

Li Guohao

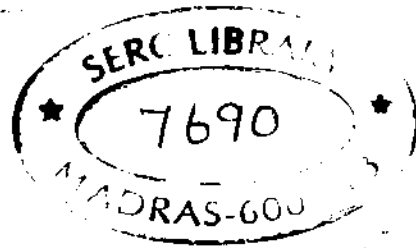
# Analysis of Box Girder and Truss Bridges

With 107 Figures

China Academic Publishers Beijing

Springer-Verlag Berlin Heidelberg New York  
London Paris Tokyo

Prof. Li Guohao  
Institute for Structure Theory  
Tong Ji University  
Shanghai/People's Republic of China



**SERC**

ISBN 7-80003-001-6/TU-13 China Academic Publishers Beijing  
ISBN 3-540-13282-1 Springer-Verlag Berlin Heidelberg New York  
ISBN 0-387-13282-1 Springer-Verlag New York Heidelberg Berlin

Library of Congress Cataloging-in-Publication Data

Li, Kuo-hao, 1913-  
Analysis of box girder and truss bridges.  
Bibliography: p. 1. Bridges, Box girder. 2. Bridges, Truss. I. Title.  
TG362.L52 1987 624'.37 87-27520  
ISBN 0-387-13282-1 (U.S.)

This work is subject to copyright. All rights are reserved, whether the whole or part of the material is concerned, specifically the rights of translation, reprinting, re-use of illustrations, recitation, broadcasting, reproduction on microfilms or in other ways, and storage in data banks. Duplication of this publication or parts thereof is only permitted under the provisions of the German Copyright Law of September 9, 1965, in its version of June 24, 1985, and a copyright fee must always be paid. Violations fall under the prosecution act of the German Copyright Law.

© China Academic Publishers, Beijing and Springer-Verlag Berlin, Heidelberg 1987  
Printed in Germany

The use of registered names, trademarks, etc. in this publication does not imply, even in the absence of a specific statement, that such names are exempt from the relevant protective laws and regulations and therefore free general use.

Typesetting: ASCO Trade Typesetting Ltd., Hong Kong  
Offsetprinting: Saladruck, Berlin. Bookbinding: Lüderitz & Bauer, Berlin  
2161/3020-543210

## Preface

In this book I discuss some of the practical experience I have gained in analyzing the box girder and the truss used in bridge engineering; the straight and curved box girder bridge, the truss bridge, and the arch-stiffened truss bridge are considered. These bridges may be either simple span or continuous over several supports, and their cross sections may be deformable. Bending and torsional stresses, lateral buckling, and vibrations are investigated, and both the analytical and the finite beam element methods of solution are developed.

It is known that the box girder and truss bridges as spatial structures can be analyzed into finite shell and plate elements or finite strips and bar members by discretization. But the computation is time consuming, and it does not yield any desirable analytical solution. Moreover, it is not possible using these methods to show the role the following play: the bending, torsional, and other rigidities of the structure or the different structural constituent parts, for instance, the chord members, the web members, the bracing systems, and the portal in a truss bridge. Determining such information is of great importance to engineers.

Applying the beam theory shown here, we can overcome all the shortcomings mentioned previously. For this reason, I have established a more accurate thin-walled beam theory of the curved box girder and developed a theory of bending and torsion of the truss bridge as an extension of the thinwalled beam theory. All these theories will be derived in detail, and the confirmation of their efficiency and accuracy by model tests or field tests will be given.

To better understand and develop the theory, the well-known analysis of the straight box girder with deformable cross section will be introduced first, then the analysis of the curved box girder with deformable trapezoidal cross section will follow.

By transforming its web members and bracing systems into continuous shearing webs, we are able to apply the theory of the box girder to the truss bridge. Thus it is only necessary to take into account the particularities of the latter type of bridge – the deformations of shearing webs and bridge portal due to shear. Finally, the arch-stiffened truss bridge will be discussed.

Many practical examples have been analyzed, and from these results, conclusions valuable to design practice have been deduced.

I hope that this book would be a contribution to the analysis and design of the bridge structures concerned.

I would like to thank deeply my research fellows for their efforts in performing the investigations based on the theories developed here and for using them in this book: Professor Shi Dong has done much for Chaps. 5 and 10, and in addition,

guided the work of Shi Jiajun for Chaps. 2 and 4, Huang Jian for Chap. 7, and Huang Dongzhou for parts of Chap. 8 and 10; Huang Dongzhou helped me to check the manuscript and the drawings. Without their help I would have hardly accomplished the task of the book.

I wish also to thank Ms. Hui Renqiu and Mr. Wu Zhenxin for improving the English of the manuscripts, and Dr. Heinz Götze for his efforts in the publication of this book.

Shanghai, People's Republic of China, July, 1986

Dr. Ing. habil Dr. Ing h.c. Li Guohao  
Honorary President, Professor of Tongji University,  
Member of Academia Sinica  
President of China Civil Engineering Society

# Contents

<b>1.</b>	<b>Bending and Torsion Theories of the Straight Box Girder</b> .....	<b>1</b>
1.1	Pure Torsion of Thin-walled Members .....	1
1.1.1	Closed Thin-walled Section .....	1
1.1.2	Open Thin-walled Section .....	3
1.2	Warping Torsion of Open Thin-walled Section .....	3
1.2.1	Torsional Warping .....	4
1.2.2	Warping Stresses and Stress Resultants .....	5
1.2.2.1	Warping Normal Stress and Bimoment .....	5
1.2.2.2	Warping Shear Stress and Warping Torsional Moment .....	6
1.3	Bending and Torsion of Box Girder with Rigid Cross Section ....	7
1.3.1	Displacements .....	8
1.3.2	Stresses and Stress Resultants .....	9
1.3.2.1	Normal Stresses and Stress Resultants .....	9
1.3.2.2	Shear Stresses and Stress Resultants .....	9
1.3.3	Strain Energy .....	10
1.3.4	Potential of External Forces .....	11
1.3.5	Equilibrium Equations .....	11
1.3.6	Differential Equations and Boundary Conditions .....	12
1.4	Torsion of Box Girder with Deformable Cross Section .....	13
1.4.1	Distortion and Warping .....	13
1.4.2	Displacements in the Section Plane .....	15
1.4.3	Shear Rigidity and Distortion Rigidity of a Box Section .....	16
1.4.4	Stresses and Stress Resultants .....	17
1.4.4.1	Normal Stresses and Stress Resultants .....	17
1.4.4.2	Shear Stresses and Stress Resultants .....	18
1.4.5	Strain Energy .....	18
1.4.6	Potential of External Forces .....	18
1.4.7	Differential Equations and Boundary Conditions .....	19
1.5	Torsion of a Box Girder Considering Shear Strain .....	19
1.5.1	Basis Equations .....	20
1.5.2	Potential of Internal and External Forces .....	20
1.5.3	Differential Equations .....	21
<b>2.</b>	<b>Stress Analysis of Straight Box Girders</b> .....	<b>22</b>
2.1	Finite Beam Element Method .....	22

2.1.1	Assumptions on the Nodal Displacement Parameters and the Displacement Functions of Beam Elements .....	22
2.1.2	Derivation of the Element Stiffness Matrix .....	24
2.1.3	Derivation of the Element Load Vector .....	27
2.1.4	Formation of the Structure Stiffness Matrix .....	27
2.1.5	Boundary Conditions .....	28
2.1.6	Evaluation of Displacements and Stresses .....	28
2.2	Analytical Method .....	29
2.2.1	Analytical Solution for a Single-span Girder .....	29
2.2.2	Treatment of a Continuous Girder .....	30
2.2.3	Numerical Example .....	31
2.2.4	Effect of Warping Torsion of Box Girders .....	35
2.2.5	Effect of Shear Strain $\gamma_w$ Due to Warping Torsion .....	35
2.3	Cross-section Distortion Analysis of Box Girders .....	37
2.3.1	Solution to the Distortion Equation of Box Girders .....	37
2.3.2	Numerical Example .....	39
2.3.3	Effect of Distortional Warping of Box Girders .....	41
2.4	Comparison of Theoretical Results with Model Test .....	41
<b>3.</b>	<b>Bending and Torsion Theories of Curved Box Girder .....</b>	<b>43</b>
3.1	Displacements and Deformations .....	43
3.2	Normal Strain .....	45
3.3	Principal Coordinates .....	46
3.3.1	Unit Torsional Warping .....	46
3.3.2	Unit Distortional Warping .....	47
3.3.3	Neutral Axis of Horizontal Bending .....	49
3.4	Stresses and Stress Resultants .....	50
3.4.1	Normal Stresses and Moments .....	50
3.4.2	Shear Stress and Torque .....	51
3.5	The Strain Energy .....	51
3.6	Potential of External Forces .....	52
3.7	Differential Equations .....	52
3.8	Boundary Conditions .....	53
3.9	Simplification in Special Cases .....	54
3.9.1	Special Case 1: $R(x) \approx R_0$ .....	54
3.9.2	Special Case 2: $R(x) = R_0, \tilde{\theta} = 0$ .....	54
3.10	Analysis Under Consideration of Shear Strain of Warping Torsion .....	55
3.10.1	Displacements and Strains .....	55
3.10.2	Differential Equations .....	56
<b>4.</b>	<b>Stress Analysis of Curved Box Girder .....</b>	<b>57</b>
4.1	Finite Beam Element Method .....	57
4.1.1	Assumptions on the Nodal Displacements and Displacement Functions .....	57
4.1.2	Derivation of Element Stiffness Matrix and Element Load Vector .....	58
4.1.3	Boundary Conditions .....	59

4.1.4	Evaluation of Displacements and Stresses . . . . .	60
4.2	Model Test . . . . .	61
4.3	Influence of Curvature on Normal Stresses . . . . .	63
4.4	Influence of the Number of Diaphragms . . . . .	65
4.5	Influence of Thickness of Plates of Box Girders . . . . .	66
4.6	Effect of the Variation of $R$ Along the Width of Cross-section . . . . .	67
4.7	Influence of Coupling on Distortion . . . . .	68
4.8	Effect of Shear Strain $\gamma_w$ on Warping Torsion . . . . .	68
<b>5.</b>	<b>Earthquake Response of Curved Box Girder Bridge . . . . .</b>	<b>70</b>
5.1	Finite Element Method . . . . .	70
5.1.1	Stress-strain . . . . .	70
5.1.2	Displacement Functions . . . . .	72
5.1.3	Nodal Forces and Element Stiffness Matrix . . . . .	73
5.1.4	Element Mass Matrix . . . . .	74
5.1.5	Seismic Mass Matrix . . . . .	76
5.1.6	Pier Element and Coordinate Transformation . . . . .	77
5.1.7	Dynamic Global Equations and Earthquake Response . . . . .	78
5.2	Example . . . . .	78
<b>6.</b>	<b>Bending and Torsion Theories of Truss Bridges . . . . .</b>	<b>81</b>
6.1	Introduction . . . . .	81
6.2	Influence of Webs of Truss . . . . .	82
6.2.1	Shear Rigidity of Webs . . . . .	82
6.2.2	Influence of Shear Strain in Bending . . . . .	83
6.2.3	Influence of Shear Strain in Warping Torsion and Distortion . . . . .	86
6.3	Boundary Conditions at Portal . . . . .	87
6.4	Determination of Internal Forces . . . . .	88
<b>7.</b>	<b>Spatial Stress Analysis of Truss Bridges . . . . .</b>	<b>90</b>
7.1	Finite Beam Element Method for Stress Analysis . . . . .	90
7.2	End Beam Element for Inclined Portal . . . . .	90
7.3	Analysis of Shear Forces in Portals and Sway Bracings . . . . .	92
7.4	Comparison of Theoretical and Experimental Results . . . . .	94
7.5	Analytical Solution of the Internal Forces . . . . .	95
7.5.1	Simplification of the Differential Equations . . . . .	95
7.5.1.1	Neglect the Effect of the Warping Torsion . . . . .	95
7.5.1.2	Neglect the Coupling of Warping Torsion and Distorsion of Cross-section as Discussed in Chaps. 1 and 2 . . . . .	95
7.5.2	Solutions of the Differential Equations . . . . .	95
7.6	Examples . . . . .	98
<b>8.</b>	<b>Lateral Stability of Truss Bridges . . . . .</b>	<b>100</b>
8.1	Derivation of Differential Equations of Lateral Buckling . . . . .	100
8.1.1	Basic Principle . . . . .	100

8.1.2	Potential of Existing Internal Forces Due Lateral Buckling	101
8.1.3	Potential of Vertical Loads Due to Lateral Buckling	103
8.1.4	Differential Equations of Lateral Buckling	103
8.2	Approximate Analytical Solution of the Lateral Buckling	104
8.3	Determination of Lateral Buckling Safety Factor	106
8.3.1	Approximate Modification of Safety Factor for Plastic Deformation	106
8.3.2	Example	107
8.4	Finite Beam Element Method for Analyzing Lateral Buckling	108
8.4.1	Basic Principle	109
8.4.2	Element Geometric Matrix	110
8.4.3	Example	110
8.5	Practical Method for Determining Critical Load	111
8.6	Influence of the Slope of Inclined Portals	113
8.7	Model Tests	114
<b>9.</b>	<b>Bending and Torsional Vibrations of Truss Bridges</b>	<b>116</b>
9.1	Energy Method	116
9.1.1	Basic Principle	116
9.1.2	Energy in Lateral Bending and Torsional Vibrations	117
9.1.3	Equation of Bending and Torsional Vibrations	117
9.1.4	Lateral Bending and Torsional Free Vibrations	120
9.2	Finite Beam Element Method	120
9.2.1	Mass Matrix of Truss Beam Element	121
9.3	Example	122
<b>10.</b>	<b>Spatial Analysis of Arch-Truss Bridges</b>	<b>126</b>
10.1	Finite Elements of the Arch-Truss	126
10.2	Nodal Displacements of the Arch-Beam Element in Lateral Bending and Torsion	128
10.3	Stiffness Matrix of Arch-Beam Element	128
10.3.1	Element Stiffness Matrix of Truss $[k]_T$	129
10.3.2	Element Stiffness Matrix of Arch $[k]_A$	129
10.3.3	Element Stiffness Matrix of the Cross-frame $[k]_F$	132
10.4	Substructure Element at the Arch Portal	133
10.5	Boundary Conditions	133
10.6	Calculation of Internal Forces	134
10.7	Comparison Between the Model Test and the Theory	134
10.8	Finite Element Method for the Lateral Buckling Analysis of Arch-Truss	135
10.9	Model Test of the Lateral Buckling of Arch-Truss Bridge	138
	<b>References</b>	<b>139</b>



# 1. Bending and Torsion Theories of the Straight Box Girder

The box girder is often used for bridges and other structures. Usually its cross section consists of a rectangular or trapezoidal box and open parts. Diaphragms are generally used, and for girders of short span, only end-diaphragms are provided. Box girders without diaphragms or with insufficient intermediate diaphragms are subjected to cross-sectional distortion under torsional loading. This will be considered in detail.

Box girders can be either straight or curved in plan. The theory and method for the analysis of bending and torsion of straight box girders have been quite well developed by Vlasov (1940), Dshanelidze and Panovko (1948), Bornscheuer (1952), Sedlacek (1971), Roik et al. (1972), and others, while for the analysis of curved box girders, improvements in their analysis can still be made.

For practical uses and as a theoretical basis for the curved box girder and truss, we will introduce the theory of bending and torsion of the straight box girder in this chapter. The discussion will be restricted to a single box cell. For multiple box cells see, for instance, Roik et al. (1972), Huang (1983). In the analysis we will assume that the displacements are small and that Hooke's law is valid.

## 1.1 Pure Torsion of Thin-walled Members

Pure torsion occurs if a straight member is subjected only to torques at its ends and the warping — out-of-plane distortion — of cross sections thereby produced is not restrained, so that only shear stresses  $\tau_c$  but no normal stresses  $\sigma$  arise.

### 1.1.1 Closed Thin-walled Section

A closed thin-walled cross section is subjected to a torque  $T_c$ , as shown in Fig. 1.1. Assuming that the shear stress  $\tau_c$  is uniformly distributed across the small wall thickness  $t$ , there is a constant shear flow  $q_c = t\tau_c$  along the contour. With the lever arm  $\rho_M$  from the shear center or center of twist, the shear flow over the whole cross section produces a moment that, due to equilibrium conditions, equals the torque  $T_c$ :

$$\oint \rho_M q_c ds = T_c .$$

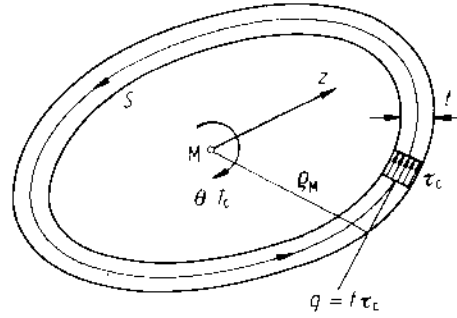


Fig. 1.1. Closed thin-walled cross section

Hence

$$q_c = t\tau_c = \frac{T_c}{2A}, \quad (1.1)$$

where

$$A = \frac{1}{2} \oint \rho_M ds. \quad (1.1a)$$

Here  $A$  denotes the area enclosed by the shear flow.

To establish the relation between the torque  $T_c$  and the angle of twist  $\theta$ , we equate the strain energy of torsion to the work done by the torque for a member element  $dz$ :

$$\frac{1}{2} dz \oint t\tau_c \gamma_c ds = \frac{1}{2} T_c \frac{d\theta}{dz} dz.$$

With Hooke's Law,  $\gamma_c = \tau_c/G$ , and  $\tau_c$  from Eq. (1.1), we obtain

$$T_c = C \frac{d\theta}{dz} = C\theta', \quad (1.2)$$

where  $C$  denotes the torsional rigidity:

$$C = GI_d, \quad (1.3)$$

and here

$$I_d = \frac{4A^2}{\oint (ds/t)}. \quad (1.3a)$$

From Eqs. (1.1) to (1.3a), it follows that the shear strain is

$$\gamma_c = \frac{\psi}{t} \theta', \quad (1.4)$$

where

$$\psi = \frac{2A}{\oint (ds/t)}. \quad (1.5)$$

$\psi/t$  is often called the torsional function and will be used later. It gives the magnitude of  $\gamma_c$  for  $\theta' = 1$  and has the dimension of "length."

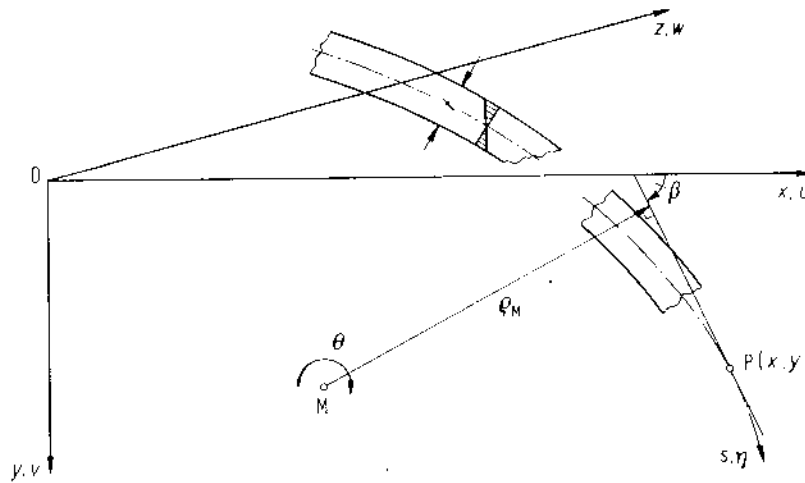


Fig. 1.2. Open thin-walled cross section

### 1.1.2 Open Thin-walled Section

The thin-walled open cross section behaves quite differently in pure torsion. No shear stress will be produced along the center line of the wall, and there is an antisymmetrical linear distribution across the wall thickness for the shear stress with  $\tau_{\max}$  at both edges, as shown in Fig. 1.2.

For a narrow rectangular section with thickness  $t$  and width  $b$ , this shear stress gives a torsional moment

$$T_c = \frac{1}{3}bt^2\tau_{\max} . \quad (1.6)$$

From energy considerations analogous to the preceding section, we also obtain Eqs. (1.2) and (1.3), where  $I_d$  for an open section is

$$I_d = \frac{1}{3}bt^3 . \quad (1.3b)$$

For box girders of cross section,  $I_d$  is the sum of that due to the closed section and the open sections; however, the open section's contribution is small and can be neglected.

Using Eqs. (1.6) and (1.3b) we can write

$$\tau_{\max} = \frac{T_c}{I_d} t . \quad (1.6a)$$

## 1.2 Warping Torsion of Open Thin-walled Section

If, owing to the action of torques, the warping of cross section is restrained, warping normal stresses and, consequently, warping shear stresses will be induced. These shear stresses form a warping torsional moment, as an addition to the pure torsional

moment. We now consider the warping torsion of a thin-walled section with the assumption that the section is not deformable.

### 1.2.1 Torsional Warping

In Fig. 1.2 a part of the open thin-walled section is shown.  $O$  denotes its centroid;  $x, y$  are the principal axes; and  $M(x_M, y_M)$  is the center of twist.  $\rho_M$  ( $\rho_0$ ) is the perpendicular from  $M$  ( $O$ ) to the tangent at  $P(x, y)$  on the centerline of the section:

$$\rho_M = (x - x_M) \sin \beta - (y - y_M) \cos \beta, \quad (1.7a)$$

or

$$\rho_M = \rho_0 - x_M \sin \beta + y_M \cos \beta. \quad (1.7b)$$

The tangential displacement  $\eta = \rho_M \theta$  and the out-of-plane displacement  $w$  produced by the torques would induce a shear strain

$$\gamma_{zs} = \frac{\partial \eta}{\partial z} + \frac{\partial w}{\partial s}, \quad (1.8)$$

where  $s$  denotes the coordinate along the centerline of section, clockwise positive.

According to the assumption that the thin-walled open section remains plane under the action of torsion, this shear strain must be zero:  $\gamma_{zs} = 0$ . It follows that with  $\eta = \rho_M \theta$  the warping is

$$w(s, z) = -\theta' \int_0^s \rho_M ds + w_0(z),$$

or

$$w(s, z) = -\omega(s)\theta'(z), \quad (1.9)$$

where

$$\omega(s) = \omega_1(s) + \omega_1(0), \quad (1.10)$$

$$\omega_1(s) = \int_0^s \rho_M ds. \quad (1.11)$$

$\omega(s)$  is called the principal unit warping.

The constant of integration  $\omega_1(0)$  and the coordinates  $(x_M, y_M)$  of the center of twist  $M$  can be determined from the equilibrium conditions for the warping normal stress induced by the torque  $T_c$ . Applying Hooke's law, we have

$$\sigma(s, z) = Ew' = -E\omega(s)\theta''(z), \quad (1.12)$$

and, from equilibrium, we have

$$N = \int_F \sigma dF = 0, \quad (1.13a)$$

$$M_x = \int_F y\sigma dF = 0, \quad (1.13b)$$

$$M_y = \int_F x\sigma dF = 0. \quad (1.13c)$$

Substituting Eqs. (1.11) and (1.12) into Eq. (1.13a), we have

$$\int_F \omega dF = 0 : \quad \omega_1(0) = -\frac{1}{F} \int_F \omega_1(s) dF . \quad (1.14)$$

Equation (1.7b), when multiplied by  $ds$ , will be

$$\rho_M ds = \rho_0 ds - x_M dy + y_M dx .$$

Using this expression, Eq. (1.11) gives

$$\omega = \omega_M = \omega_0 - x_M y + y_M x , \quad (1.15)$$

where  $\rho_0$  and  $\omega_0$  refer to the centroid  $O$ . With Eqs. (1.12) and (1.15), we obtain from Eqs. (1.13b) and (1.13c):

$$\begin{aligned} \int_F y \omega dF = 0 : \quad x_M &= \frac{F_{y\omega_0}}{F_{yy}} ; \\ \int_F x \omega dF = 0 : \quad y_M &= -\frac{F_{x\omega_0}}{F_{xx}} , \end{aligned} \quad (1.16)$$

where the following notation is used for cross-sectional integrals:

$$F = \int_F dF , \quad F_r = \int_F r dF , \quad F_{rs} = \int_F rs dF . \quad (1.17)$$

For principal axes  $x$  and  $y$ , as is known in the bending analysis, there are similar expressions as Eqs. (1.14) and (1.16) for  $\omega$ . All these can be interpreted as the orthogonal relationship

$$F_{x_i x_k} = \int_F x_i x_k dF = \begin{cases} F_{x_i x_i}, & \text{if } i = k \\ 0, & \text{if } i \neq k \end{cases} \quad (1.18)$$

between the four principal coordinates

$$[x_i] = [x \ y \ \omega \ 1] . \quad (1.19)$$

It is this orthogonality that makes it possible to analyze the torsion, the bending about the  $x$  and  $y$  axes, and the axial tension of a straight member independently.

## 1.2.2 Warping Stresses and Stress Resultants

### 1.2.2.1 Warping Normal Stress and Bimoment

The warping normal stress is given in Eq. (1.12). Multiplying both sides of the equation by  $\omega$  and integrating over the entire cross section, we obtain an expression for the so called bimoment,

$$M_\omega = \int_F \omega \sigma dF = -D_{\omega\omega} \theta'' , \quad (1.20)$$

where the warping torsional rigidity is given by

$$D_{\omega\omega} = EF_{\omega\omega} = E \int_F \omega\omega dF. \quad (1.21)$$

The warping normal stress is often determined from the bimoment:

$$\sigma = \frac{M_{\omega}}{F_{\omega\omega}} \omega. \quad (1.22)$$

### 1.2.2.2 Warping Shear Stress and Warping Torsional Moment

Since we have assumed that the shear strain  $\gamma_{zs} = 0$ , the warping shear stress  $\tau$  can only be determined from warping normal stress  $\sigma$  by considering the equilibrium in the longitudinal direction of an element of the member, as shown in Fig. 1.3:

$$\frac{\partial(t\tau)}{\partial s} + \frac{\partial(t\sigma)}{\partial z} = 0. \quad (1.23)$$

Hence

$$t\tau = q = q_0 - \int_0^s \frac{\partial(t\sigma)}{\partial z} ds. \quad (1.24)$$

Taking the free edge of section as the start of  $s$  where  $q_0 = 0$  if there is no external longitudinal force acting along the edge, and substituting Eq. (1.12) into the integral, we get

$$q(s, z) = EF_{\omega}(s)\theta'''(z), \quad (1.25)$$

where

$$F_{\omega}(s) = \int_0^s \omega(s)t ds. \quad (1.25a)$$

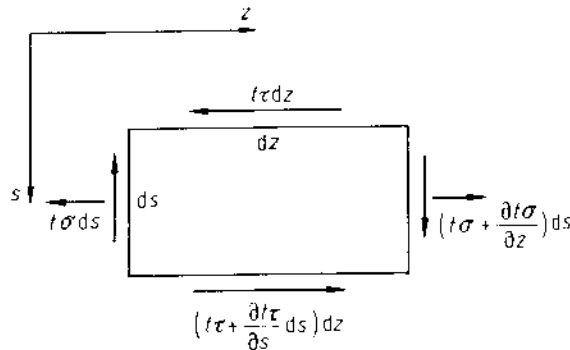


Fig. 1.3. A plate element

The warping torsional moment provided by  $q$  is

$$\begin{aligned} T_{\omega} &= \int_s q \rho_M ds = \int_s q d\omega \\ &= [q \omega] - \int_s \frac{\partial q}{\partial s} \omega ds . \end{aligned} \quad (1.26)$$

The first term on the right-hand side represents the boundary values that vanish because at the ends of the section  $q = 0$ . Substituting Eq. (1.25) into the integral we get

$$T_{\omega} = -D_{\omega\omega} \theta''' . \quad (1.27)$$

Comparing this with Eq. (1.20), yields

$$T_{\omega} = M'_{\omega} . \quad (1.28)$$

Thus, the warping shear stress given in Eq. (1.25) can be determined from the warping torsional moment

$$\tau = -\frac{T_{\omega}}{t F_{\omega\omega}} F_{\omega}(s) . \quad (1.29)$$

### 1.3 Bending and Torsion of Box Girder with Rigid Cross Section

We consider the bending, torsion, and axial tensions of a straight box girder with cross section subjected to distributed loading  $q_x, q_y, q_z$  in three directions  $x, y, z$  as shown in Fig. 1.4. The effects of the deformation of the cross section and that of the shear on the torsion will be discussed later, while the local stresses induced by loadings are neglected.

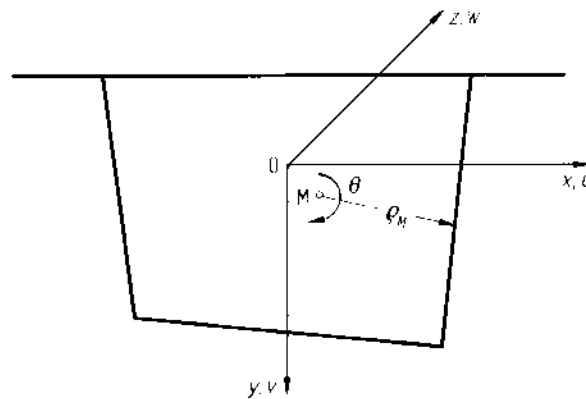


Fig. 1.4. A composed cross section

### 1.3.1 Displacements

In Fig. 1.4  $O$  denotes the centroid,  $M$  is the shear center,  $x, y$  are the principal axes, and  $z$  is the girder axis. Suppose under the action of loads  $q_x, q_y, q_z$  the cross section has undergone three uniform displacements  $u_0(z), v_0(z), w_0(z)$  in directions  $x, y, z$ , and an angle of twist  $\theta(z)$  about the shear center  $M$ , the out-of-plane displacement  $w(x, y, z)$  of the section has to be determined, in order to evaluate the stresses.

Let us at first consider the torsional warping of the thin-walled closed section, which can also be given in a form similar to Eqs. (1.9) and (1.10) for open sections. Only the evaluation of unit warping  $\omega$  is different, because in a closed section the shear strain  $\gamma_0$  is not zero as in the case of open section, but is of the magnitude given by Eq. (1.4). Substituting this into Eq. (1.8) we have

$$w = -\theta' \int_0^s \left( \rho_M - \frac{\psi}{t} \right) ds + w_0.$$

Therefore,

$$w = -\omega \theta',$$

$$\omega = \int_0^s \left( \rho_M - \frac{\psi}{t} \right) ds + \omega_1(0). \quad (1.30)$$

The constant of integration  $\omega_1(0)$  and the coordinates  $(x_M, y_M)$  of the center of twist  $M$  can also be determined from Eqs. (1.14) and (1.16).

For box girders usually used in practice, the unit warping consists of two parts, which are given in Eqs. (1.30) and (1.11) for closed and open sections, respectively, as shown in Fig. 1.5. It is antisymmetrically distributed about the vertical axis for the symmetrical cross section.

As to the bending, according to the assumption that after deformation the cross section remains plane and perpendicular to the girder axis, it is easy to see that the longitudinal displacement  $w$  equals the slopes  $u'_0$  and  $v'_0$  of the deflections  $u_0$  and  $v_0$  multiplied by  $x$  and  $y$ , respectively.

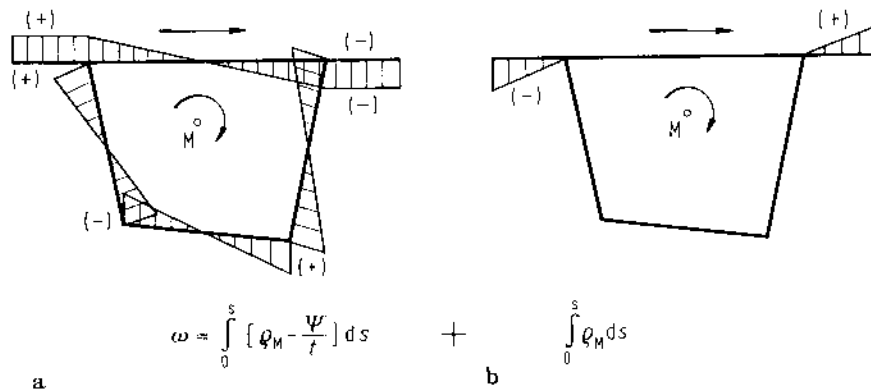


Fig. 1.5a, b.  $\omega$  diagrams of closed and open section parts



Thus, the displacement  $w(x, y, z)$  over the cross section can be given as follows:

$$w(x, y, z) = -xu'_0 - yv'_0 - \omega\theta' + w_0. \quad (1.31)$$

Finally, we list the displacements in directions  $x$  and  $y$  for future use:

$$\begin{aligned} u(x, y, z) &= u_0(z) - (y - y_M)\theta(z), \\ v(x, y, z) &= v_0(z) + (x - x_M)\theta(z). \end{aligned} \quad (1.32)$$

### 1.3.2 Stresses and Stress Resultants

#### 1.3.2.1 Normal Stresses and Stress Resultants

Using Hooke's law, the normal stresses of bending, warping torsion, and axial tension can be evaluated from the strain  $\epsilon$  obtained by differentiating Eq. (1.31):

$$\begin{aligned} \sigma(x, y, z) &= E\epsilon = Ew'(x, y, z) \\ &= -E(xu''_0 + yv''_0 + \omega\theta'' - w'_0). \end{aligned} \quad (1.33a)$$

Considering the orthogonal relationship of the four principal coordinates given in Eqs. (1.18) and (1.19), we obtain the bending moments  $M_y$ ,  $M_x$ , the bimoment of warping torsion  $M_\omega$ , and the axial tension  $N$  as follows

$$M_y = \int_F x\sigma dF = -D_{xx}u''_0, \quad (1.34a)$$

$$M_x = \int_F y\sigma dF = -D_{yy}v''_0, \quad (1.34b)$$

$$M_\omega = \int_F \omega\sigma dF = -D_{\omega\omega}\theta'', \quad (1.34c)$$

$$N = \int_F \sigma dF = EFw'_0 = Dw'_0, \quad (1.34d)$$

where the third expression (1.34c) has been given in Eq. (1.20), and the flexural rigidities  $D_{xx}$  and  $D_{yy}$  are defined analogously as  $D_{\omega\omega}$  in Eq. (1.21).

By using Eq. (1.34), the normal stress is often evaluated according to the following equation:

$$\sigma = \frac{M_y}{F_{xx}}x + \frac{M_x}{F_{yy}}y + \frac{M_\omega}{F_{\omega\omega}}\omega + \frac{N}{F}. \quad (1.33b)$$

#### 1.3.2.2 Shear Stresses and Stress Resultants

The shear stress due to pure torsion  $\tau_c$  in a closed section is given in Eq. (1.1). The shear stress  $\tau$  in equilibrium with the normal stress  $\sigma$  has to be calculated according to Eq. (1.24) deduced from Eq. (1.23). In order to determine  $q_0$  in a closed section we imagine a cut in the box;  $q_0$  is applied in the cut so that the continuity is

maintained:

$$\oint \gamma ds = \frac{1}{G} \oint \tau ds = 0. \quad (1.35)$$

On substituting Eq. (1.33a) or (1.33b) into Eq. (1.24) and this in turn into Eq. (1.35), we obtain

$$q_0 = -\frac{E}{\oint (ds/t)} \left\{ u_0''' \oint F_x(s) \frac{ds}{t} + v_0''' \oint F_y(s) \frac{ds}{t} + \theta''' \oint F_\omega(s) \frac{ds}{t} - w_0'' \oint F(s) \frac{ds}{t} \right\}.$$

Denoting

$$S_\omega(s) = F_\omega(s) - \frac{1}{\oint (ds/t)} \oint F_\omega(s) \frac{ds}{t}, \quad (1.36)$$

and similarly for  $S_x$ ,  $S_y$ , and  $S$ , where  $F_\omega(s)$ , analogously  $F_x(s)$ ,  $F_y(s)$ ,  $F(s)$ , is defined by Eq. (1.25a), we finally obtain the shear stress due to bending, warping torsion, and axial tension in a closed section:

$$\tau = \frac{E}{t} \{ u_0''' S_x(s) + v_0''' S_y(s) + \theta''' S_\omega(s) - w_0'' S(s) \}, \quad (1.37a)$$

or

$$\tau = -\frac{1}{t} \left\{ \frac{Q_x}{F_{xx}} S_x(s) + \frac{Q_y}{F_{yy}} S_y(s) + \frac{T_\omega}{F_{\omega\omega}} S_\omega(s) + \frac{N'}{F} S(s) \right\}, \quad (1.37b)$$

where the shear forces  $Q_x$ ,  $Q_y$  and the warping torsional moment  $T_\omega$  are

$$\begin{aligned} Q_x &= M'_y, \\ Q_y &= M'_x, \\ T_\omega &= M'_\omega. \end{aligned} \quad (1.38)$$

For open sections,  $q_0$  vanishes at the free edge if no external longitudinal force is acting there, and this point can be taken as the origin of local coordinate  $s$ .

In the closed section, the shear stress is the sum of  $\tau_c$  and  $\tau$  given by Eqs. (1.1) and (1.37a) or (1.37b).

### 1.3.3 Strain Energy

The elastic strain energy, or the potential of internal forces of bending, torsion, and axial tension, consists of two parts provided by the normal strain  $\varepsilon$  and the shear strain  $\gamma_c$  of a closed section induced by pure torsion:

$$U_e = \frac{E}{2} \int_1 \int_F \varepsilon^2 dF dz + \frac{G}{2} \int_1 \int_F \gamma_c^2 dF dz. \quad (1.39)$$

Using  $\varepsilon$  and  $\gamma_c$  from Eqs. (1.33a) and (1.4), respectively, we get, after integration over

the cross sectional area,

$$U_e = \frac{1}{2} \int \{ D_{xx}(u_0'')^2 + D_{yy}(v_0'')^2 + D_{\omega\omega}(\theta'')^2 + C(\theta')^2 + D(w_0')^2 \} dz, \quad (1.40a)$$

where the rigidities  $D_{ii}$  ( $D = D_{ii}$ ) and  $C$  are given in Eqs. (1.21) and (1.3).

Substituting expressions (1.34) and (1.2) into the preceding equation, we can express the strain energy in another form:

$$U_e = -\frac{1}{2} \int \{ M_y u_0'' + M_x v_0'' + M_{\omega\omega} \theta'' - T_c \theta' - N w_0' \} dz. \quad (1.40b)$$

### 1.3.4 Potential of External Forces

The potential of external forces — the loadings  $q_x, q_y, q_z$  — equals the negative value of the work done by the loadings

$$U_p = - \int \int \int (q_x u + q_y v + q_z w) dx dy dz. \quad (1.41)$$

Substituting  $u, v, w$ , given by Eqs. (1.32) and (1.31), into the integral and using the following notation

$$\begin{aligned} p_x &= \int \int q_x dx dy, & p_y &= \int \int q_y dx dy, & p_z &= \int \int q_z dx dy, \\ m_x &= \int \int y q_z dx dy, & m_y &= \int \int x q_z dx dy, \\ m_z &= \int \int \{ (x - x_M) q_y - (y - y_M) q_x \} dx dy, \\ m_\omega &= \int \int \omega q_z dx dy, \end{aligned} \quad (1.42)$$

we obtain

$$U_p = - \int \{ p_x u_0 - m_y u_0' + p_y v_0 - m_x v_0' + m_z \theta - m_\omega \theta' + p_z w_0 \} dz. \quad (1.43)$$

### 1.3.5 Equilibrium Equations

An elastic system is in equilibrium when total potential energy is an extremum; that means that the variation of the potential equals zero:

$$\delta U = \delta U_e + \delta U_p = 0. \quad (1.44)$$

Using Eq. (1.40b) we obtain, after partial integration, the variation of  $U_e$

$$\begin{aligned} \delta U_e &= - \int \{ (M_y'' \delta u_0 + M_x'' \delta v_0 + T' \delta \theta + N' \delta w_0) dz - [M_y \delta u_0'] + [Q_x \delta u_0] \\ &\quad - [M_x \delta v_0'] + [Q_y \delta v_0] - [M_\omega \delta \theta'] + [T \delta \theta] + [N \delta w_0] \}, \end{aligned} \quad (1.45)$$

where the brackets [ ] denote boundary values, and the torque  $T$  is

$$T = T_\omega + T_c. \quad (1.46)$$

$Q_x, Q_y$ , and  $T_\omega$  are defined in Eq. (1.38).

The variation of  $U_p$  can be calculated analogously from Eq. (1.43). It is

$$\begin{aligned} \delta U_p = - \int \{ & (p_x + m'_y) \delta u_0 + (p_y + m'_x) \delta v_0 + (m_z + m'_\omega) \delta \theta + p_z \delta w_0 \} dz \\ & + [m_y \delta u_0] + [m_x \delta v_0] + [m_\omega \delta \theta]. \end{aligned} \quad (1.47)$$

The substitution of  $\delta U_e$  and  $\delta U_p$  into Eq. (1.44) under the condition that the integrands belonging to the four independent displacement variations  $\delta u_0$ ,  $\delta v_0$ ,  $\delta \theta$ ,  $\delta w_0$  must be zero, yields the following equilibrium equations:

$$Q'_x + p_x + m'_y = 0, \quad (1.48a)$$

$$Q'_y + p_y + m'_x = 0, \quad (1.48b)$$

$$T' + m_z + m'_\omega = 0, \quad (1.48c)$$

$$N' + p_z = 0. \quad (1.48d)$$

### 1.3.6 Differential Equations and Boundary Conditions

Using Eqs. (1.46), (1.38), (1.34), and (1.2), Eqs. (1.48) can be transformed into the required differential equations, containing four displacement variables, of bending, torsion, and axial tension of a straight box girder. However, owing to the orthogonal relationship of the principal coordinates given in Eqs. (1.18) and (1.19), these equations are independent as mentioned above:

$$(D_{xx} u_0'')'' = p_x + m'_y, \quad (1.49a)$$

$$(D_{yy} v_0'')'' = p_y + m'_x, \quad (1.49b)$$

$$(D_{\omega\omega} \theta'')'' - (C\theta')' = m_z + m'_\omega, \quad (1.49c)$$

$$-Dw_0' = p_z. \quad (1.49d)$$

To fulfill Eq. (1.44), the boundary values in it that contain  $\delta u_0$ ,  $\delta v_0$ ,  $\delta \theta$ ,  $\delta w_0$  must also be zero. This gives the boundary conditions. When there are no external forces and moments acting at the boundaries, we have:

$$[M_y \delta u_0'] = 0, \quad [Q_x \delta u_0] = 0, \quad (1.50a)$$

$$[M_x \delta v_0'] = 0, \quad [Q_y \delta v_0] = 0, \quad (1.50b)$$

$$[M_\omega \delta \theta'] = 0, \quad [T \delta \theta] = 0, \quad (1.50c)$$

$$[N \delta w_0] = 0. \quad (1.50d)$$

According to these equations, at the end either the displacement (or slope) is given, so that its variation vanishes, or the corresponding force (or moment) equals zero. For example, either  $\delta u_0 = 0$  (supported end) or  $Q_x = -D_{xx} u_0''' = 0$  (free end), or either  $\delta u_0' = 0$  (fixed end) or  $M_y = -D_{xx} u_0'' = 0$  (simple support).

## 1.4 Torsion of Box Girder with Deformable Cross Section

### 1.4.1 Distortion and Warping

We consider a single box section. Its distortion can be represented in two parts as shown in Fig. 1.6, where  $O$  denotes the centroid;  $x$  and  $y$  are the principal axes;  $N$  is the center of distortion;  $\tilde{x}$ ,  $\tilde{y}$  are the axes parallel to  $x$ ,  $y$ ;  $d_i$  ( $i = 1, 2, 3, 4$ ) is the side length of the closed section;  $\beta_i$  is its slope referred to  $x$  axis (clockwise positive); and  $\alpha_i$  is the angle at the box corner.

Assuming that the  $\tilde{y}$  and  $\tilde{x}$  axis rotate about  $N$  an angle  $\phi = \bar{\theta}$  (clockwise positive) and  $\psi = -v\bar{\theta}$ , respectively, and that the sides, as hinged at their joints, follow these rotations, the distortion of the cross section can be expressed by

$$\tilde{\gamma}_N = \phi - \psi = (1 + v)\bar{\theta}, \quad (1.51)$$

where the factor  $v$  is used in order to ensure the continuity of warping caused by  $\phi$  and  $\psi$ .

Analogously to torsion, the distortional warping can be derived from Eq. (1.8) with  $\gamma_{zs} = 0$  for open and closed sections. The result is similar to Eqs. (1.9), (1.10), (1.11):

$$\tilde{w}(z, s) = -\tilde{\omega}(s)\tilde{\theta}(z), \quad (1.52)$$

where the unit distortional warping

$$\tilde{\omega}(s) = \int_0^s \tilde{\rho}_N ds, \quad (1.53a)$$

with

$$\begin{aligned} \tilde{\rho}_N(\phi) &= \rho_N, & \tilde{\rho}_N(\psi) &= v_n \rho_N, \\ v_n &= 1 & \text{for } n &= 1, 3, \end{aligned} \quad (1.53b)$$

and

$$v_n = -v \quad \text{for } n = 2, 4. \quad (1.54)$$

$n = 1, 2, 3, 4$  denotes the side number, and  $\rho_N$  is the perpendicular from  $N$  to the sides as shown in Fig. 1.6.

The continuity of distortional warping means

$$\tilde{\omega}(-0) = \tilde{\omega}(+0) - \oint \tilde{\rho}_N ds = \tilde{\omega}(+0),$$

that is

$$\oint \tilde{\rho}_N ds = 0.$$

It follows that

$$v = \frac{\rho_1 d_1 + \rho_3 d_3}{\rho_2 d_2 + \rho_4 d_4}. \quad (1.55)$$

For a rectangular box,  $v = 1$ .

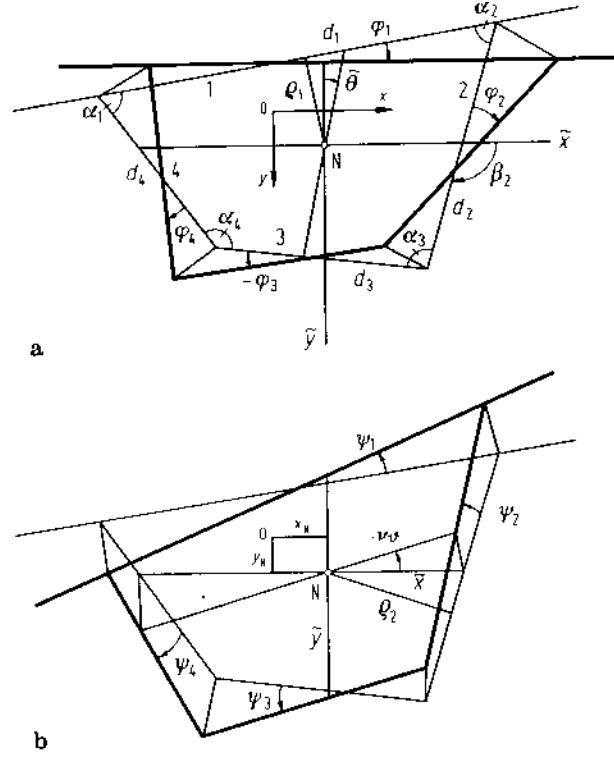


Fig. 1.6. Distortion of box section with respect to (a) angle  $\tilde{\theta}$  and (b) to angle  $-v\tilde{\theta}$

Like the unit torsional warping  $\omega(s)$ , the unit distortional warping  $\tilde{\omega}(s)$  has to be and can be orthogonalized to the principal coordinates  $[x \ y \ 1]$  in order to make the stress state induced by it independent from that of bending and axial tension. The equations concerned are similar to Eqs. (1.14) to (1.16):

$$\int_F \tilde{\omega} dF = 0 : \quad \tilde{\omega}_1(0) = -\frac{1}{F} \int_F \tilde{\omega} dF, \quad (1.56)$$

$$\tilde{\omega}(s) = \tilde{\omega}_N(s) = \tilde{\omega}_0(s) - x_N v_n y + y_N v_n x; \quad (1.57)$$

$$\int_F y \tilde{\omega} dF = 0 : \quad x_N = \frac{\sum_n F_y^{(n)} \tilde{\omega}_0}{\sum_n v_n F_{yy}^{(n)}}; \quad (1.58)$$

$$\int_F x \tilde{\omega} dF = 0 : \quad y_N = -\frac{\sum_n F_x^{(n)} \tilde{\omega}_0}{\sum_n v_n F_{xx}^{(n)}},$$

where the index  $N$  denotes the center of distortion and  $O$  denotes the centroid.

There is, however, no possibility of orthogonalizing  $\tilde{\omega}(s)$  to  $\omega(s)$ . Therefore, the distortion, if any, and the warping torsion are coupled, although usually the link is weak.

### 1.4.2 Displacements in the Section Plane

The displacements in the section plane at the center line  $s$  of section in the tangential direction  $\tilde{\eta}(s)$  (clockwise positive) and in the normal direction  $\tilde{\xi}(s)$  (outward positive) can be given as follows (see Fig. 1.5):

$$\tilde{\eta}_n = \tilde{\rho}_n \tilde{\theta}, \quad (1.59)$$

$$\tilde{\xi}_n = (\tilde{\eta}_n \cot \alpha_n + \tilde{\eta}_{n-1} \operatorname{cosec} \alpha_n) - (\phi_n + \psi_n) s_n, \quad (1.60)$$

where  $n = 1, 2, 3, 4$  cyclically and  $s_n$  is the coordinate of side  $n$  (clockwise positive) with the origin at the box corner. The rotation angles in Fig. 1.6a are:

$$\phi_n = \frac{\tilde{\eta}_n}{d_n} (\cot \alpha_n + \cot \alpha_{n+1}) \quad \text{for } n = 1, 3, \quad (1.61)$$

$$\phi_n = \frac{1}{d_n} (\tilde{\eta}_{n-1} \operatorname{cosec} \alpha_n + \tilde{\eta}_n \operatorname{cosec} \alpha_{n+1}) \quad \text{for } n = 2, 4.$$

Switching the even and odd numbers in Eq. (1.61) gives the expressions for  $\psi_n$  in Fig. 1.6b.

Using expressions of  $\phi_n$  and  $\psi_n$ , Eq. (1.60) will be

$$\tilde{\xi}_n = \tilde{\lambda}_n \tilde{\theta},$$

where

$$\tilde{\lambda}_n = (\tilde{\rho}_{n-1} \operatorname{cosec} \alpha_n + \tilde{\rho}_n \cot \alpha_n)(1 - \bar{s}_n) - (\tilde{\rho}_n \cot \alpha_{n+1} + \tilde{\rho}_{n+1} \operatorname{cosec} \alpha_{n+1}) \bar{s}_n \quad (1.62)$$

with  $\bar{s}_n = s_n/d_n$ .

With the transformation matrix

$$[T_n] = \begin{bmatrix} \sin \beta_n & \cos \beta_n \\ -\cos \beta_n & \sin \beta_n \end{bmatrix}, \quad (1.63)$$

we obtain from  $\xi_n, \eta_n$  the displacements  $\tilde{u}_n, \tilde{v}_n$  in  $x, y$  directions:

$$\begin{Bmatrix} \tilde{u}_n \\ \tilde{v}_n \end{Bmatrix} = [T_n] \begin{Bmatrix} \tilde{\xi}_n \\ \tilde{\eta}_n \end{Bmatrix}, \quad (1.64)$$

or

$$\begin{Bmatrix} \tilde{u}_n \\ \tilde{v}_n \end{Bmatrix} = - \begin{Bmatrix} \tilde{r}_{un} \\ \tilde{r}_{vn} \end{Bmatrix} \tilde{\theta}, \quad (1.65)$$

where

$$\begin{Bmatrix} \tilde{r}_{un} \\ \tilde{r}_{vn} \end{Bmatrix} = - [T_n] \begin{Bmatrix} \tilde{\lambda}_n \\ \tilde{\rho}_n \end{Bmatrix}.$$

For a symmetrical trapezoidal box section, as shown in Fig. 1.7,

$$v = \frac{d_3 - 2j_1 \cot \beta}{d_1 + 2j_1 \cot \beta}, \quad j_1 = (h_1 + y_N), \quad (1.66)$$

$$\tilde{u}(x, y, z) = -(y - y_N) \tilde{\theta}(z) = -\tilde{y} \tilde{\theta}, \quad (1.67)$$

$$\tilde{v}(x, y, z) = -\tilde{r}_v \tilde{\theta},$$

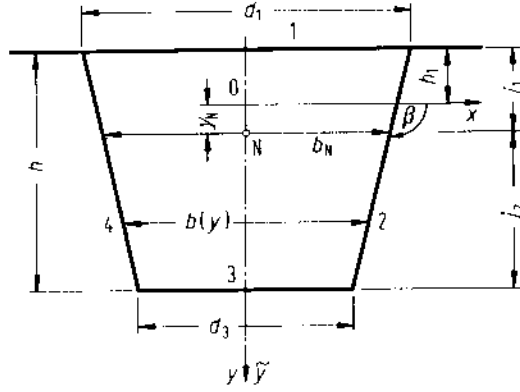


Fig. 1.7. Symmetrical trapezoidal box section

where

$$\tilde{r}_v = (vb_N - 2(y - y_N) \cot \beta) \frac{x}{b(y)}$$

and  $y_N$  referring to Eq. (1.58).

For a symmetrical rectangular box section,  $v = 1$  and

$$\begin{aligned} \tilde{u}(x, y, z) &= -(y - y_N)\tilde{\theta}(z), \\ \tilde{v}(x, y, z) &= -x\tilde{\theta}(z). \end{aligned} \tag{1.68}$$

### 1.4.3 Shear Rigidity and Distortion Rigidity of a Box Section

Let us consider a box section of unit length rigidly connected at the corners. Assuming that the section is supported at both lower corners and subjected to a unit force  $H_1 = 1$  causing a displacement  $\tilde{\eta}_1$ , as shown in Fig. 1.8, the distortion

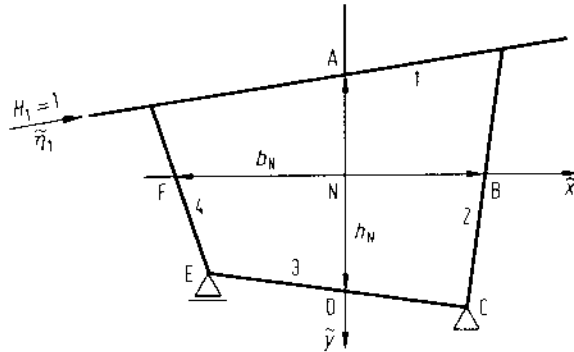


Fig. 1.8. Mechanical model of a box section for determining its shear rigidity and distortion rigidity



defined in Eq. (1.51) is

$$\tilde{\gamma} = \frac{u_A}{h_N} - \frac{1}{b_N}(v_B - v_F).$$

Using the equations in the preceding section, we have

$$\tilde{\gamma} = \frac{\tilde{\eta}_1}{h_i}, \quad (1.69)$$

where

$$\begin{aligned} h_i &= \frac{h_N}{\mu}, \\ \mu &= \cos \beta_1 - [(1 - \bar{s}_{1A}) \cot \alpha_1 - \bar{s}_{1A} \cot \alpha_2] \sin \beta_1 \\ &\quad - \frac{h_N}{b_N} \{ (1 - \bar{s}_{2B})(\cot \alpha_2 \cos \beta_1 - \sin \beta_1) \\ &\quad + \bar{s}_{4F}(\cot \alpha_1 \cos \beta_1 + \sin \beta_1) \}. \end{aligned} \quad (1.70)$$

For a symmetrical trapezoidal box section as shown in Fig. 1.7,

$$\mu = 1 - \frac{2j_2}{b_N} \cot \alpha_1. \quad (1.71)$$

For a rectangular box,  $\mu = 1$ .

The force  $H$  or the moment  $Hh_i$  causing unit distortion  $\tilde{\gamma} = 1$  is defined as shear rigidity  $R$  or distortion rigidity  $K$ . It can, therefore, be given in the following form:

$$R = \frac{1}{\tilde{\gamma}_1} = \frac{h_i}{\tilde{\eta}_1}, \quad (1.72)$$

$$K = Rh_i = \frac{h_i^2}{\tilde{\eta}_1}, \quad (1.73)$$

where  $\tilde{\eta}_1$  induced by unit force  $H_1 = 1$  can be determined according to methods known in structural theory.

## 1.4.4 Stresses and Stress Resultants

### 1.4.4.1 Normal Stresses and Stress Resultants

The normal stress induced by torsion and distortion can be calculated from the warping given in Eqs. (1.31) and (1.52). Thus,

$$\sigma = E\varepsilon = Ew' = -E\omega\theta'' - E\tilde{\omega}\theta'' = \sigma_\omega + \sigma_{\tilde{\omega}}. \quad (1.74a)$$

Since both principal coordinates  $\omega(s)$  and  $\tilde{\omega}(s)$  are nonorthogonal, we define the bimoments, different from Eq. (1.34), as follows:

$$M_{\omega} = \int_F \omega \sigma_{\omega} dF = -D_{\omega\omega} \theta'' , \quad (1.75a)$$

$$\tilde{M}_{\tilde{\omega}} = \int_F \tilde{\omega} \sigma_{\tilde{\omega}} dF = -D_{\tilde{\omega}\tilde{\omega}} \theta'' . \quad (1.75b)$$

Using these equations, the normal stress can be written

$$\sigma = \frac{M_{\omega}}{F_{\omega\omega}} \omega + \frac{\tilde{M}_{\tilde{\omega}}}{F_{\tilde{\omega}\tilde{\omega}}} \tilde{\omega} . \quad (1.74b)$$

#### 1.4.4.2 Shear Stresses and Stress Resultants

In a closed section, the shear stress  $\tau_c$  caused by pure torsion is given in Eqs. (1.1) and (1.2), while that induced by the normal stress  $\sigma$  can be determined as shown in Eqs. (1.37a) or (1.37b) and (1.36). We have here

$$\tau = \frac{E}{t} \{ \theta''' S_{\omega}(s) + \tilde{\theta}''' S_{\tilde{\omega}}(s) \} , \quad (1.76)$$

or

$$\tau = -\frac{1}{t} \left\{ \frac{T_{\omega}}{F_{\omega\omega}} S_{\omega}(s) + \frac{T_{\tilde{\omega}}}{F_{\tilde{\omega}\tilde{\omega}}} S_{\tilde{\omega}}(s) \right\} ,$$

and the moments

$$\begin{aligned} T_{\omega} &= M'_{\omega} , \\ \tilde{T}_{\tilde{\omega}} &= \tilde{M}'_{\tilde{\omega}} . \end{aligned} \quad (1.77)$$

#### 1.4.5 Strain Energy

The strain energy consists of three parts, induced by normal strain  $\epsilon$ , shear strain  $\gamma_c$  of pure torsion, and distortion  $\tilde{\gamma}_N$ :

$$U_c = \frac{1}{2} \int_l \int_F (E\epsilon^2 + G\gamma_c^2) dF dz + \frac{1}{2} \int_l K \tilde{\gamma}_N^2 dz . \quad (1.78)$$

Using  $\epsilon$ ,  $\tilde{\gamma}_N$ ,  $\gamma_c$  given in Eqs. (1.74a), (1.51), (1.2), we obtain

$$U_c = \frac{1}{2} \int_l \{ D_{\omega\omega} (\theta'')^2 + 2D_{\omega\tilde{\omega}} \theta'' \tilde{\theta}'' + D_{\tilde{\omega}\tilde{\omega}} (\tilde{\theta}'')^2 + C(\theta')^2 + \tilde{A} \tilde{\theta}^2 \} dz , \quad (1.79)$$

where

$$\tilde{A} = (1 + \nu)^2 K \quad (1.80)$$

#### 1.4.6 Potential of External Forces

The general expression for the potential of external forces  $q_x$ ,  $q_y$ ,  $q_z$  is given in Eq. (1.41). Using Eqs. (1.65), (1.52), (1.32), (1.9), we obtain

$$U_p = - \int_l (m_z \theta + \tilde{m}_z \tilde{\theta} - m_{\omega} \theta' - m_{\tilde{\omega}} \tilde{\theta}') dz, \quad (1.81)$$

where  $m_z$  and  $m_{\omega}$  are defined in Eq. (1.42), and

$$\begin{aligned} \tilde{m}_z &= - \sum_n \iint (\tilde{r}_{vn} q_y + \tilde{r}_{un} q_x) dx dy, \\ m_{\tilde{\omega}} &= \iint \tilde{\omega} q_z dx dy. \end{aligned} \quad (1.82)$$

### 1.4.7 Differential Equations and Boundary Conditions

The differential equations and boundary conditions for torsion and distortion can be derived in the same way as in Sects. 1.3.5 and 1.3.6. The result is

$$\begin{aligned} (D_{\omega\omega} \theta'')' - (C\theta')' + (D_{\omega\tilde{\omega}} \tilde{\theta}'')' &= m_z + m'_{\omega}, \\ (D_{\omega\tilde{\omega}} \theta'')' + (D_{\tilde{\omega}\tilde{\omega}} \tilde{\theta}'')' + \tilde{A}\tilde{\theta} &= \tilde{m}_z + m'_{\tilde{\omega}}, \end{aligned} \quad (1.83)$$

with the boundary conditions

$$\begin{aligned} [(D_{\omega\omega} \theta'' + D_{\omega\tilde{\omega}} \tilde{\theta}'') \delta\theta'] &= 0, \\ [\{(D_{\omega\omega} \theta'' - C\theta' + (D_{\omega\tilde{\omega}} \tilde{\theta}'')') \} \delta\theta] &= 0, \\ [(D_{\omega\tilde{\omega}} \theta'' + D_{\tilde{\omega}\tilde{\omega}} \tilde{\theta}'') \delta\tilde{\theta}'] &= 0, \\ [\{(D_{\omega\tilde{\omega}} \theta'' + (D_{\tilde{\omega}\tilde{\omega}} \tilde{\theta}'')') \} \delta\tilde{\theta}] &= 0. \end{aligned} \quad (1.84)$$

See the discussions after Eqs. (1.50) for the meaning of the boundary conditions.

As mentioned previously, the angle of twist  $\theta(z)$  and the distortion of section  $\tilde{\theta}(z)$  are coupled with each other, in both differential equations and boundary conditions. However, the mutual influence is usually insignificant, so that the torsion and the distortion may also be analyzed separately, by neglecting the linking terms containing  $D_{\omega\tilde{\omega}}$  in Eqs. (1.83) and (1.84).

## 1.5 Torsion of a Box Girder Considering Shear Strain

The influence of shear strain on bending and torsion will usually be neglected, as was done in Sect. 1.3. However, for a box girder this may yield incorrect values of torsional warping stresses at sections and fixed ends where concentrated torques are acting.

In the following we will introduce an extended torsion theory taking the influence of shear strain into account, which was mainly developed by Dshanelidze and Panovko (1948). It is based on two displacement functions, similar to the extended bending theory given by Timoshenko (1921). See also Hu (1981).

### 1.5.1 Basic Equations

The shear strain  $\gamma_w$  in a box girder induced by the shear stress due to torsional warping is coupled with that caused by pure torsion, and will produce an additional warping of the cross section. Assuming that this has the same shape as  $\omega$ , the total warping of torsion is

$$w(z, s) = -\omega(\theta' + \gamma_w), \quad (1.85)$$

and

$$\varepsilon = w' = -\omega(\theta'' + \gamma_w'). \quad (1.86)$$

Using Eqs. (1.85) and (1.30) and  $\eta = \rho_M \theta$ , we have the shear strain

$$\begin{aligned} \gamma &= \frac{\partial w}{\partial s} + \frac{\partial \eta}{\partial z} \\ &= -\left(\rho_M - \frac{\psi}{t}\right)(\theta' + \gamma_w) + \rho_M \theta', \end{aligned}$$

or

$$\gamma = \frac{\psi}{t} \theta' - \left(\rho_M - \frac{\psi}{t}\right) \gamma_w. \quad (1.87)$$

### 1.5.2 Potentials of Internal and External Forces

The potential of internal forces or the strain energy according to Eq. (1.39) can be evaluated with  $\varepsilon$  and  $\gamma$  from Eqs. (1.86) and (1.87). Considering

$$\oint \left(\rho_M \frac{\psi}{t}\right) t ds = \oint \left(\frac{\psi}{t}\right)^2 t ds = I_d, \quad (1.88a)$$

$$\int_F \rho_M^2 dF = I_p, \quad (1.88b)$$

the result is

$$U_e = -\frac{1}{2} \int \{M_\omega(\theta'' + \gamma_w') - T\theta' - T_\gamma \gamma_w\} dz, \quad (1.89)$$

where

$$\begin{aligned} M_\omega &= -D_{\omega\omega}(\theta'' + \gamma_w'), \\ T_\gamma &= C_\gamma \gamma_w, \\ C_\gamma &= C_p - C = GI_p - GI_d, \end{aligned} \quad (1.90)$$

and  $D_{\omega\omega}$  is given in Eq. (1.21).

The potential of external forces can be deduced from Eq. (1.43):

$$U_p = -\int \{m_z \theta - m_\omega(\theta' + \gamma_w)\} dz. \quad (1.91)$$

### 1.5.3 Differential Equations

With  $U_e$  and  $U_p$  given in Eqs. (1.89) and (1.91), the equilibrium equation (1.44) yields two differential equations and boundary conditions for  $\theta(z)$  and  $\gamma_w(z)$ . The differential equations are:

$$(D_{\omega\omega}(\theta'' + \gamma_w'))' - (C\theta')' = m_z + m'_\omega, \quad (1.92a)$$

$$(D_{\omega\omega}(\theta'' + \gamma_w'))' - C_\gamma \gamma_w = m_\omega. \quad (1.92b)$$

Differentiating the second equation and then subtracting it from the first, we obtain for constant cross section

$$\gamma_w' = \frac{1}{C_\gamma} (C\theta'' + m_z), \quad (1.93)$$

Substituting this into Eq. (1.92b), we obtain

$$\gamma_w = \frac{D_{\omega\omega}}{C_\gamma^2} (C_p \theta''' + m_z') - \frac{1}{C_\gamma} m_\omega. \quad (1.94)$$

After substituting  $\gamma_w$  into Eq. (1.92a), we have

$$D_{\omega\omega}^* \theta^{IV} - C\theta'' = m_z + m'_\omega - m_z^*, \quad (1.95)$$

where

$$D_{\omega\omega}^* = \frac{C_p}{C_\gamma} D_{\omega\omega} = \frac{I_p}{I_p - I_d} D_{\omega\omega} = v_\gamma D_{\omega\omega} \quad (1.96)$$

$$m_z^* = \frac{D_{\omega\omega}}{C_\gamma} m_z. \quad (1.97)$$

Comparing Eq. (1.95) with Eq. (1.49c), it can be seen that the influence of the shear strain  $\gamma_w$  leads mainly to a modification of the warping torsional rigidity from  $D_{\omega\omega}$  to  $D_{\omega\omega}^*$ . This is also true for evaluating the bimoment, since substituting  $\gamma_w'$  from Eq. (1.93) into Eq. (1.86) for  $\varepsilon$  yields, according to Eq. (1.34c),

$$M_\omega = -D_{\omega\omega}^* \theta'' + m_z^*. \quad (1.98)$$

The boundary conditions for integrating differential equation (1.95) are the same as given in Eq. (1.50c).

## 2. Stress Analysis of Straight Box Girders

The bending and torsion theories of box girders with deformable cross-section were presented in Chap. 1. The solution to the differential equations of bending of straight box girders and the stresses due to bending can be obtained according to the general beam theory. The stresses due to warping torsion and distortion of the cross-section can be evaluated by first solving the displacement differential equations and then using the formulas for the stresses.

Equation (1.83) can be solved by converting it into a differential equation with one variable and its higher derivatives or a set of differential equations in terms of multiple variables and their first derivatives. However, by either one of the two ways we will encounter difficulty in satisfying the accuracy requirement when one large number is subtracted from the other. For a general box girder in practice, it is thus very difficult to obtain the stresses due to warping torsion and distortion of cross-section by solving Eq. (1.83) directly.

At the beginning of this chapter a procedure is described through which the displacements and stresses caused by torsion of straight box girders are evaluated by the finite beam element method. From the analyses of specific examples using this method, it turns out that the coupling term of torsional and distortional warping has little effect on the displacements and stresses. Without consideration of the coupling effect the problem of warping torsion and distortion of straight box girders has already been solved, and the results are briefly presented here. Finally, a discussion about the effects of warping torsion and distortion is given along with a numerical example.

### 2.1 Finite Beam Element Method

#### 2.1.1 Assumptions on the Nodal Displacement Parameters and the Displacement Functions of Beam Elements

The shape of a beam element is shown in Fig. 2.1; its length is  $2\lambda$ . To satisfy the accuracy of normal stresses concerned, we take the angle of twist  $\theta$  and distortion  $\bar{\theta}$  as well as their first and second derivatives  $\theta'$ ,  $\theta''$ ,  $\bar{\theta}'$ ,  $\bar{\theta}''$  at ends  $i$  and  $j$  of the element as the nodal displacement parameters. Thus the nodal displacement parameter vector of an element is defined as

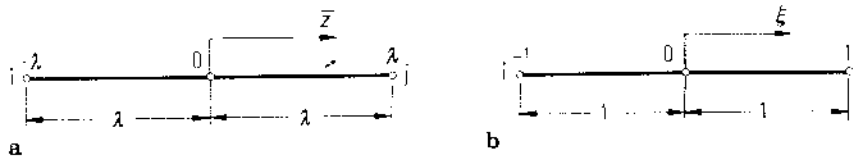


Fig. 2.1a,b. Beam element

$$\{\delta\}^e = \begin{Bmatrix} \delta_i \\ \delta_j \end{Bmatrix},$$

$$\{\delta_i\} = [\theta_i \ \theta_i' \ \theta_i'' \ \tilde{\theta}_i \ \tilde{\theta}_i' \ \tilde{\theta}_i'']^T,$$

$$\{\delta_j\} = [\theta_j \ \theta_j' \ \theta_j'' \ \tilde{\theta}_j \ \tilde{\theta}_j' \ \tilde{\theta}_j'']^T.$$

To ensure the continuities of  $\theta''$  and  $\tilde{\theta}''$  at the ends, we select quintic parabolic curves to interpolate various displacement components within the element, for example, for the angle of twist  $\theta$

$$\theta(\bar{z}) = a + b\bar{z} + c\bar{z}^2 + d\bar{z}^3 + e\bar{z}^4 + f\bar{z}^5, \quad (2.1)$$

in which coefficients  $a, b, c, d, e, f$  are determined by the following equations:

$$\bar{z} = -\lambda: \quad \theta(\bar{z}) = \theta_i, \quad \theta'(\bar{z}) = \theta_i', \quad \theta''(\bar{z}) = \theta_i'';$$

$$\bar{z} = \lambda: \quad \theta(\bar{z}) = \theta_j, \quad \theta'(\bar{z}) = \theta_j', \quad \theta''(\bar{z}) = \theta_j''.$$

The above six equations give a set of simultaneous equations. On solving and substituting into Eq. (2.1), we have

$$\{\delta\} = \begin{Bmatrix} \theta \\ \tilde{\theta} \end{Bmatrix} = [N] \{\delta\}^e, \quad (2.2)$$

where

$$[N] = \begin{bmatrix} N_1 & N_2 & N_3 & 0 & 0 & 0 & N_4 & N_5 & N_6 & 0 & 0 & 0 \\ 0 & 0 & 0 & N_1 & N_2 & N_3 & 0 & 0 & 0 & N_4 & N_5 & N_6 \end{bmatrix}, \quad (2.3)$$

in which

$$N_1 = \frac{1}{16}(8 - 15\xi + 10\xi^3 - 3\xi^5),$$

$$N_2 = \frac{1}{16}\lambda(5 - 7\xi + 6\xi^2 + 10\xi^3 + \xi^4 - 3\xi^5),$$

$$N_3 = \frac{1}{16}\lambda^2(1 - \xi - 2\xi^2 + 2\xi^3 + \xi^4 - \xi^5),$$

$$N_4 = \frac{1}{16}(8 + 15\xi - 10\xi^3 + 3\xi^5),$$

$$N_5 = \frac{1}{16}\lambda(-5 - 7\xi + 6\xi^2 + 10\xi^3 - \xi^4 - 3\xi^5),$$

$$N_6 = \frac{1}{16}\lambda^2(1 + \xi - 2\xi^2 - 2\xi^3 + \xi^4 + \xi^5),$$

with  $\xi = \bar{z}/\lambda$ .

### 2.1.2 Derivation of the Element Stiffness Matrix

Differential equations (1.83) can be rewritten in the form of

$$[D] \begin{Bmatrix} \theta^{(4)} \\ \tilde{\theta}^{(4)} \end{Bmatrix} - [C] \begin{Bmatrix} \theta^{(2)} \\ \tilde{\theta}^{(2)} \end{Bmatrix} + [A] \begin{Bmatrix} \theta \\ \tilde{\theta} \end{Bmatrix} = \{p\}, \quad (2.4)$$

where

$$[D] = \begin{bmatrix} D_{\omega\omega} & D_{\omega\tilde{\omega}} \\ D_{\omega\tilde{\omega}} & D_{\tilde{\omega}\tilde{\omega}} \end{bmatrix}, \quad [C] = \begin{bmatrix} C & 0 \\ 0 & 0 \end{bmatrix}, \quad [A] = \begin{bmatrix} 0 & 0 \\ 0 & \tilde{A} \end{bmatrix}, \quad \{p\} = \begin{bmatrix} m_z + m'_\omega \\ \tilde{m}_z + \tilde{m}'_{\tilde{\omega}} \end{bmatrix}.$$

Using the notation

$$[L] = [D]d^4 - [C]d^2 + [A] \text{ and } \{\delta\} = \begin{Bmatrix} \theta \\ \tilde{\theta} \end{Bmatrix},$$

differential equations (2.4) can be rewritten as

$$[L]\{\delta\} - \{p\} = 0, \quad (2.5)$$

where

$$d = d/dz.$$

Now we evaluate element stiffness matrices using the principle of virtual work. For the force system in equilibrium  $[L]\{\delta\} - \{p\} = 0$ , the total work done by the virtual displacements  $\{\delta^*\}$  within a box girder is the summation of that done within all the beam elements and is equal to zero, i.e.

$$\begin{aligned} A^* &= \int \{\delta^*\}^T ([L]\{\delta\} - \{p\}) dz \\ &= \sum_{i=1}^n \int_{z_i}^{z_{i+1}} \{\delta^*\}^T ([L]\{\delta\} - \{p\}) d\bar{z} = 0. \end{aligned} \quad (2.6)$$

Substituting  $\{\delta^*\} = [N]\{\delta^*\}^e$  into Eq. (2.6) gives

$$A^* = \sum_{i=1}^n \int_{z_i}^{z_{i+1}} ([N]\{\delta^*\}^e)^T ([L]\{\delta\} - \{p\}) d\bar{z} = 0, \quad (2.7)$$

i.e.,

$$A^* = \sum_{i=1}^n (\{\delta^*\}^e)^T \int_{z_i}^{z_{i+1}} ([N]^T [L] [N] \{\delta\}^e - [N]^T \{p\}) d\bar{z} = 0. \quad (2.8)$$

As Eqs. (2.8) are true for arbitrary nodal virtual displacements  $\{\delta^*\}^e$ , thus we have to hold

$$\int_{z_i}^{z_{i+1}} ([N]^T [L] [N] \{\delta\}^e - [N]^T \{p\}) d\bar{z} = 0, \quad (2.9)$$

in which each equation is in fact the statement of the equilibrium in each nodal generalized displacement direction. The nodal elastic force vector of an element and the equivalent load vector (i.e., the element load vector) are of the forms

$$\{F\}^e = [K]_e \{\delta\}^e, \quad (2.10)$$

and



$$\{F\}_p^e = \int_0^e [N]^T \{p\} d\bar{z}, \quad (2.11)$$

respectively in which

$$\begin{aligned} [K]_e &= \int_0^e [N]^T [L] [N] d\bar{z} \\ &= \int_0^e [N]^T [D] [N^{(4)}] d\bar{z} - \int_0^e [N]^T [C] [N''] d\bar{z} \\ &\quad + \int_0^e [N]^T [A] [N] d\bar{z}. \end{aligned}$$

Using integration by parts, we have

$$\begin{aligned} \int_0^e [N]^T [D] [N^{(4)}] d\bar{z} &= [N]^T [D] [N''']|_e \\ &\quad - [N']^T [D] [N'']|_e + \int_0^e [N'']^T [D] [N''] d\bar{z}, \quad (2.12) \end{aligned}$$

and

$$\begin{aligned} \int_0^e [N]^T [C] [N''] d\bar{z} &= [N] [C] [N']|_e \\ &\quad - \int_0^e [N']^T [C] [N'] d\bar{z}, \quad (2.13) \end{aligned}$$

The first and second terms of the right-hand side of Eq. (2.12) and the first term of Eq. (2.13) are boundary values (forces). With reference to Eq. (2.6) it can be found that these values cancel at the nodes between two adjacent elements and can be treated at the boundaries by imposing boundary conditions. Thus, without consideration of the terms just mentioned, we can write  $[k]$  in the form of

$$[K]_e = [K_D] + [K_C] + [K_A], \quad (2.14)$$

in which

$$\begin{aligned} [K_D] &= \lambda \int_{-1}^1 [N'']^T [D] [N''] d\xi, \\ [K_C] &= \lambda \int_{-1}^1 [N']^T [C] [N'] d\xi, \end{aligned}$$

and

$$[K_A] = \lambda \int_{-1}^1 [N]^T [A] [N] d\xi,$$

where

$$\begin{aligned} [K_D] &= \begin{bmatrix} D_{\omega\omega}[A_1] & D_{\omega\bar{\omega}}[A_1] & D_{\omega\omega}[A_2] & D_{\omega\bar{\omega}}[A_2] \\ & D_{\bar{\omega}\bar{\omega}}[A_1] & D_{\bar{\omega}\bar{\omega}}[A_2] & D_{\bar{\omega}\bar{\omega}}[A_2] \\ & & D_{\omega\bar{\omega}}[A_3] & D_{\omega\bar{\omega}}[A_3] \\ & \text{symmetry} & & D_{\bar{\omega}\bar{\omega}}[A_3] \end{bmatrix}, \\ [K_C] &= \begin{bmatrix} C[B_1] & 0 & C[B_2] & 0 \\ & 0 & 0 & 0 \\ & & C[B_3] & 0 \\ & \text{symmetry} & & 0 \end{bmatrix}, \end{aligned}$$

and

$$[K_{\lambda}] = \begin{bmatrix} 0 & 0 & 0 & 0 \\ \tilde{A}[C_1] & 0 & \tilde{A}[C_2] & \\ & 0 & 0 & \\ \text{symmetry} & & \tilde{A}[C_3] & \end{bmatrix},$$

in which  $[A_1]$ ,  $[A_2]$ ,  $[A_3]$ ,  $[B_1]$ ,  $[B_2]$ ,  $[B_3]$ ,  $[C_1]$ ,  $[C_2]$ ,  $[C_3]$  are  $3 \times 3$  square matrices and are given as

$$[A_1] = \frac{1}{\lambda^3} \begin{bmatrix} \frac{15}{7} & \frac{15}{7}\lambda & \frac{3}{14}\lambda^2 \\ \frac{15}{7}\lambda & \frac{96}{35}\lambda^2 & \frac{11}{35}\lambda^3 \\ \frac{3}{14}\lambda^2 & \frac{11}{35}\lambda^3 & \frac{6}{35}\lambda^4 \end{bmatrix},$$

$$[A_2] = \frac{1}{\lambda^3} \begin{bmatrix} -\frac{15}{7} & \frac{15}{7}\lambda & -\frac{3}{14}\lambda^2 \\ -\frac{15}{7}\lambda & \frac{54}{35}\lambda^2 & -\frac{4}{35}\lambda^3 \\ -\frac{3}{14}\lambda^2 & \frac{4}{35}\lambda^3 & \frac{1}{35}\lambda^4 \end{bmatrix},$$

$$[A_3] = \frac{1}{\lambda^3} \begin{bmatrix} \frac{15}{7} & -\frac{15}{7}\lambda & \frac{3}{14}\lambda^2 \\ -\frac{15}{7}\lambda & \frac{96}{35}\lambda^2 & -\frac{11}{35}\lambda^3 \\ \frac{3}{14}\lambda^2 & -\frac{11}{35}\lambda^3 & \frac{6}{35}\lambda^4 \end{bmatrix},$$

$$[B_1] = \frac{1}{\lambda} \begin{bmatrix} \frac{15}{21} & \frac{3}{14}\lambda & \frac{1}{42}\lambda^2 \\ \frac{3}{14}\lambda & \frac{16}{35}\lambda^2 & \frac{1}{15}\lambda^3 \\ \frac{1}{42}\lambda^2 & \frac{1}{15}\lambda^3 & \frac{4}{315}\lambda^4 \end{bmatrix},$$

$$[B_2] = \frac{1}{\lambda} \begin{bmatrix} -\frac{15}{21} & \frac{3}{14}\lambda & -\frac{1}{42}\lambda^2 \\ -\frac{3}{14}\lambda & -\frac{1}{35}\lambda^2 & \frac{2}{105}\lambda^3 \\ -\frac{1}{42}\lambda^2 & -\frac{2}{105}\lambda^3 & \frac{2}{315}\lambda^4 \end{bmatrix},$$

$$[B_3] = \frac{1}{\lambda} \begin{bmatrix} \frac{15}{21} & -\frac{3}{14}\lambda & \frac{1}{42}\lambda^2 \\ -\frac{3}{14}\lambda & \frac{16}{35}\lambda^2 & -\frac{1}{15}\lambda^3 \\ \frac{1}{42}\lambda^2 & -\frac{1}{15}\lambda^3 & \frac{4}{315}\lambda^4 \end{bmatrix},$$

$$[C_1] = \lambda \begin{bmatrix} \frac{181}{231} & \frac{311}{1155}\lambda & \frac{281}{6930}\lambda^2 \\ \frac{311}{1155}\lambda & \frac{416}{3465}\lambda^2 & \frac{69}{3465}\lambda^3 \\ \frac{281}{6930}\lambda^2 & \frac{69}{3465}\lambda^3 & \frac{4}{1155}\lambda^4 \end{bmatrix},$$

$$[C_2] = \lambda \begin{bmatrix} \frac{60}{231} & -\frac{151}{1155}\lambda & \frac{181}{6930}\lambda^2 \\ \frac{151}{1155}\lambda & -\frac{266}{3465}\lambda^2 & \frac{52}{3465}\lambda^3 \\ \frac{181}{6930}\lambda^2 & -\frac{52}{3465}\lambda^3 & \frac{2}{693}\lambda^4 \end{bmatrix},$$

$$[C_3] = \lambda \begin{bmatrix} -\frac{181}{231} & -\frac{311}{1155}\lambda & \frac{281}{6930}\lambda^2 \\ -\frac{311}{1155}\lambda & \frac{416}{3465}\lambda^2 & -\frac{69}{3465}\lambda^3 \\ \frac{281}{6930}\lambda^2 & -\frac{69}{3465}\lambda^3 & \frac{4}{1155}\lambda^4 \end{bmatrix}.$$

### 2.1.3 Derivation of the Element Load Vector

The element load vector is of the form

$$\{F\}_p^e = \int_0^e [N]^T \{p\} dz \quad (2.15)$$

from which we can evaluate element load vectors. Two types of element load vectors are presented here for (a) a concentrated load applied at the left end of element and (b) loads uniformly distributed on a whole element; they are:

$$\{F\}_p^e = \begin{bmatrix} a_i \\ a_j \end{bmatrix} \begin{Bmatrix} (m_z + m'_\omega) \\ (i\tilde{m}_z + \tilde{m}'_\omega) \end{Bmatrix}. \quad (2.16)$$

Case (a)

$$[a_i] = \begin{bmatrix} 1 \\ 0 & 0 \\ 0 \\ & 1 \\ 0 & 0 \\ & 0 \end{bmatrix}, \quad [a_j] = [0]; \quad (2.17a)$$

Case (b)

$$[a_i] = \begin{bmatrix} \lambda \\ \frac{2}{5}\lambda^2 & 0 \\ \frac{1}{15}\lambda^3 & \\ & \lambda \\ 0 & \frac{2}{5}\lambda^2 \\ & \frac{1}{15}\lambda^3 \end{bmatrix}, \quad [a_j] = -[a_i(-\lambda)]. \quad (2.17b)$$

### 2.1.4 Formation of the Structure Stiffness Matrix

Assume the element stiffness matrix is in the form of

$$[K]_e = \begin{bmatrix} K_{ii}^e & K_{ij}^e \\ K_{ji}^e & K_{jj}^e \end{bmatrix} \quad (2.18)$$

and the element load vector

$$\{F\}_p^e = \begin{Bmatrix} F_i \\ F_j \end{Bmatrix}, \quad (2.19)$$

where  $[K_{ii}]^e$ ,  $[K_{ij}]^e$ ,  $[K_{ji}]^e$ ,  $[K_{jj}]^e$  are  $6 \times 6$  square matrices and  $\{F_i\}$ ,  $\{F_j\}$  are column vectors of order 6.

Since only two elements are connected at each node, the equilibrium conditions at any node  $r$  in the girder can be written as

$$\begin{aligned}
& [K_{jj}]_{(r-1)}^e \{\delta_{r-1}\} + ([K_{jj}]_{(r-1)}^e + [K_{ii}]_{(r)}^e) \{\delta_r\} + [K_{ij}]_{(r)}^e \{\delta_{r+1}\} \\
& = \{F_j\}_{(r-1)} + \{F_i\}_{(r)}, \quad (2.20)
\end{aligned}$$

in which subscripts  $r - 1$  and  $r$  of the submatrices in the element stiffness matrix and element load vector refer to the element to the left of node  $r$  and the element to the right, respectively;  $\{\delta_{r-1}\}$ ,  $\{\delta_r\}$ , and  $\{\delta_{r+1}\}$  denote the displacement vectors of nodes  $r - 1$ ,  $r$ , and  $r + 1$  in turn.

By assembling all the above nodal equilibrium equations, we get a set of linear algebraic equations in terms of nodal displacements,

$$[K] \{\delta\} = \{F\}_p, \quad (2.21)$$

in which  $[K]$  is the structure stiffness matrix,  $\{F\}_p$  is the structure load vector, and  $\{\delta\}$  is the structure displacement vector.

### 2.1.5 Boundary Conditions

Before imposing boundary conditions to Eqs. (2.21) we are unable to solve the set of equations in a normal way because the matrix  $[K]$  is singular. Boundary conditions depend on the support conditions of the structure, and two types of boundary conditions for two different supports are as follows.

At a fixed support, there is neither the displacements of the cross-section in the vertical, transverse, and longitudinal directions, nor the rotation and distortion of the cross-section, thus the boundary conditions can be expressed as

$$\begin{aligned}
[\theta] &= 0, & [\tilde{\theta}] &= 0; \\
[\theta'] &= 0, & [\tilde{\theta}'] &= 0.
\end{aligned} \quad (2.22)$$

At a simple support, the cross-section is not permitted to move in the vertical and transverse directions, to rotate, and or to be distorted, but it can be freely warped, owing to the existing diaphragms with infinite rigidity in-plane while zero out-plane. Hence, the boundary conditions can be formulated as

$$\begin{aligned}
[\theta] &= 0, & [\tilde{\theta}] &= 0; \\
[\theta''] &= 0, & [\tilde{\theta}'] &= 0.
\end{aligned} \quad (2.23)$$

The same is true at the nodes where a rigid intermediate diaphragm is provided. For elastic intermediate diaphragms at nodes we can easily consider their effect in stiffness matrix by taking their virtual work into account.

### 2.1.6 Evaluation of Displacements and Stresses

By solving the set of linear equations for the equilibrium of the structure, we can obtain angle of twist  $\theta$  and distortion  $\tilde{\theta}$  of cross-sections as well as their first and second derivatives  $\theta'$ ,  $\theta''$ ,  $\tilde{\theta}'$ , and  $\tilde{\theta}''$ . Then the normal stresses due to warping torsion and distortion of cross-section at any specified section can be evaluated according

to Eqs. (1.74b) and (1.75):

$$\sigma = \sigma_{\omega} + \sigma_{\tilde{\omega}} = \frac{M_{\omega}}{F_{\omega\omega}} \omega + \frac{\tilde{M}_{\tilde{\omega}}}{F_{\tilde{\omega}\tilde{\omega}}} \tilde{\omega},$$

where  $M_{\omega} = -D_{\omega\omega}\theta''$ ,  $\tilde{M}_{\tilde{\omega}} = -D_{\tilde{\omega}\tilde{\omega}}\tilde{\theta}''$ , that is

$$\sigma = -E(\theta''\omega + \tilde{\theta}''\tilde{\omega}). \quad (2.24)$$

## 2.2 Analytical Method

Results from specific numerical examples by the finite beam element method reveal that the coupling term  $D_{\omega\tilde{\omega}}$  in the equations

$$\begin{aligned} D_{\omega\omega}\theta^{(4)} + D_{\omega\tilde{\omega}}\tilde{\theta}^{(4)} - C\theta^{(2)} &= m_z + m'_{\omega}, \\ D_{\omega\tilde{\omega}}\theta^{(4)} + D_{\tilde{\omega}\tilde{\omega}}\tilde{\theta}^{(4)} + \tilde{A}\tilde{\theta} &= \tilde{m}_z + \tilde{m}'_{\tilde{\omega}} \end{aligned}$$

has little effect on the final results (for  $\theta$ ,  $\tilde{\theta}$ , the effect is generally less than 5%) and is negligible. Thus, the set of differential equations are converted into two independent equations:

$$\begin{aligned} D_{\omega\omega}\theta^{(4)} - C\theta^{(2)} &= m_z + m'_{\omega}, \\ D_{\tilde{\omega}\tilde{\omega}}\tilde{\theta}^{(4)} + \tilde{A}\tilde{\theta} &= \tilde{m}_z + \tilde{m}'_{\tilde{\omega}}. \end{aligned} \quad (2.25)$$

That is to say, the problem of warping torsion of box girders with deformable cross-section is simplified into two independent problems: warping torsion of box girders with rigid cross-section and distortion of box girders with deformable cross-section. In the case of constant cross-section, the two differential equations can be solved easily, and analytical solutions to them are given in the next section.

### 2.2.1 Analytical Solution for a Single-span Girder

We rewrite the first equation of Eqs. (2.25) as

$$\theta^{(4)} - \frac{C}{D_{\omega\omega}}\theta'' = (m_z + m'_{\omega})/D_{\omega\omega}. \quad (2.26)$$

Denoting  $\lambda = \sqrt{C/D_{\omega\omega}}$ , gives

$$\theta^{(4)} - \lambda^2\theta'' = (m_z + m'_{\omega})/D_{\omega\omega}. \quad (2.27)$$

The characteristic equation is

$$r^2(r^2 - \lambda^2) = 0, \quad (2.28)$$

with roots  $r_1, r_2 = 0, r_3 = \lambda, r_4 = -\lambda$ .

Hence, the homogeneous solution to Eq. (2.26) is

$$\theta = C_1 + C_2z + C_3e^{\lambda z} + C_4e^{-\lambda z}$$

Furthermore, the general solution of Eq. (2.26) can be written in the form of

$$\theta = C_1 + C_2 z + C_3 e^{\lambda z} + C_4 e^{-\lambda z} + \theta_p. \quad (2.29)$$

If the exponential terms in the above equation are written in the form of hyperbolic functions, then Eq. (2.29) becomes

$$\theta = C_1 + C_2 z + C_3 \cdot \cosh \lambda z + C_4 \cdot \sinh \lambda z + \theta_p, \quad (2.30)$$

in which coefficients  $C_1, C_2, C_3, C_4$  are constants and can be determined by boundary conditions.

For a single-span girder, solutions for various boundary conditions and various forms of loads have already been developed and can be applied.

## 2.2.2 Treatment of a Continuous Girder

For the problem of warping torsion of continuous girders, we can use the known solution to a single-span girder by analogy with the method of solving the planar bending problem of a continuous beam. We take a series of simply supported single-span girders as a fundamental structure system, as shown in Fig. 2.2, in which unknown redundant forces are the bimoments at the cross-sections on supports and apply the deformation compatibility conditions on the supports that the warping — the slope angle of twist  $\theta$  at adjacent cross-sections — is the same.

### Notations

$M_{k-1}, M_k, M_{k+1}$  the unknown bimoments at the cross-sections on supports  $k-1, k, k+1$ , respectively.

$\theta'_{k,m_l}$  — the slope of angle of twist  $\theta$  at support  $k$  caused by a unit bimoment applied at the left end of span  $m$  of the fundamental structure;

$\theta'_{k,m_r}$  — the slope of angle of twist  $\theta$  at support  $k$  caused by a unit bimoment applied at the right end of span  $m$  of the fundamental structure;

$\theta'_{k,n_l}$  — the slope of angle of twist  $\theta$  at support  $k$  caused by a unit bimoment applied at the left end of span  $n$ ;

$\theta'_{k,n_r}$  — the slope of angle of twist  $\theta$  at support  $k$  caused by a unit bimoment applied at the right end of span  $n$ ;

$\theta'_{k,p_l}, \theta'_{k,p_r}$  — the slopes of angle of twist  $\theta$  caused by load  $p$  applied within span  $m$  and span  $n$ , respectively.

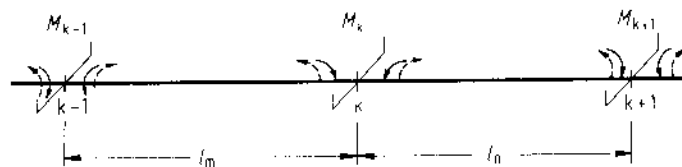


Fig. 2.2. Continuous girder

Using the deformation compatibility conditions, the relative warping caused by external load and redundant forces vanishes at any intermediate support  $k$ , i.e.

$$M_{k-1} \theta'_{k,m_1} + M_k (\theta'_{k,m_1} + \theta'_{k,n_1}) + M_{k+1} \theta'_{k,n_1} = -(\theta'_{k,p_m} + \theta'_{k,p_n}) \quad (2.31)$$

in which  $k$  is the number of supports of the continuous girder and

$$\begin{aligned} \theta'_{k,m_1} &= \frac{1}{C_m l_m} \left( 1 - \frac{x_m}{\sinh x_m} \right), \\ \theta'_{k,m_1} &= \frac{1}{C_m l_m} (x_m \cdot \cosh x_m - 1), \\ \theta'_{k,n_1} &= \frac{1}{C_n l_n} (x_n \cdot \cosh x_n - 1), \\ \theta'_{k,n_1} &= \frac{1}{C_n l_n} \left( 1 - \frac{x_n}{\sinh x_n} \right), \end{aligned} \quad (2.32)$$

with

$$x_m = \sqrt{C_m/D_{\omega\omega m}} \times l_m \quad \text{and} \quad x_n = \sqrt{C_n/D_{\omega\omega n}} \times l_n. \quad (2.33)$$

Equations (2.32) can be calculated from Eq. (2.30) in which  $\theta_p$  is the special solution for the case of a unit bimoment applied at the end of the girder.

For every intermediate support we can write an equation similar to Eq. (2.31), and thus a set of equations is established. After solving the equations, the unknown redundant forces, i.e., the bimoments at intermediate supports, are obtained. Thus the continuous girder can be analyzed according to the existing formulas for single-span girders.

### 2.2.3 Numerical Example

*Data:* dimensions of a cross-section of a steel box girder are indicated in Fig. 2.3; the span length  $l = 2400$  cm; uniform torque  $m_z = 1000$  N·m/m; the modulus of elasticity  $E = 2.06 \times 10^5$  MPa and modulus of shearing  $G = 7.848 \times 10^4$  MPa.

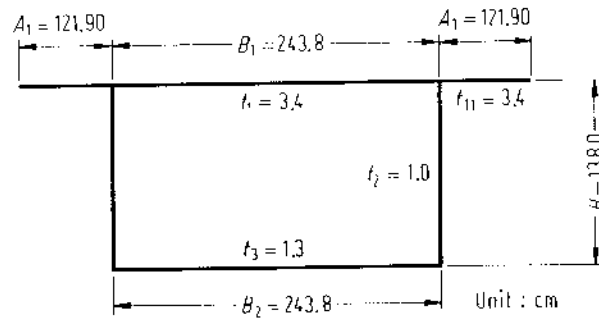


Fig. 2.3. Dimensions of a bridge cross section

The area of cross-section is

$$F = \sum F_i = 2250.78 \text{ cm}^2 .$$

The distance from the centroid to the top plate is

$$h_1 = \sum F_i \cdot y_i / F = 27.89 \text{ cm} .$$

The torsional rigidity is

$$\begin{aligned} C &= G \times [(B_1 + B_2) \times H]^2 / (B_1/t_1 + B_2/t_2 + 2 \times H/t_3) \\ &= 6.638 \times 10^{13} \text{ N} \cdot \text{cm}^2 , \\ \psi &= 2A/\oint (ds/t) = 125.71 \text{ cm}^2 . \end{aligned}$$

The sectorial coordinate is

$$\omega = \int_0^s \left( \rho_M - \frac{\psi}{t} \right) ds$$

shown in Fig. 2.4.

$$y_M = -\frac{F_{x\omega_0}}{F_{xx}} = 0.85 \text{ cm} ,$$

$$D_{\omega\omega} = EF_{\omega\omega} = E \int_F \omega^2 dF = 4.595 \times 10^{16} \text{ N} \cdot \text{cm}^4 .$$

For a box girder simply supported at two ends subject to uniform torsional moments, Eq. (2.30) is modified:

$$\theta = \frac{m_z}{C} \left[ \frac{z(l-z)}{2} - \frac{1}{\lambda^2} \left( 1 - \frac{\sinh \lambda z + \sinh \lambda(l-z)}{\sinh \lambda l} \right) \right] ,$$

in which  $\lambda = \sqrt{C/D_{\omega\omega}}$ . The values of  $\theta$ ,  $T_c$ ,  $M_\omega$ , and  $T_\omega$  are plotted in Figs. 2.5 to 2.8.

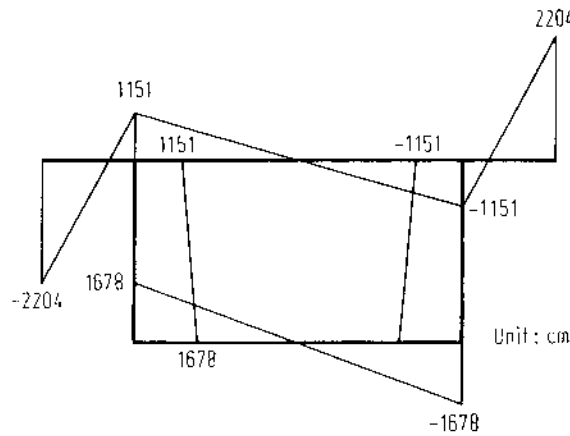
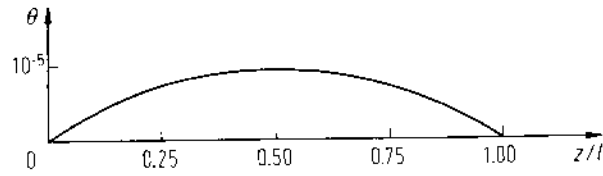
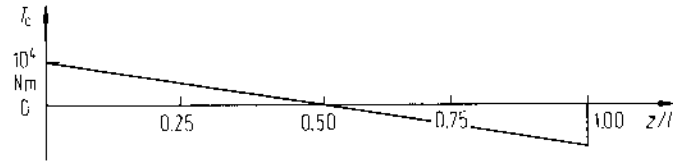
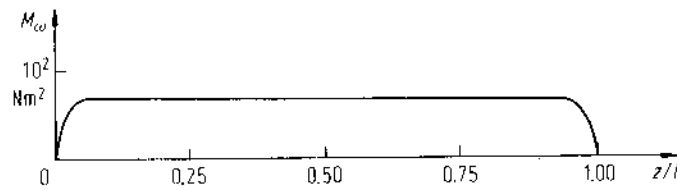
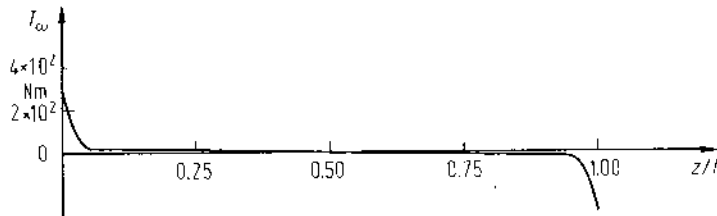


Fig. 2.4.  $\omega$  diagram of the cross section



Fig. 2.5. Angle of twist  $\theta$  as a function of  $z/l$ Fig. 2.6. Torque  $T_c$  as a function of  $z/l$ Fig. 2.7. Bimoment  $M_w$  as a function of  $z/l$ Fig. 2.8. Torque  $T_w$  as a function of  $z/l$ 

$$\theta = \frac{m_z}{C} \left[ \frac{z(l-z)}{2} - \frac{1}{\lambda^2} \left( 1 - \frac{\sinh \lambda z + \sinh \lambda(l-z)}{\sinh \lambda l} \right) \right],$$

$$T_c = C\theta' = m_z \left( \frac{l}{2} - z + \frac{1}{\lambda} \frac{\cosh \lambda z - \cosh \lambda(l-z)}{\sinh \lambda l} \right),$$

$$M_w = \frac{m_z}{\lambda^2} \left( 1 - \frac{\sinh \lambda z + \sinh \lambda(l-z)}{\sinh \lambda l} \right),$$

$$T_w = -\frac{m_z}{\lambda} \frac{\cosh \lambda z - \cosh \lambda(l-z)}{\sinh \lambda l},$$

$$\sigma_{\omega} = \frac{M_{\omega}}{F_{\omega\omega}} \cdot \omega, \quad F_{\omega\omega} = 2.230 \times 10^9 \text{ cm}^6,$$

in which  $\omega$  diagram is shown in Fig. 2.4. As an example, on the cross-section at the mid-span, the warping torsion stresses at the edges of top plate are  $\sigma_{\omega} = \pm 0.683 \text{ N/cm}^2$ , being quite small.

The shearing stresses due to pure torsion are of the form

$$\tau_{ci} = \frac{T_c}{2A} \cdot \frac{1}{t_i},$$

in which  $T_c$  is given in Fig. 2.6. As an example, shearing stresses on the cross-section at quarter point are calculated and given in Fig. 2.9.

The shearing stresses due to warping torsion can be calculated according to the form

$$(\tau_{\omega}) = -\frac{T_{\omega}}{F_{\omega\omega}} \left( F_{\omega} - \int \frac{F_{\omega}(ds/t)}{\int (ds/t)} \right) = -\frac{T_{\omega}}{F_{\omega\omega}} S_{\omega},$$

in which  $T_{\omega}$  can be seen in Fig. 2.8.

$$F_{\omega} = \int_0^s \omega t ds, \quad \text{as shown in Fig. 2.10 .}$$

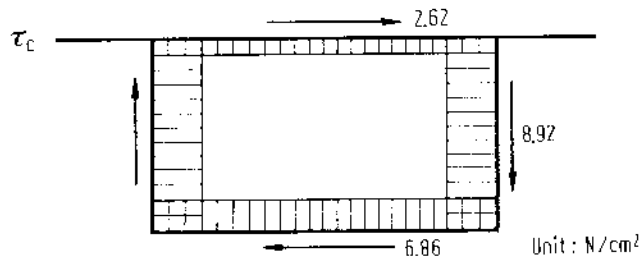


Fig. 2.9. Shear stresses  $\tau_c$  on the cross section at quarter point

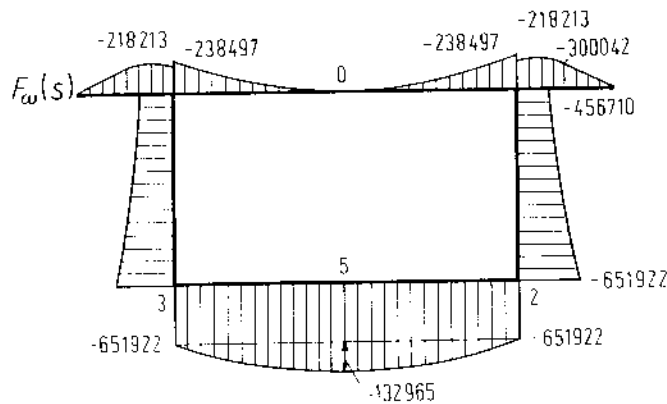


Fig. 2.10.  $F_{\omega}$  diagram of the cross section

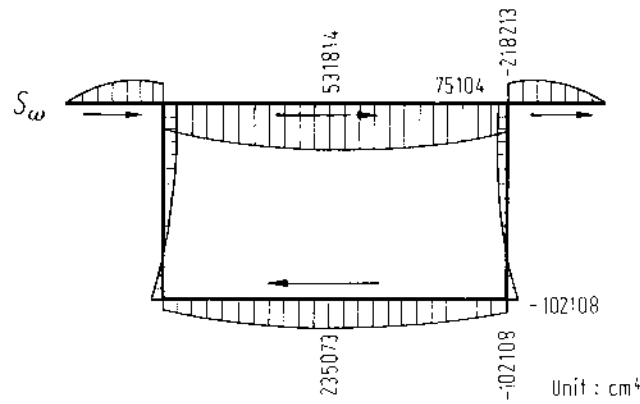


Fig. 2.11.  $S_{\omega}$  diagram of the cross section

$$\oint F_{\omega} \frac{ds}{t} = -284520312 \text{ cm} ,$$

$$\oint \frac{ds}{t} = 535.2 ,$$

$$S_{\omega} = F_{\omega} - \frac{\oint F_{\omega}(ds/t)}{\oint (ds/t)} , \text{ as shown in Fig. 2.11 .}$$

$\max(t\tau_w)$  is very small in comparison with  $\max(t\tau_c)$ .

#### 2.2.4 Effect of Warping Torsion of Box Girders

The torsion of a thin walled structure is generally a combination of pure torsion and warping torsion.

The question, in which torsion is dominant in the case when a girder is subjected to torsional moments, can be answered by distinguishing the torsion characteristic parameter  $\kappa = \sqrt{C/D_{\omega\omega}} \cdot l = \lambda l$ , which is the product of  $\lambda = \sqrt{C/D_{\omega\omega}}$ , the ratio of the torsional rigidity  $C$  to the warping torsion rigidity, and the length  $l$  of the girder. If the value of parameter  $\kappa$  is very small, then the effect of warping torsion is dominant and conversely, the pure torsion is dominant. In other cases we have to consider the two effects of warping and pure torsions together.

Figure 2.12 indicates the curve of bimoment  $M_{\omega}(\chi)$  due to warping torsion at the mid-span of a simply supported girder under uniform torque  $m_x$ . In the figure the abscissa  $\chi$  is a logarithmic coordinate, while the value of the  $M_{\omega}(\chi)/M_{\omega}(\chi = 0)$  is from zero (pure torsion) to one (warping torsion).

#### 2.2.5 Effect of Shear Strain $\gamma_w$ Due to Warping Torsion

We apply the theory given in Sect. 1.5 to analyzing the effect of shear strain  $\gamma_w$ , also using the numerical example in Sect. 2.2.3.

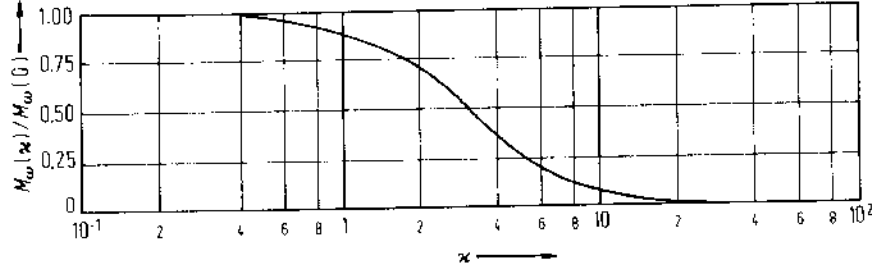


Fig. 2.12. Ratio  $M_w(x)/M_w(0)$  as a function of  $\chi$

From the calculation in the previous section we have

$$C_p = G \cdot I_p = G \int_s \rho_M^2 t ds = 7.239 \times 10^{13} \text{ N} \cdot \text{cm}^2,$$

$$C_\gamma = C_p - C = 6.014 \times 10^{12} \text{ N} \cdot \text{cm}^2,$$

$$v_\gamma = C_p/C_\gamma = 12.04,$$

$$D_{\omega\omega}^* = v_\gamma \cdot D_{\omega\omega} = 5.53 \times 10^{17} \text{ N} \cdot \text{cm}^4,$$

$$\lambda = \sqrt{C/D_{\omega\omega}^*} = 1.095 \times 10^{-2} \text{ cm}^{-1}.$$

In the case of a concentrated torsional moment  $T$  acting at the mid-span we have

$$\theta = \frac{T}{C} \left( \frac{z}{2} - \frac{\sinh \lambda l/2}{v_\gamma \lambda \sinh \lambda l} \cdot \sinh \lambda z \right),$$

$$\theta' = \frac{T}{C} \left( \frac{1}{2} - \frac{\sinh \lambda l/2}{v_\gamma \sinh \lambda l} \cdot \cosh \lambda z \right),$$

$$M_\omega = T \cdot \frac{\sinh \lambda l/2}{v_\gamma \lambda \sinh \lambda l} \cdot \sinh \lambda z, \quad (z < l/2).$$

$$T_c = C\theta' = T \left( \frac{1}{2} - \frac{\sinh \lambda l/2}{v_\gamma \sinh \lambda l} \cdot \cosh \lambda z \right),$$

$$T_\omega = -EF_{\omega\omega} \cdot \theta'' = T \cdot \frac{\sinh \lambda l/2}{v_\gamma \sinh \lambda l} \cdot \cosh \lambda z,$$

Assume  $T = 5 \times 10^6 \text{ N} \cdot \text{cm}$ . The values of  $\theta$ ,  $T_c$ ,  $T_\omega$  and  $M_\omega$  with consideration of  $\gamma_w$  are shown in Figs. 2.13 to 2.16.

Computation results show that the shear strain  $\gamma_w$  remarkably reduces the stress  $\sigma_\omega$  due to torsional warping on cross-sections where a concentrated torque is applied or the warping is perfectly restrained — a fixed support. The reduction depends on the factor  $v_\gamma = C_p/C_\gamma$ . The ratio of bimoments  $M_\omega(1)$  and  $M_\omega(v_\gamma)$  obtained by neglecting  $\gamma_w$  (i.e.  $v_\gamma = 1$ ) and considering  $\gamma_w$  can be given roughly as

$$\frac{M_\omega(1)}{M_\omega(v_\gamma)} \approx \sqrt{v_\gamma}.$$

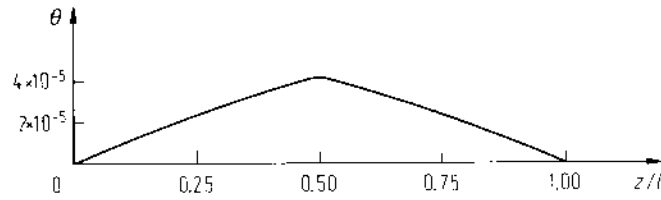


Fig. 2.13. Angle of twist  $\theta$  as a function of  $z/l$

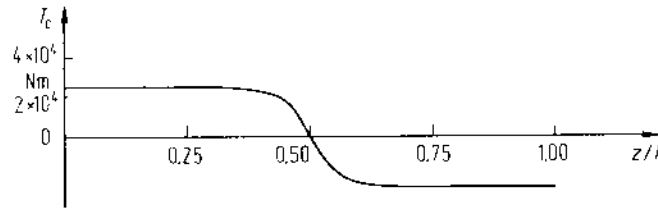


Fig. 2.14. Torque  $T_c$  as a function of  $z/l$

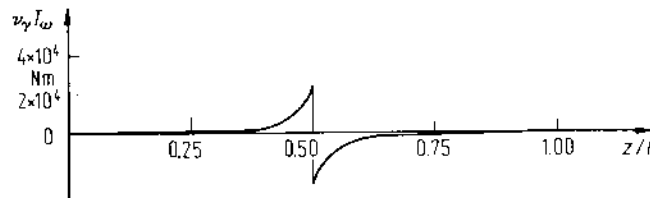


Fig. 2.15. Torque  $T_w$  as a function of  $z/l$

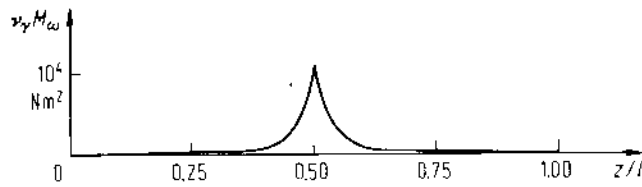


Fig. 2.16. Bimoment  $M_w$  as a function of  $z/l$

## 2.3 Cross-section Distortion Analysis of Box Girders

### 2.3.1 Solution to the Distortion Equation of Box Girders

We rewrite the second equation of Eqs. (2.25) as

$$\tilde{\theta}^{(4)} + \frac{\tilde{A}}{D_{\tilde{\omega}\tilde{\omega}}} \tilde{\theta} = \frac{\tilde{m}_z}{D_{\tilde{\omega}\tilde{\omega}}} \quad (2.34)$$

Denoting

$$\tilde{\lambda} = \sqrt{\tilde{A}/4D_{\omega\omega}}$$

the characteristic equation of Eq. (2.34) is

$$\gamma^4 + 4\tilde{\lambda}^4 = 0,$$

with roots

$$\begin{aligned} \gamma_1 &= (1 + i)\tilde{\lambda}, & \gamma_2 &= (1 - i)\tilde{\lambda}, \\ \gamma_3 &= (-1 + i)\tilde{\lambda}, & \gamma_4 &= (-1 - i)\tilde{\lambda}. \end{aligned} \quad (2.35)$$

Thus, the homogeneous solution to Eq. (2.34) can be constructed as

$$\tilde{\theta} = e^{\tilde{\lambda}z}(C_1 \cos \tilde{\lambda}z + C_2 \sin \tilde{\lambda}z) + e^{-\tilde{\lambda}z}(C_3 \cos \tilde{\lambda}z + C_4 \sin \tilde{\lambda}z). \quad (2.36)$$

In the case when a simple supported girder is subjected to uniformly distributed loads  $\tilde{m}_z$ , the general solution to Eq. (2.34) is

$$\tilde{\theta} = \frac{\tilde{m}_z}{\tilde{A}} + e^{\tilde{\lambda}z}(C_1 \cos \tilde{\lambda}z + C_2 \sin \tilde{\lambda}z) + e^{-\tilde{\lambda}z}(C_3 \cos \tilde{\lambda}z + C_4 \sin \tilde{\lambda}z) \quad (2.37)$$

in which coefficients  $C_1$ ,  $C_2$ ,  $C_3$ , and  $C_4$  can be determined by imposing the boundary conditions,

$$\begin{aligned} \text{for } z = 0: & \quad \tilde{\theta}(0) = 0, \quad \tilde{\theta}''(0) = 0; \\ \text{for } z = l: & \quad \tilde{\theta}(l) = 0, \quad \tilde{\theta}''(l) = 0, \end{aligned}$$

and will be

$$\begin{aligned} C_1 &= \frac{\tilde{m}_z}{\tilde{A}} \cdot \frac{\frac{1}{2}(e^{2\tilde{\lambda}l} - \cos 2\tilde{\lambda}l) - \sinh \tilde{\lambda}l \cos \tilde{\lambda}l - \cosh 2\tilde{\lambda}l + \cos 2\tilde{\lambda}l}{\cosh 2\tilde{\lambda}l - \cos 2\tilde{\lambda}l}, \\ C_2 &= C_4 = \frac{\tilde{m}_z \sin \tilde{\lambda}l (\cos \tilde{\lambda}l - \cosh \tilde{\lambda}l)}{\tilde{A} (\cosh 2\tilde{\lambda}l - \cos 2\tilde{\lambda}l)}, \\ C_3 &= -\frac{\tilde{m}_z}{\tilde{A}} \cdot \frac{\frac{1}{2}(e^{2\tilde{\lambda}l} - \cos 2\tilde{\lambda}l) - \sinh \tilde{\lambda}l \cos \tilde{\lambda}l}{\cosh 2\tilde{\lambda}l - \cos 2\tilde{\lambda}l}. \end{aligned} \quad (2.38a)$$

In the case when a girder is subjected to a concentrated moment  $\tilde{T}$ , the homogeneous solution Eq. (2.36) is the general solution. Using boundary conditions and deformation compatibility conditions at the mid-span, coefficients  $C_1$ ,  $C_2$ , etc., can be determined:

$$\begin{aligned} C_1 &= -C_3 = \frac{\tilde{T}}{8D_{\omega\omega}\tilde{\lambda}^3} \cdot \frac{\sinh \frac{\tilde{\lambda}l}{2} \sin \frac{\tilde{\lambda}l}{2} + \cosh \frac{\tilde{\lambda}l}{2} \cos \frac{\tilde{\lambda}l}{2}}{\cosh \tilde{\lambda}l + \cos \tilde{\lambda}l}, \\ C_2 &= C_4 = \frac{\tilde{T}}{8D_{\omega\omega}\tilde{\lambda}^3} \cdot \frac{\sinh \frac{\tilde{\lambda}l}{2} \sin \frac{\tilde{\lambda}l}{2} - \cosh \frac{\tilde{\lambda}l}{2} \cos \frac{\tilde{\lambda}l}{2}}{\cosh \tilde{\lambda}l + \cos \tilde{\lambda}l}. \end{aligned} \quad (2.38b)$$

### 2.3.2 Numerical Example

Data: The example shown in Sect. 2.2.3 is reused. For the data see Sect. 2.2.3.

$$y_N = -\frac{F_{x\tilde{\omega}_0}}{F_{xx}} = -14.19 \text{ cm}$$

$\tilde{\omega}$ -diagram is shown in Fig. 2.17.

$$F_{\tilde{\omega}\tilde{\omega}} = \oint_F \tilde{\omega} \tilde{\omega} dF = 4.9476 \times 10^{10} \text{ cm}^6$$

$$\tilde{A} = 8.63 \times 10^5 \text{ N}$$

$$C_1 = 3.0630 \times 10^{-4}$$

$$C_2 = C_4 = 2.1875 \times 10^{-3}$$

$$C_3 = 0.01105$$

The values of  $\tilde{\theta}$  and  $\tilde{M}_{\tilde{\omega}}$  are plotted in Figs. 2.18 and 2.19.

$$\tilde{M}_{\tilde{\omega}} = -D_{\tilde{\omega}\tilde{\omega}} \tilde{\theta}'' , \quad \tilde{M}_{\tilde{\omega}}(l/2) = -5.24 \times 10^4 \text{ Nm}^2$$

As an example,  $\sigma_{\tilde{\omega}} = \frac{\tilde{M}_{\tilde{\omega}}}{F_{\tilde{\omega}\tilde{\omega}}} \tilde{\omega}$  on the cross-section at mid-span and at the lower box corner is  $160.59 \text{ N/cm}^2$ .

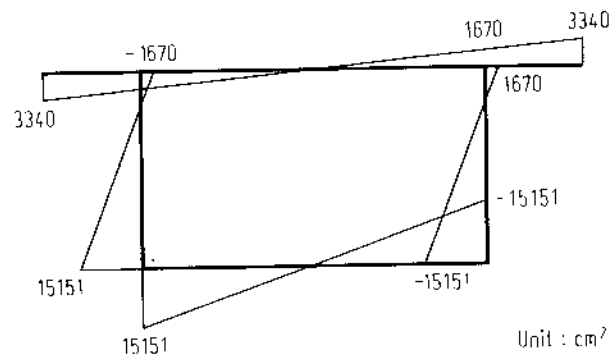


Fig. 2.17.  $\tilde{\omega}$  diagram of the cross section

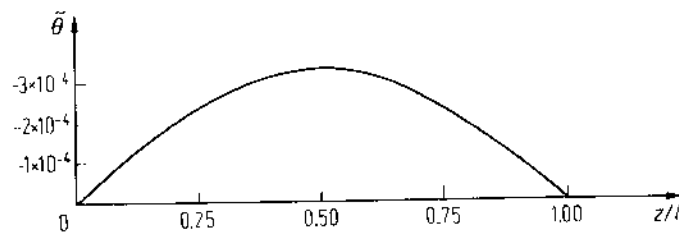


Fig. 2.18. Distortion  $\tilde{\theta}$  as a function of  $z/l$

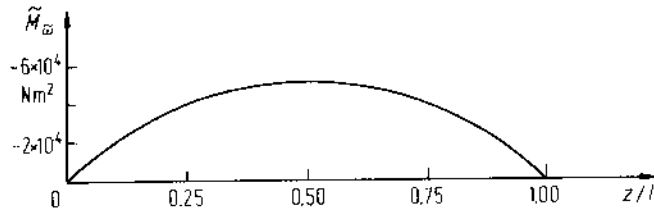


Fig. 2.19. Bimoment  $\tilde{M}_b$  as a function of  $z/l$

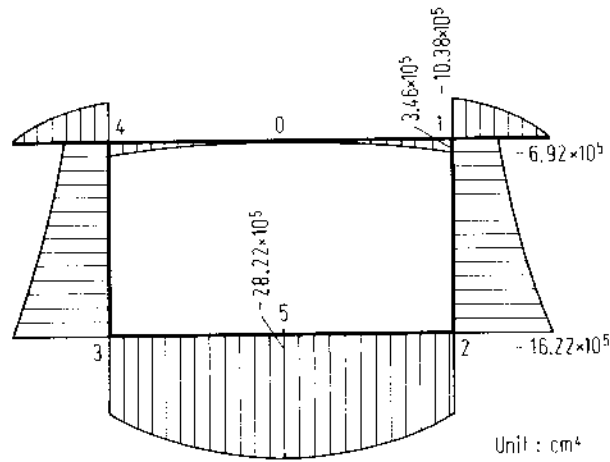


Fig. 2.20.  $F_b$  diagram of the cross section

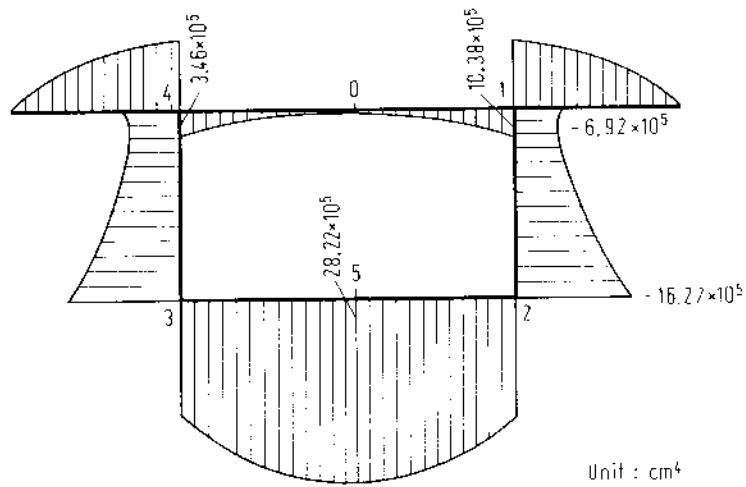


Fig. 2.21.  $S_b$  diagram



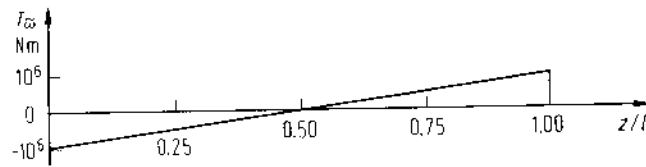


Fig. 2.22. Torque  $T_{\omega}$  as a function of  $z/l$

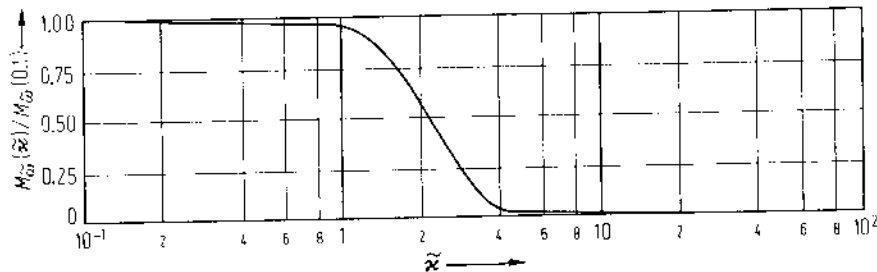


Fig. 2.23. Variation of the ratio  $M_{\omega}(\tilde{x})/M_{\omega}(0.1)$  with respect to  $\tilde{x}$

$F_{\omega}^*$  is shown in Fig. 2.20,  $s_{\omega} = F_{\omega} - \left( \oint F_{\omega} \frac{ds}{t} / \oint \frac{ds}{t} \right)$  is shown in Fig. 2.21, and  $T_{\omega} = -EF_{\omega\omega}\tilde{\theta}'''$  is shown in Fig. 2.22.

The shear on the cross-section at the support is  $(t\tau_{\omega}) = 1.825S_{\omega}$ .

### 2.3.3 Effect of Distortional Warping of Box Girders

As was previously mentioned, the general torsional rigidity of a thin walled box girder is composed of two parts, one of which is the pure torsional rigidity  $C$  and the other is the warping torsional rigidity  $D_{\omega\omega}$ . The characteristics of torsion of thin walled box girders are related to the dimensionless parameters  $\kappa = \lambda l = \sqrt{C/D_{\omega\omega}}l$ . Similarly, the distortional rigidity of cross-section of thin walled box girder is the combination of the shearing rigidity  $\bar{A}$  and the warping distortional rigidity  $D_{\omega\hat{\omega}}$ . The distortional warping box girder is related to dimensionless parameter  $\tilde{\kappa} = \sqrt[4]{\bar{A}/4D_{\omega\hat{\omega}}} \cdot l$ . With the increase of the value of  $\tilde{\kappa}$ , the effect of distortional warping decreases. The variation of warping distortional moment at mid-span with respect to  $\tilde{x}$  under uniform loads  $\tilde{m}_z$  is shown in Fig. 2.23, where the ordinate represents  $M_{\omega}(\tilde{x})/M_{\omega}(0.1)$ , while the abscissa  $\tilde{x}$  is a logarithmic value.

## 2.4 Comparison of Theoretical Results with Model Test

To verify the correctness of the theoretical analyses, we performed a loading test with a girder model made of Perspex.

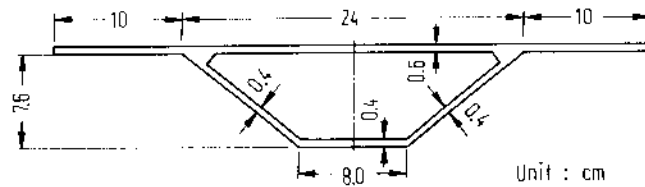


Fig. 2.24. Dimensions of the model cross section

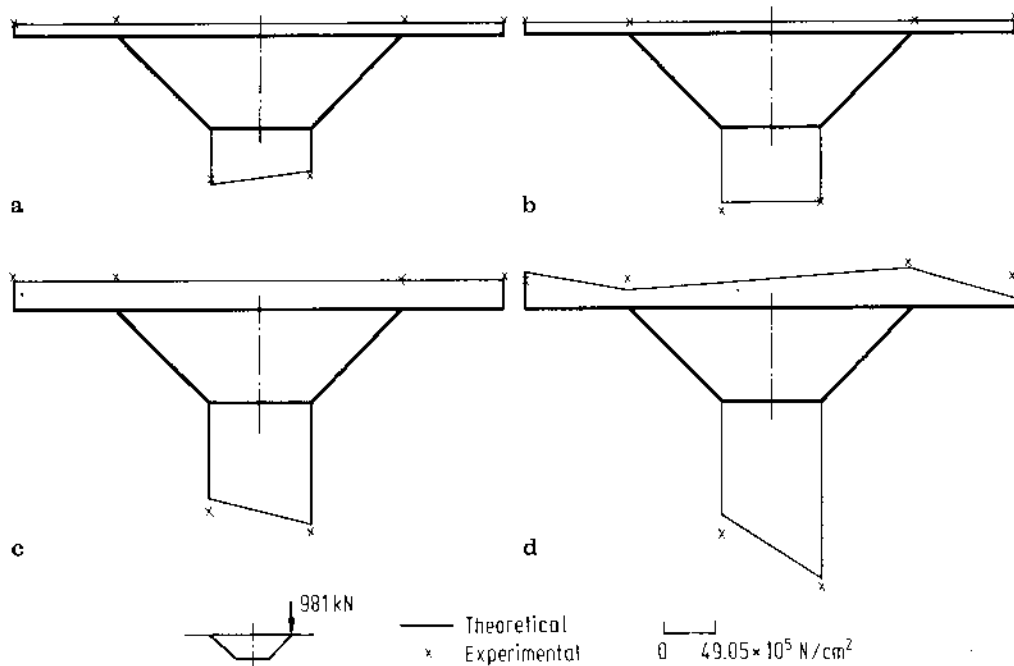


Fig. 2.25. Normal stresses  $\sigma$  on the cross sections at (a)  $\frac{3}{8}l$ , (b)  $\frac{5}{8}l$ , (c)  $\frac{7}{8}l$ , (d) mid-span

Dimensions of the constant cross-section are indicated in Fig. 2.24. The span length of the girder model is 200 cm. Two diaphragms were located at the two ends, each of which was supported at two points. One end was supported on two linking rods and the other on two bearings.

The modulus of elasticity of Perspex is  $E = 2943 \text{ MPa}$  and its Poisson's ratio is  $\mu = 0.4$ .

A concentrated force of 981 N was symmetrically or eccentrically applied at the mid-span.

Figures 2.25a–d show the normal stresses on the cross-sections at  $\frac{3}{8}l$ ,  $\frac{5}{8}l$ ,  $\frac{7}{8}l$  and the mid-span, which are theoretically and experimentally obtained under an eccentric concentrated force applied at the mid-span of the model. It can be seen that the agreement between the results from the theory and the test is good.

### 3. Bending and Torsion Theories of Curved Box Girder

The bending and torsion of the curved box girder can, in principle, be analyzed analogously to those of the straight box girder. However, because of the presence of initial curvature, the analysis becomes more complicated. Many authors have contributed to the development of this theory, for instance Vlasov (1961), Dabrowski (1964). In this chapter a practical theory of bending and torsion of the box girder for wide initial curvature range will be developed. That means it includes the cases where the initial curvature radius of the girder axis is rather small and, therefore, the nonlinear distribution of normal strains and stresses over the cross section must be taken into account.

The curved box girder of symmetrical trapezoidal section, as shown in Fig. 3.1, is widely applied in bridge engineering, and will be considered here. For simplicity, we assume that the cross section and the radius  $R_0$  of girder axis are constant along the girder length. The cross section may be distorted due to torsion, and its distortional rigidity is assumed to be continuously distributed.

The cylindrical coordinates  $r, n, z$  will be used, and the centroidal principal axes  $x, y$  coincide with  $r, n$ , as shown in Fig. 3.2.

The distributed loading  $q_r, q_n, q_z$  acting in the directions  $r, n, z$ , respectively, will be considered. As in the case of a straight box girder, the local stresses induced by the loading are not included in the investigation, and the influence of shear strain caused by the warping torsion will be analyzed last.

#### 3.1 Displacements and Deformations

As in Chap. 1, there are five basic displacements, namely, the uniform displacements  $u_0(z), v_0(z), w_0(z)$  in the directions  $r, n, z$ , respectively, the angle of twist  $\theta(z)$ , and the distortion  $\tilde{\theta}(z)$ :

$$\{A\} = [A]^T = [u_0 \ v_0 \ \theta \ \tilde{\theta} \ w_0]^T. \quad (3.1)$$

The displacements  $u(x, y, z)$  and  $v(x, y, z)$  in the directions  $r$  and  $n$ , respectively, at point  $(x, y)$  of the section  $(z)$  can be expressed in the following form:

$$\begin{aligned} u(x, y, z) &= u_0 - (y - y_M)\theta - (y - y_N)\tilde{\theta}, \\ v(x, y, z) &= v_0 - (x - x_M)\theta - \tilde{r}_v\tilde{\theta}, \end{aligned} \quad (3.2)$$

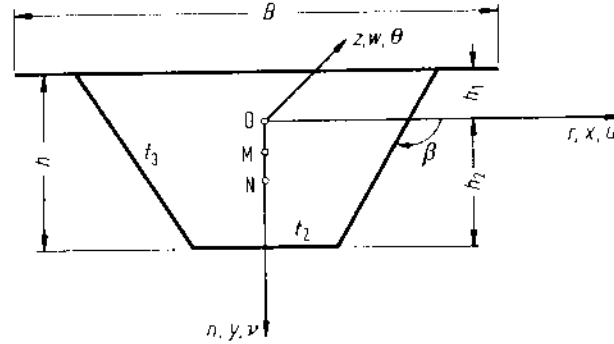


Fig. 3.1. Symmetrical trapezoidal section and its coordinate system

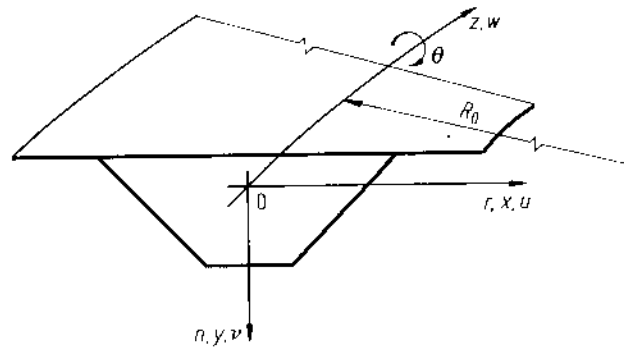


Fig. 3.2. Cylindrical coordinate system

where the indices M and N denote the center of twist and center of distortion of the cross section of the curved girder, respectively, and  $\tilde{r}_v$  is defined in Eq. (1.67).

In order to determine the normal displacement  $w(x, y, z)$ , let us consider the rotations and twist of the section. The rotation vector in direction  $r$  is

$$\phi_r = -\frac{dv_0}{dz} = -v'_0, \quad (3.3)$$

while the rotation vector in direction  $n$  consists of two parts, namely,  $u'_0$  due to the horizontal deflection  $u_0$ , and  $w_0/R_0$  due to the uniform axial displacement  $w_0$ , as shown in Fig. 3.3. The sum is therefore,

$$\phi_n = u'_0 + \chi w_0, \quad (3.4)$$

where

$$\chi = 1/R_0. \quad (3.5)$$

As to the twist, aside from  $\theta$  due to the torsion, there is a contribution due to the vertical deflection  $v_0$ . It may be seen from Fig. 3.4 that the displacement  $v_0$  induces a relative rotation  $-dv_0/R_0$  about the  $z$ -axis between two adjacent cross sections of an element  $dz$  of the curved girder. Hence a twist  $dv_0/R_0$  will occur if

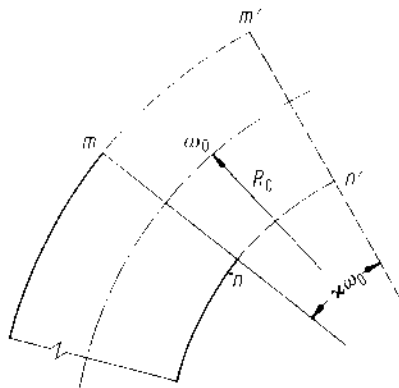


Fig. 3.3. Rotation due to uniform axial displacement  $w_0$

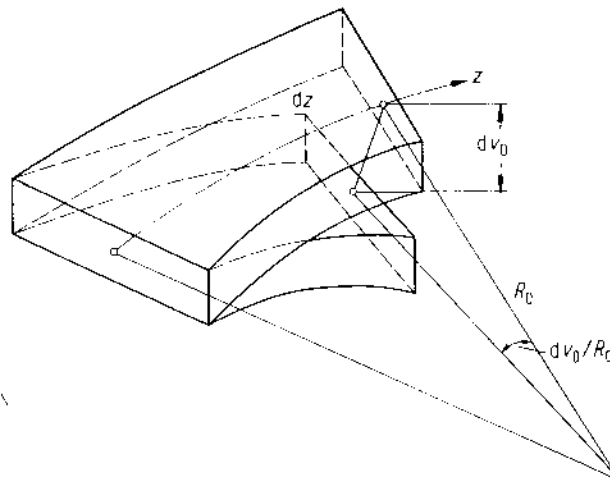


Fig. 3.4. Twist due to vertical displacement  $v_0$

the angle  $\theta$  remains unchanged. The total twist per unit length is therefore

$$k_z = \theta' + \chi v_0' \tag{3.6}$$

By using the expressions of  $\phi_r, \phi_n, k_z$ , the normal displacement can be determined according to the following equation:

$$w(x, y, z) = -(x - e)\phi_n + y\phi_r - \omega_R k_z - \tilde{\omega}_R \tilde{\theta}' + w_0, \tag{3.7}$$

where  $\omega_R$  and  $\tilde{\omega}_R$  are principal coordinates for torsional warping and distortional warping of a curved girder, respectively, and  $e$  denotes the eccentricity of neutral axis of bending in the horizontal plane caused by the initial curvature of the girder. The calculation of  $\omega_R, \tilde{\omega}_R, e$  will be given later.

### 3.2 Normal Strain

In the analysis of the normal strain of the curved girder, the variation of the initial radius across the width of the cross section

$$R(x) = R_0 - x \tag{3.8}$$

will be taken into account.

In order to establish a practical method, the following approximation will be adopted:

$$\frac{1}{R(x)} = \chi(1 + \chi x), \tag{3.9}$$

where  $\chi$  is given in Eq. (3.5). It is the term  $\chi x$  wherein the variation of the initial curvature across the section width is considered.

The normal strain of a curved girder is given by the equation

$$\varepsilon_z(x, y, z) = \frac{\partial w}{R(x)\partial\phi} - \frac{u}{R(x)}.$$

Using Eq. (3.9) and  $R(x)\partial\phi = (1 - \chi x)\partial z$ , we can put the above equation in the following form:

$$\varepsilon_z = (1 + \chi x)(w' - \chi u). \quad (3.10)$$

Substituting Eqs. (3.7), (3.6), (3.4), (3.3), (3.2) into the preceding equation, we obtain

$$\varepsilon_z = (1 + \chi x)[\hat{x}][d]\{\mathcal{A}\}, \quad (3.11a)$$

or

$$\varepsilon_z = -(1 + \chi x)[\hat{x}]\{k\}, \quad (3.11b)$$

where the matrix of the principal coordinates is

$$[\hat{x}] = [(x - e) \ y \ \omega_R \ \tilde{\omega}_R \ 1] \quad (3.12)$$

The matrix of differentiation operator  $d = d/dz$  is

$$[d] = \begin{bmatrix} -d^2 & 0 & 0 & 0 & -\chi d \\ 0 & -d^2 & \chi & \chi & 0 \\ 0 & -\chi d^2 & -d^2 & 0 & 0 \\ 0 & 0 & 0 & -d^2 & 0 \\ -\chi & 0 & -\chi y_M & -\chi y_N & d \end{bmatrix} \quad (3.13)$$

and the matrix of curvatures is  $\{k\} = -[d]\{\mathcal{A}\}$ , i.e.,

$$\{k\} = \left\{ \begin{array}{l} k_y \\ k_x \\ k'_z \\ \tilde{k}'_z \\ -\varepsilon_0 \end{array} \right\} = \left\{ \begin{array}{l} u''_0 + \chi w'_0 \\ v''_0 - \chi(\theta + \tilde{\theta}) \\ \theta'' + \chi v''_0 \\ \tilde{\theta}'' \\ -(w'_0 - \chi(u_0 + y_M\theta + y_N\tilde{\theta})) \end{array} \right\}. \quad (3.14)$$

From Eq. (3.11) it can be seen that, owing to the term  $\chi x$ , the normal strain  $\varepsilon_z$  is no longer linearly distributed over the section, and the nonlinearity is considered only up to the square of  $x$ .

### 3.3 Principal Coordinates

#### 3.3.3 Unit Torsional Warping

The torsional warping of a curved box girder can be determined from the equation for shear strain:

$$\gamma_{zs} = \frac{\partial \eta}{\partial z} + \frac{\partial w}{\partial s} + \frac{w}{R_0} \cos \beta(s), \quad (3.15)$$

where  $s, \beta, \eta$  are shown in Fig. 1.2. In comparison with Eq. (1.8) for a straight girder, the above equation has one extra term on the right-hand side, namely, the third term containing  $1/R_0$ . This  $R_0$  has been taken for  $R(x)$ , since it is only a term modifying  $w$ .

For this reason, Eq. (3.15) can be integrated by successive approximation. Using the unit torsional warping  $\omega$  of the straight box girder given by Eq. (1.30) as the first approximate solution, we obtain the first modified warping

$$w(x, s) = -\omega_R k_z, \quad (3.16)$$

where

$$\omega_R = \omega(s) - \chi \Omega(s), \quad (3.17)$$

$$\begin{aligned} \Omega(s) &= \int_0^s \omega \cos \beta ds + \Omega_1(0) \\ &= \Omega_1(s) + \Omega_1(0). \end{aligned} \quad (3.18)$$

A further step of approximation yielding modification with  $\chi^2$  can be omitted.

To orthogonalize  $\omega_R$  to the principal coordinates ( $x, y$ ), the integration constant  $\Omega_1(0)$  must be

$$\Omega_1(0) = -\frac{1}{F} \int \Omega_1(s) dF \quad (3.19)$$

and the position of the center of twist  $M(x_M^0, y_M^0)$  of  $\omega(s)$  in Eq. (3.17) has to be adjusted. From the relation

$$\omega_R(x_M^0 + \Delta x_M, y_M^0 + \Delta y_M) = \omega_R(x_M^0, y_M^0) - \Delta x_M y + \Delta y_M x, \quad (3.20)$$

i.e.,  $\omega_R(x_M, y_M) = \omega(x_M^0, y_M^0) - \chi \Omega(s) - \Delta x_M y + \Delta y_M x$  follows the adjustment similar to Eq. (1.16):

$$\begin{aligned} \Delta x_M &= -\chi \frac{F_{y\Omega}}{F_{yy}}, \\ \Delta y_M &= \chi \frac{F_{x\Omega}}{F_{xx}}. \end{aligned} \quad (3.21)$$

Figure 3.5 shows an example of  $\omega_R$ . For a symmetrical box section,  $\omega$  is anti-symmetric,  $\Omega$  symmetric,  $\Delta y_M = 0$ , but  $\Delta x_M \neq 0$ . Therefore, the center of twist  $M$  of a curved girder is not on the axis of symmetry and  $\omega_R$  is asymmetric involving the nonlinear term  $\Omega$ , which in addition to  $\chi x$  in Eq. (3.10) makes the distribution of torsional warping stress  $\sigma_\omega$  over the cross section of a curved girder is no longer linear.

### 3.3.2 Unit Distortional Warping

Referring to the calculation of  $\omega_R$  in the preceding section and  $\tilde{\omega}$  in Sect. 1.4, the unit distortional warping of a curved box girder  $\tilde{\omega}_R$  can be given as follows:

$$\tilde{\omega}_R(x_N, y_N) = \tilde{\omega}(x_N^0, y_N^0) - \chi \tilde{\Omega} - \Delta x_N v_n y + \Delta y_N v_n x, \quad (3.22)$$

where

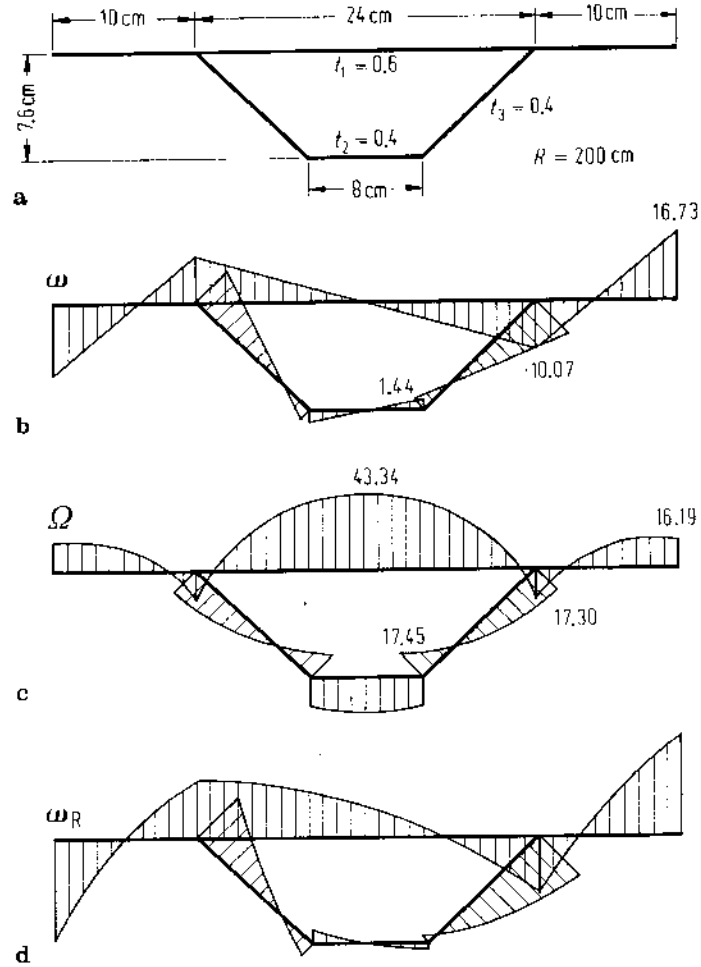


Fig. 3.5a-d.  $\omega$ ,  $\Omega$ , and  $\omega_R$  diagrams of the model section given in Fig. 2.24

$$\tilde{\Omega}(s) = \tilde{\Omega}_1(s) + \tilde{\Omega}_1(0), \quad (3.23)$$

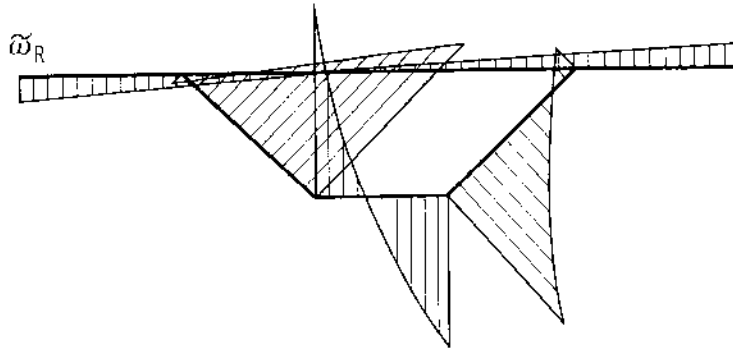
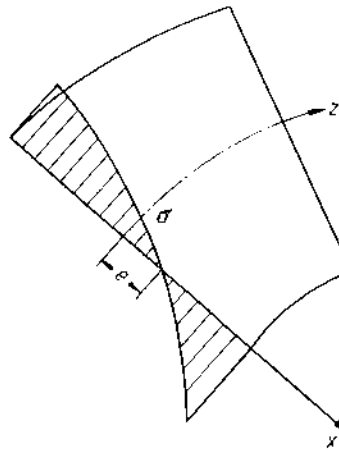
$$\tilde{\Omega}_1(s) = \int_0^s \tilde{\omega} \cos \beta ds, \quad (3.24)$$

$$\tilde{\Omega}_1(0) = -\frac{1}{F} \int_P \tilde{\Omega}_1 dF,$$

$$\Delta x_N = -\chi \frac{\sum_n F_{y\tilde{\Omega}}^{(n)}}{\sum_n v_n F_{yy}^{(n)}}, \quad (3.25)$$

$$\Delta y_N = \chi \frac{\sum_n F_{x\tilde{\Omega}}^{(n)}}{\sum_n v_n F_{xx}^{(n)}},$$



Fig. 3.6.  $\tilde{\omega}_R$  diagram of the model sectionFig. 3.7. Distribution of the normal stress  $\sigma$  in horizontal bending

and

$$v_n = \begin{cases} 1 & \text{for } n = 1, 3 \text{ (top and bottom plate),} \\ -v & \text{for } n = 2, 4 \text{ (web plates).} \end{cases}$$

An example of  $\tilde{\omega}_R$  is shown in Fig. 3.6. The foregoing statement about  $\omega_R$  is also valid for  $\tilde{\omega}_R$ .

### 3.3.3 Neutral Axis of Horizontal Bending

Owing to the initial curvature of the girder, the neutral axis of the bending in the horizontal plane shifts from  $y$ -axis ( $x = 0$ ) to  $x = e$ , as denoted in Eqs. (3.7), (3.12), and shown in Fig. 3.7.

The eccentricity  $e$  can be determined from the equilibrium condition that the sum of the bending stress  $\sigma$  over the whole cross section must equal zero. This

requires using  $\varepsilon_z$  given in Eq. (3.11),

$$\iint_F (1 + \chi x)(x - e) dF = 0. \quad (3.26)$$

Hence it follows

$$e = \chi \frac{F_{xx}}{F} = \chi r_y^2, \quad (3.27)$$

where  $r_y$  is the radius of gyration with respect to  $y$ -axis.

### 3.4 Stresses and Stress Resultants

#### 3.4.1 Normal Stresses and Moments

The normal stresses in the curved box girder can readily be given with the normal strain  $\varepsilon$  from Eq. (3.11):

$$\sigma_z = -E(1 + \chi x)[\tilde{x}]\{k\} \quad (3.28)$$

It can also be expressed in another form by using the stress resultants:

$$\sigma_z = (1 + \chi x) \left\{ \frac{M_y^0}{F_{xx}} (x - e) + \frac{M_x^0}{F_{yy}} y + \frac{M_\omega^0}{F_{\omega\omega}} \omega_R + \frac{\tilde{M}_{\tilde{\omega}}^0}{F_{\tilde{\omega}\tilde{\omega}}} \tilde{\omega}_R + \frac{N^0}{F} \right\}, \quad (3.29)$$

where

$$\begin{aligned} [M^0] &= [M_y^0 M_x^0 M_\omega^0 \tilde{M}_{\tilde{\omega}}^0 N^0] \\ &= [-\tilde{D}_{xx} k_y - D_{yy} k_x - D_{\omega\omega} k'_z - D_{\tilde{\omega}\tilde{\omega}} \tilde{k}'_z D\varepsilon_0], \end{aligned} \quad (3.30)$$

$$[D] = E[F], \quad (3.31)$$

$$\begin{aligned} [F] &= \iint_F (1 + \chi x)[\tilde{x}^2] dF \\ &= [\tilde{F}_{xx} F_{yy} F_{\omega\omega} F_{\tilde{\omega}\tilde{\omega}} F], \end{aligned} \quad (3.32)$$

$$\tilde{F}_{xx} = F_{xx}(1 - \chi^2 r_y^2). \quad (3.33)$$

The small terms  $\chi F_{xyy}$ ,  $\chi F_{x\omega\omega}$ ,  $\chi F_{x\tilde{\omega}\tilde{\omega}}$  are neglected. The indices  $\omega$  and  $\tilde{\omega}$  denote  $\omega_R$  and  $\tilde{\omega}_R$ , respectively.

It must be noted that the stress resultants ( $M^0$ ) are built up by  $\sigma_z$  induced by the curvature  $k$  multiplying its corresponding coordinate  $\tilde{x}$ . If the total normal stress  $\sigma_z$  is taken for building the moment, then

$$\{M\} = -E \iint_F (1 + \chi x)[\tilde{x}]^T [\tilde{x}] dF \{k\},$$

i.e.,

$$\{M\} = [M_y M_x M_\omega \tilde{M}_{\tilde{\omega}} N]^T = -E[F_x] \{k\}, \quad (3.34)$$

where

$$[F_\chi] = \begin{bmatrix} \bar{F}_{xx} & \chi F_{xxy} & \chi F_{xx\omega} & \chi F_{xx\bar{\omega}} & 0 \\ (F_{yy} + \chi F_{xyy}) & \chi F_{xy\omega} & \chi F_{xy\bar{\omega}} & 0 & 0 \\ (F_{\omega\bar{\omega}} + \chi F_{x\omega\bar{\omega}}) & (F_{\omega\bar{\omega}} + \chi F_{x\omega\bar{\omega}}) & (F_{\omega\bar{\omega}} + \chi F_{x\omega\bar{\omega}}) & 0 & 0 \\ (F_{\bar{\omega}\omega} + \chi F_{x\bar{\omega}\omega}) & (F_{\bar{\omega}\omega} + \chi F_{x\bar{\omega}\omega}) & (F_{\bar{\omega}\omega} + \chi F_{x\bar{\omega}\omega}) & 0 & 0 \\ \text{symmetric} & & & & F \end{bmatrix}. \quad (3.35)$$

It can be seen that  $[F]$  contains only the diagonal elements without  $\chi$  of  $[F_\chi]$ , and, therefore,  $\{M^0\} \neq \{M\}$ , but  $N^0 = N$ .

### 3.4.2 Shear Stress and Torque

The shear stress in the curved box girder caused by pure torsion as well as by warping torsion and bending can be determined just as that in the straight box girder (see Sect. 1.3), because the influence of the initial curvature of the girder upon the shear stress  $\tau$ , even in the top and bottom plates, is very small, and in the web where  $\tau$  dominates it is smaller still.

The expression for the torque of pure torsion here is different from that of the straight box girder, namely, it is

$$T_c = Ck_z = C(\theta + \chi v_0)'. \quad (3.36)$$

## 3.5 The Strain Energy

The strain energy  $U_e$  in the girder consists of three parts induced by the normal strain  $\varepsilon_z$ , the shear strain of pure torsion  $\gamma_c$ , and the distortion of the section  $\bar{\gamma}_N$ :

$$U_e = U_e(\varepsilon_z) + U_e(\gamma_c) + U_e(\bar{\gamma}_N). \quad (3.37)$$

The first part is

$$U_e(\varepsilon_z) = \frac{E}{2} \iiint \varepsilon_z^2 dx dy R(x) d\phi.$$

Using  $R(x) d\phi = (1 - \chi x) dz$  and Eqs. (3.11) to (3.14) and (3.34), (3.35), we have

$$U_e(\varepsilon_z) = \frac{E}{2} \int \{k\}^T [F_\chi] \{k\} dz, \quad (3.38)$$

or

$$= -\frac{1}{2} \int \{k\}^T \{M\} dz.$$

The second part can readily be given as

$$U_e(\gamma) = \frac{C}{2} \int k_z^2 dz,$$

or

$$= \frac{1}{2} \int T_c k_z dz . \quad (3.39)$$

The third part is the same as for the straight box girder, see Eqs. (1.79) and (1.80),

$$U_c(\tilde{y}_N) = \frac{K}{2} \int \tilde{y}_N^2 dz$$

or

$$= \frac{1}{2} \int \tilde{m} \tilde{\theta} dz . \quad (3.40)$$

### 3.6 Potential of External Forces

The potential of the loadings  $q_r$ ,  $q_n$ ,  $q_z$  on the curved girder can be determined by using the same equations (1.41) and (1.81) for the straight box girder where only  $\omega$  and  $\tilde{\omega}$  have to be substituted by  $\omega_R$  and  $\tilde{\omega}_R$ , respectively. It is

$$\begin{aligned} U_p &= -\iiint (q_r u + q_n v + q_z w) dx dy dz \\ &= -\int \{ p_x u_0 - m_y u'_0 + (p_y + \chi m_z) v_0 \\ &\quad - (m_x + \chi m_\omega) v'_0 + m_z \theta - m_\omega \theta' \\ &\quad + \tilde{m}_z \tilde{\theta} - \tilde{m}_\omega \tilde{\theta}' + (p_z - \chi m_y) w_0 \} dz . \end{aligned} \quad (3.41)$$

### 3.7 Differential Equations

The differential equations of bending and torsion of the curved box girder can be derived, analogous to the straight box girder in Chap. 1, by means of the calculus of variations. Using  $U_c$  and  $U_p$  given in Eqs. (3.37) to (3.41), we obtain from

$$\delta U = \delta U_c + \delta U_p = 0 \quad (3.42)$$

after partial integrations the following equations of equilibrium:

$$\left\{ \begin{array}{l} -M_y'' - \chi N \\ -M_x'' - \chi(M_\omega'' + T_c') \\ -M_\omega'' - T_c' + \chi(M_x - N y_M) \\ -\tilde{M} \tilde{\omega}'' + \chi(M_x - N y_N) + \tilde{m} \\ N' - \chi M_y' \end{array} \right\} = \left\{ \begin{array}{l} p_x + m_y' \\ p_y + m_x' + \chi(m_z + m_\omega') \\ m_z + m_\omega' \\ \tilde{m}_z + \tilde{m}_\omega' \\ -p_z + \chi m_y \end{array} \right\} . \quad (3.43)$$

The substitution of Eqs. (3.34) and (3.36) for  $\{M\}$  and  $T_c$  into the above equations gives the differential equations

$$[D]\{A\} = \{p\} , \quad (3.44)$$

where  $\{p\}$  denotes the loading matrix in Eq. (3.43),  $\{A\}$  is the displacement matrix given by Eq. (3.1), and  $[D]$  is the stiffness and differential operator matrix. The elements  $D_{ik}$  containing  $\chi$  and the indices  $(xxy)$ ,  $(xx\omega)$ ,  $(xx\bar{\omega})$ ,  $(x\omega\omega)$ ,  $(x\omega\bar{\omega})$ ,  $(x\bar{\omega}\bar{\omega})$ , as shown in Eq. (3.35), are small and can therefore be neglected. Then we have

$$\begin{aligned}
D_{11} &= \bar{D}_{xx}d^4 + \chi^2D, & d &= d/dz, \\
D_{12} &= 0, \\
D_{13} &= \chi^2y_M D, \\
D_{14} &= \chi^2y_N D, \\
D_{15} &= \chi\bar{D}_{xx}d^3 - \chi Dd, \\
D_{22} &= (D_{yy} + 2\chi^2D_{xy\omega} + \chi^2D_{\omega\omega})d^4 - \chi^2Cd^2, \\
D_{23} &= \chi(D_{xy\omega} + D_{\omega\omega})d^4 - \chi(C + D_{yy} + \chi^2D_{xy\omega})d^2, \\
D_{24} &= \chi(D_{xy\bar{\omega}} + D_{\omega\bar{\omega}})d^4 - \chi(D_{yy} + \chi^2D_{xy\bar{\omega}})d^2, \\
D_{25} &= 0, \\
D_{33} &= D_{\omega\omega}d^4 - (C + 2\chi^2D_{xy\omega})d^2 + \chi^2(D_{yy} + y_M^2D), \\
D_{34} &= D_{\omega\bar{\omega}}d^4 - (\chi^2D_{xy\omega} + \chi^2D_{xy\bar{\omega}})d^2 + \chi^2(D_{xy} + y_M y_N D), \\
D_{35} &= -\chi y_M Dd, \\
D_{44} &= D_{\bar{\omega}\bar{\omega}}d^4 - 2\chi^2D_{xy\bar{\omega}}d^2 + \chi^2(D_{yy} + y_N^2D) + \bar{A}, \\
D_{45} &= -\chi y_N Dd, \\
D_{55} &= (D + \chi^2\bar{D}_{xx})d^2.
\end{aligned} \tag{3.45}$$

### 3.8 Boundary Conditions

Setting each of the boundary values from the partial integrations of Eq. (3.42) equal to zero yields the boundary conditions for integrating the differential equations (3.44). When there are no external forces acting at the ends, we have

$$[M_y \delta u'_0] = 0, \quad [M'_y \delta u_0] = 0, \tag{3.46a}$$

$$[(M_x + \chi M_\omega) \delta v'_0] = 0, \quad [(M'_x + \chi M'_\omega + \chi T_c) \delta v_0] = 0, \tag{3.46b}$$

$$[M_\omega \delta \theta'] = 0, \quad [(M'_\omega + T_c) \delta \theta] = 0, \tag{3.46c}$$

$$[\tilde{M}_{\bar{\omega}} \delta \tilde{\theta}'] = 0, \quad [\tilde{M}'_{\bar{\omega}} \delta \tilde{\theta}] = 0, \tag{3.46d}$$

$$[(N - \chi M_y) \delta w_0] = 0. \tag{3.46e}$$

The equations illustrate that at the ends either the displacement (or the rotation angle) or the corresponding force (or moment) is equal to zero. The substitution of Eqs. (3.34) to (3.36) into the preceding equations gives the boundary conditions in

terms of displacements. Owing to the initial curvature  $\chi$  and the eccentricities  $y_M$  and  $y_N$  of the shear center and distortional center from the centroid  $O$ , the displacements are coupled in the boundary conditions as in the differential equations (3.44), (3.45).

### 3.9 Simplification in Special Cases

#### 3.9.1 Special Case 1: $R(x) \approx R_0$

When the ratio of initial curvature radius  $R_0$  to the section width  $B$  is greater than 10,  $R_0/B > 10$ , the difference between the normal stresses  $\sigma$ , computed by taking  $R(x) = R_0 - x$  and  $R(x) = R_0$  along the section width, does not exceed 4%. In this case we can substitute the following without significant error:

$$R(x) \approx R(0) = R_0. \quad (3.47)$$

Thus,

$$\begin{aligned} (1 + \chi x) &= (1 - \chi x) = 1, \\ \hat{X} &= x - e = x, \\ \hat{F}_{xx} &= F_{xx}, \quad \hat{D}_{xx} = D_{xx}. \end{aligned} \quad (3.48)$$

In Eqs. (3.35) and (3.45) the terms having three indices, for example,  $F_{xy\omega}$  and  $D_{xy\omega}$ , vanish.

#### 3.9.2 Special Case 2: $R(x) = R_0, \bar{\theta} = 0$

If, in addition to  $R_0/B > 10$ , the box girder has sufficient intermediate diaphragms so that the section is practically indeformable, we have this special case 2. The basic displacements are

$$\{\Delta\} = [u_0 \ v_0 \ \theta \ w_0]^T \quad (3.49)$$

The matrix  $[D]$  in differential equation (3.44) will be simplified from Eq. (3.45) to

$$[D] = \begin{bmatrix} (D_{xx}d^4 + \chi^2 D) & 0 & \chi^2 y_M D & (\chi D_{xx}d^3 - \chi Dd) \\ [(D_{yy} + \chi^2 D_{\omega\omega})d^4 & \chi D_{\omega\omega}d^4 & & 0 \\ -\chi^2 C d^2] & -\chi(C + D_{yy})d^2] & & \\ [D_{\omega\omega}d^4 - C d^2 & & -\chi y_M D d & \\ + \chi^2 (D_{yy} + y_M^2 D)] & & & \\ & & & (D + \chi^2 D_{xx})d^2 \end{bmatrix}. \quad (3.50)$$

The initial curvature  $\chi$  tends toward zero with increasing  $R_0$ , and it can be seen from the preceding matrix that the differential equations will be independent, as shown in Eq. (1.49) for the straight girder.

### 3.10 Analysis Under Consideration of Shear Strain of Warping Torsion

We will, as in the analysis for the straight box girder described in Sec. (1.5), consider the influence of shear strain induced by torsional warping on the torsion of the curved box girder for the case just discussed, namely,  $R(x) \approx R(0) = R_0$  and  $\tilde{\theta} = 0$ .

#### 3.10.1 Displacements and Strains

Let  $\gamma_w$  denote the shear strain caused by the shear stress  $\tau_w$  of warping torsion, and assume that  $\gamma_w$  produces approximately a warping of the section  $w = -\omega_R \gamma_w$ , as given in Eq. (1.85).

Denoting the displacement and deformation matrix by

$$\{A\} = \{A\}^T = [u_0 \ v_0 \ \theta \ \gamma_w \ w_0], \quad (3.51)$$

the normal displacement  $w(x, y, z)$  can be given, analogous to Eq. (3.7), in the following form:

$$w(x, y, z) = [-xd \ -(y + \chi\omega_R)d \ -\omega_R d - \omega_R (1 - \chi x)] \{A\}. \quad (3.52)$$

As to  $u(x, y, z)$  and  $v(x, y, z)$ , Eqs. (3.2) remain valid, if we substitute  $\tilde{\theta} = 0$ .

Analogous to Eqs. (3.11) to (3.14), the normal strain  $\epsilon_z$  in this case can be given as

$$\epsilon_z = [x][d]\{A\} = -[x]\{k\}, \quad (3.53)$$

where

$$[x] = [x \ y \ \omega_R \ 1], \quad (3.54)$$

$$[d] = \begin{bmatrix} -d^2 & 0 & 0 & 0 & -\chi d \\ 0 & -d^2 & \chi & 0 & 0 \\ 0 & -\chi d^2 & -d^2 & -d & 0 \\ -\chi & 0 & -\chi y_M & 0 & d \end{bmatrix}, \quad (3.55)$$

$$\{k\} = -[d]\{A\} = \begin{Bmatrix} k_y \\ k_x \\ k_\omega \\ -\epsilon_0 \end{Bmatrix} = \begin{Bmatrix} u_0'' + \chi w_0' \\ v_0'' - \chi \theta \\ \theta'' + \chi v_0'' + \gamma_w' \\ -[w_0' - \chi(u_0 + y_M \theta)] \end{Bmatrix}. \quad (3.56)$$

For the shear strain it follows readily from Eq. (1.87), by substituting  $k_z = \theta' + \chi v_0'$  for  $\theta'$ , that

$$\gamma = \frac{\psi}{t} (\theta' + \chi v_0') - \left( \rho_M - \frac{\psi}{t} \right) \gamma_w. \quad (3.57)$$

### 3.10.2 Differential Equations

Referring to the calculations in Sects. 1.5 and 3.5, 3.6, and 3.7, we obtain by using the calculus of variations the following equations of equilibrium, similar to Eqs. (3.43),

$$\begin{Bmatrix} -M_y'' - \chi N \\ -M_x'' - \chi(M_\omega'' + T_c') \\ -M_\omega'' - T_c' + \chi(M_x - Ny_M) \\ -M_\omega' - T_y \\ N' - \chi M_y' \end{Bmatrix} = \begin{Bmatrix} p_x + m_y' \\ p_y + m_x' + \chi(m_z + m_\omega') \\ m_z + m_\omega' \\ m_\omega \\ -p_z + \chi m_y \end{Bmatrix}, \quad (3.58)$$

where, as in Eq. (3.30),

$$[M_y \ M_x \ M_\omega \ N] = [-D_{xx}k_y \ -D_{yy}k_x \ -D_{\omega\omega}k_\omega \ D\epsilon_0]. \quad (3.59)$$

$T_c$ ,  $T_y$  are as given in Eqs. (3.36) and (1.90), respectively.

Comparing Eqs. (3.58) with (3.43), it can be seen that they are different in the fourth pair only.

Substituting the preceding expressions into Eq. (3.58), we have the differential equations

$$[D]\{A\} = \{p\}, \quad (3.60)$$

where  $\{p\}$  denotes the loading matrix in Eq. (3.58), and the stiffness and differential operator matrix is as follows:

$$[D] = \begin{bmatrix} (D_{11}) & 0 & (D_{13}) & 0 & (D_{14}) \\ & (D_{22}) & (D_{23}) & \chi D_{\omega\omega} d^3 & 0 \\ & & (D_{33}) & D_{\omega\omega} d^3 & (D_{34}) \\ & & & (D_{\omega\omega} d^2 - C_\gamma) & 0 \\ & & \text{symmetric} & & (D_{44}) \end{bmatrix}, \quad (3.61)$$

where  $(D_{ik})$  denotes the element of the matrix given in Eq. (3.50).

It can be seen from this matrix and more clearly from Eq. (3.58) that, owing to the initial curvature  $\chi$ , there is a term  $\chi(M_x - Ny_M)$  in the third equation. This makes it impossible to obtain a simple expression for  $\gamma_w$  in terms of  $\theta$  from the third and fourth equations, as done in the case of the straight box girder in Sect. 1.5.

As boundary conditions for integrating differential equation (3.60) we have Eqs. (3.46a-c) and

$$[M_\omega \ \delta\gamma_w] = 0. \quad (3.62)$$

This condition means that at the girder ends it is either  $M_\omega = 0$  (no torsional warping strain) or  $\gamma_w = 0$  (torsional warping constrained).



## 4. Stress Analysis of Curved Box Girder

In Chap. 3 we derived the bending and torsion theories of a curved box girder with deformable cross-section. As with straight box girders, curved box girders can also be analyzed by solving the equilibrium differential equations (3.44) to obtain the displacements as well as their derivatives, normal stresses, and shear stresses. In solving the equations, however, the difficulty of satisfying the numerical accuracy requirement is also encountered and thus the analytical solution method is impractical.

In this chapter the procedure for evaluating the displacements and stresses by the finite beam element method is presented, and using a specific example a comparison is given between the three results, which are obtained by the finite beam element method, the finite element method of plate and shell, and a model test. Finally, the influence of various factors on the normal stresses is discussed, such as the initial curvature of a curved box girder, the number of the diaphragms, and the thicknesses of plates of a box girder.

### 4.1 Finite Beam Element Method

#### 4.1.1 Assumptions on the Nodal Displacements and Displacement Functions

A typical beam element is shown in Fig. 4.1; its length is  $2\lambda$ . We take lateral displacement  $u_0$ , vertical displacement  $v_0$ , angle of twist  $\theta$ , distortion  $\tilde{\theta}$ , and longitudinal displacement  $w_0$  as well as their first and second derivatives as element displacement parameters. It should be mentioned that it is unnecessary to let the second derivative  $w_0''$  be a parameter, and it was taken for the sake of convenience in calculation. Thus, the displacement parameter column vector  $\{\delta\}^e$  can be defined as

$$\{\delta\}^e = \begin{Bmatrix} \delta_1 \\ \delta_2 \end{Bmatrix}, \quad (4.1)$$

where

$$\begin{aligned} \{\delta_1\} &= [u_i \ u_i' \ u_i'' \ v_i \ v_i' \ v_i'' \ \theta_i \ \theta_i' \ \theta_i'' \ \tilde{\theta}_i \ \tilde{\theta}_i' \ \tilde{\theta}_i'' \ w_i \ w_i' \ w_i'']^T, \\ \{\delta_2\} &= [u_j \ u_j' \ u_j'' \ v_j \ v_j' \ v_j'' \ \theta_j \ \theta_j' \ \theta_j'' \ \tilde{\theta}_j \ \tilde{\theta}_j' \ \tilde{\theta}_j'' \ w_j \ w_j' \ w_j'']^T. \end{aligned}$$

As in the analysis of a straight box girder in Sect. 2.1, we select quintic parabolic curves to interpolate all displacement components within the element and obtain

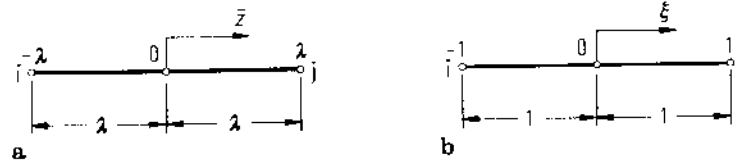


Fig. 4.1a,b. Beam element

$$\{\delta\} = \begin{Bmatrix} u_0 \\ v_0 \\ \theta \\ \tilde{\theta} \\ w_0 \end{Bmatrix} = [N] \{\delta\}^e, \quad (4.2)$$

where

$$[N] = [N_i \ N_j],$$

$$[N_i] = \begin{bmatrix} N_1 & N_2 & N_3 & 0 & 0 & 0 & 0 & 0 & 0 & 0 & 0 & 0 & 0 & 0 \\ 0 & 0 & 0 & N_1 & N_2 & N_3 & 0 & 0 & 0 & 0 & 0 & 0 & 0 & 0 \\ 0 & 0 & 0 & 0 & 0 & 0 & N_1 & N_2 & N_3 & 0 & 0 & 0 & 0 & 0 \\ 0 & 0 & 0 & 0 & 0 & 0 & 0 & 0 & 0 & N_1 & N_2 & N_3 & 0 & 0 \\ 0 & 0 & 0 & 0 & 0 & 0 & 0 & 0 & 0 & 0 & 0 & 0 & N_1 & N_2 & N_3 \end{bmatrix} \quad (4.3)$$

and  $[N_j]$  can be produced by replacing subscript  $n$  (with 1, 2, 3) of element  $N_n$  in the above matrix by  $n + 3$ , in which  $N_1, \dots, N_6$  can be seen in Eq. (2.3).

#### 4.1.2 Derivation of Element Stiffness Matrix and Element Load Vector

For convenience of calculation the differential equations (3.44) of a curved box girder can be written as follows:

$$([D^{(4)}]d^4 + [D^{(3)}]d^3 - [D^{(2)}]d^2 - [D^{(1)}]d + [D^{(0)}])\{\delta\} = \{p\},$$

or abbreviated

$$[L]\{\delta\} = \{p\}, \quad (4.4)$$

in which

$$d = d/dz$$

$$[D^{(4)}] = \begin{bmatrix} \bar{D}_{xx} & 0 & 0 & 0 & 0 \\ (D_{yy} + \chi^2 D_{\omega\omega} + 2\chi^2 D_{xy\omega}) & \chi(D_{\omega\omega} + D_{xy\omega}) & \chi(D_{\omega\tilde{\omega}} + D_{xy\tilde{\omega}}) & 0 & 0 \\ & D_{\omega\omega} & D_{\omega\tilde{\omega}} & 0 & 0 \\ & & D_{\tilde{\omega}\tilde{\omega}} & 0 & 0 \\ \text{symmetry} & & & & 0 \end{bmatrix},$$

$$\begin{aligned}
[D^{(3)}] &= \begin{bmatrix} 0 & 0 & 0 & 0 & \chi D_{xx} \\ & 0 & 0 & 0 & 0 \\ & & 0 & 0 & 0 \\ & & & 0 & 0 \\ \text{symmetric} & & & & 0 \end{bmatrix}, \\
[D^{(2)}] &= \begin{bmatrix} 0 & 0 & 0 & 0 & 0 \\ \chi^2 C & \chi(D_{yy} + \chi^2 D_{xy\omega} + C) & \chi(D_{yy} + \chi^2 D_{xy\omega}) & 0 & 0 \\ & (C + 2\chi^2 D_{xy\omega}) & \chi^2(D_{xy\omega} + D_{xy\bar{\omega}}) & 0 & 0 \\ & & 2\chi^2 D_{xy\bar{\omega}} & 0 & 0 \\ & \text{symmetry} & & & -(D + \chi^2 D_{xx}) \end{bmatrix}, \\
[D^{(1)}] &= \begin{bmatrix} 0 & 0 & 0 & 0 & \chi D \\ & 0 & 0 & 0 & 0 \\ & & 0 & 0 & \chi y_M D \\ & & & 0 & \chi y_N D \\ \text{symmetric} & & & & 0 \end{bmatrix}, \\
[D^{(0)}] &= \begin{bmatrix} \chi^2 D & 0 & \chi^2 y_M D & \chi^2 y_N D & 0 \\ & 0 & 0 & 0 & 0 \\ & & \chi^2(D_{yy} + y_M^2 D) & \chi^2(D_{yy} + y_M y_N D) & 0 \\ & & & \tilde{A} + \chi^2(D_{yy} + y_N^2 D) & 0 \\ & \text{symmetry} & & & 0 \end{bmatrix}, \\
\{p\} &= \begin{Bmatrix} (p_x + m'_y) \\ (p_y + m'_x + \chi(m_z + m'_\omega)) \\ (m_z + m'_\omega) \\ (\tilde{m}_z + \tilde{m}'_\omega) \\ (-p_z + \chi m_y) \end{Bmatrix},
\end{aligned}$$

and

$$\{\delta\} = [u_0 \ v_0 \ \theta \ \bar{\theta} \ w_0]^T. \quad (4.5)$$

By analogy with the treatment of straight box girders given in Chap. 2, we can obtain the element stiffness matrix and the element load column vector:

$$[K]_e = \int_0^e [N]^T [L] [N] d\bar{z}, \quad (4.6)$$

$$\{F\}_p^e = \int_0^e [N]^T \{p\} d\bar{z}. \quad (4.7)$$

### 4.1.3 Boundary Conditions

From different support conditions we can obtain different boundary conditions.

For the cross-section at a fixed support, the vertical displacement, the horizontal radial displacement, the rotation, the distortion, and the longitudinal displacement

are not allowed. For this case the boundary conditions can be expressed as

$$\begin{aligned} [u_0] = 0 \quad [v_0] = 0 \quad [\theta] = 0 \quad [\tilde{\theta}] = 0 \quad [w_0] = 0 \\ [u'_0] = 0 \quad [v'_0] = 0 \quad [\theta'] = 0 \quad [\tilde{\theta}'] = 0. \end{aligned} \quad (4.8)$$

For the cross-section at a simple support, the vertical and horizontally radial displacements are suppressed, and for an end diaphragm with infinite stiffness in its own plane while the out-plane stiffness is zero, the section cannot be rotated and distorted but can freely warp. Hence, the boundary conditions are

$$\begin{aligned} [u_0] = 0 \quad [v_0] = 0 \quad [\theta] = 0 \quad [\tilde{\theta}] = 0 \quad [w_0] = 0 \\ [u''_0] = 0 \quad [v''_0] = 0 \quad [\theta''] = 0 \quad [\tilde{\theta}''] = 0 \quad [w'_0] = 0. \end{aligned} \quad (4.9)$$

#### 4.1.4 Evaluation of Displacements and Stresses

In an identical manner as for straight box girders, we can obtain the equilibrium equations for all nodes in the form of

$$[K]\{\delta\} = \{F\}_p. \quad (4.10)$$

After solving the above equations on which boundary conditions have been imposed, we obtain at each node lateral displacement  $u_0$ , vertical displacement  $v_0$ , angle of twist  $\theta$ , distortion  $\tilde{\theta}$ , and longitudinal displacement  $w_0$  as well as their first and second derivatives.

Then we can further evaluate normal stresses over each specified cross-section according to Eqs. (3.28):

$$\sigma_z = -E(1 + \chi_x)[\tilde{x}]\{k\},$$

where  $\chi$ ,  $[\tilde{x}]$ ,  $\{k\}$  are given in Eqs. (3.5), (3.12), (3.14).

To verify the accuracy of the finite beam element method, the differential equations of curved box girders have been converted into a set of differential equations of first order and then solved analytically. The results from a numerical example by the analytical method and the finite beam element method reveal that they have a very good agreement.

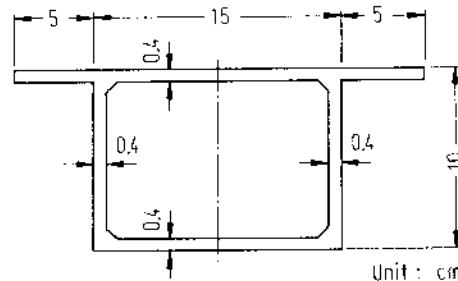


Fig. 4.2. Dimensions of the model cross section

### 4.2 Model Test

To verify the reliability of theoretical analyses, a test was performed with a girder model made of Perspex.

Dimensions of the constant cross-section of the model are indicated in Fig. 4.2.

The axial line of the box girder is a circular curve with radius  $R_0 = 160$  cm. The angle is  $60^\circ$  between the two radial lines that coincide with the two end cross-sections. End diaphragms were placed at the two ends of the girder. The girder was supported on both ends, one of which was on two linking rods and the other on two bearings.

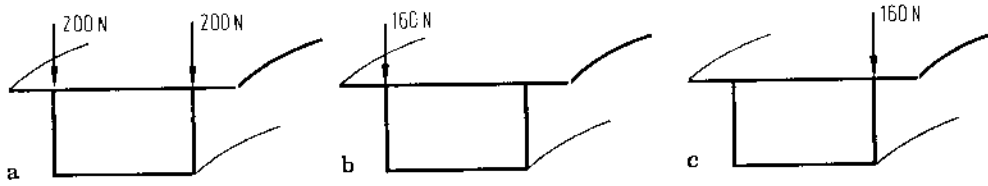


Fig. 4.3a-c. Three loading cases

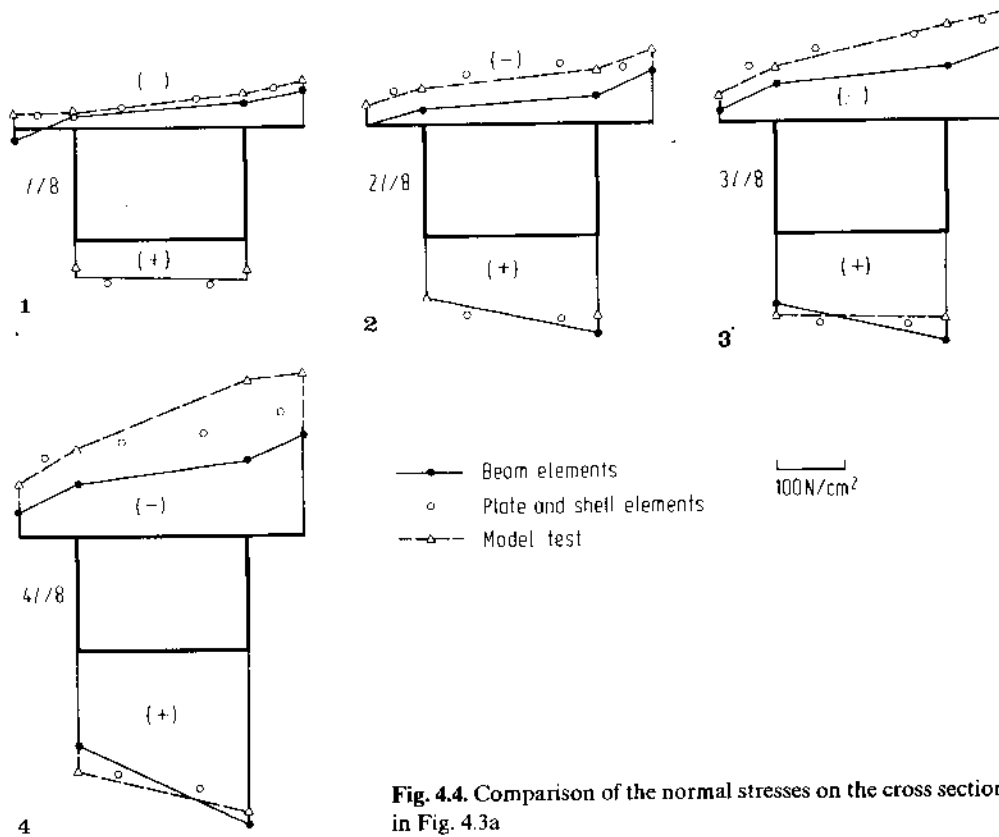


Fig. 4.4. Comparison of the normal stresses on the cross sections in Fig. 4.3a

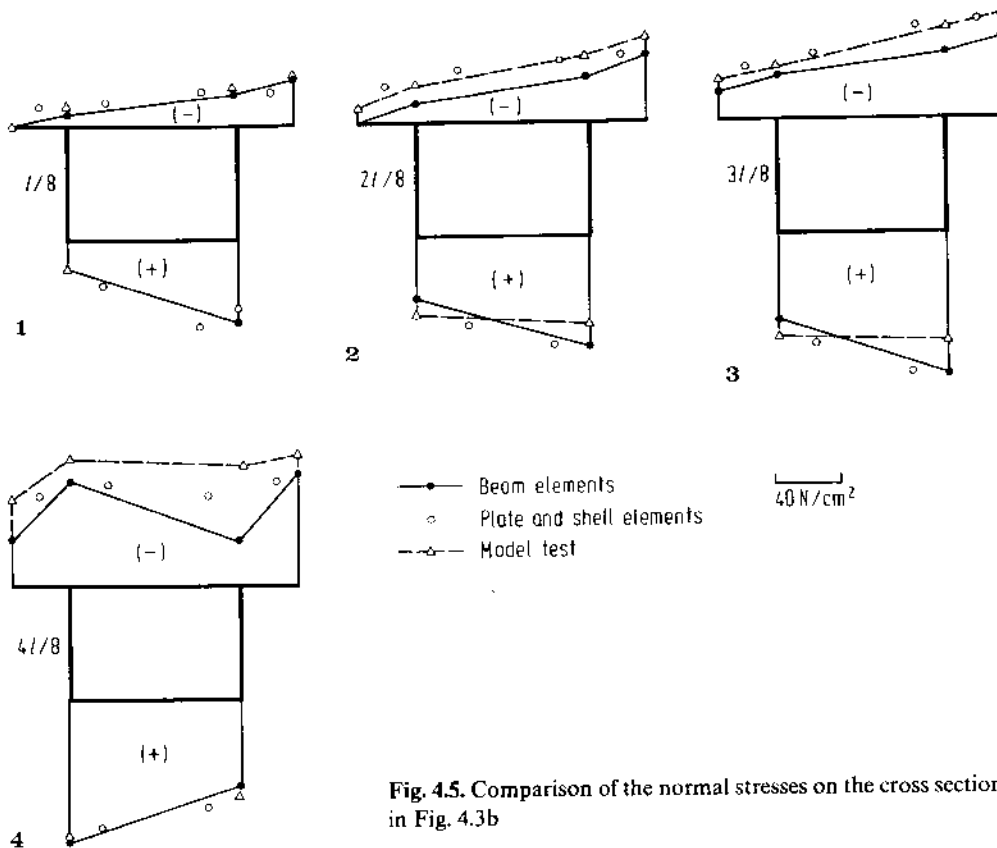


Fig. 4.5. Comparison of the normal stresses on the cross sections in Fig. 4.3b

The modulus of elasticity of the Perspex used in the model is  $E = 2943$  MPa and its Poisson's ratio is  $\mu = 0.4$ .

Loads were applied at the mid-span. For the three cases of loading, shown in Fig. 4.3, we took the strain measurements.

To verify the accuracy of the results obtained by the finite beam element method, the comparison of the results obtained by the FEM of beam elements, the FEM of plate and shell, and the model test is given in Figs. 4.4 to 4.6 for three loading cases. The stresses at the control points on the radical cross-sections at  $\frac{1}{8}L$ ,  $\frac{2}{8}L$ ,  $\frac{3}{8}L$  and  $\frac{4}{8}L$  are shown in the figures. From the figures it can be observed that the distributions of the stresses obtained by the two methods agree well with those from the model test. The relative error between the theoretical and the experimental values is within the range of  $\pm 20\%$  with a few exceptions.

The analysis of the model by the finite element method of plate and shell is accomplished with the aid of the Structure Analysis Programme SAP5. The finite beam element method presented herein is superior to the finite element method of plate and shell in the reduction of the necessary ROM storage and computer time, in the simplicity of input data, and in the clarity of output data.

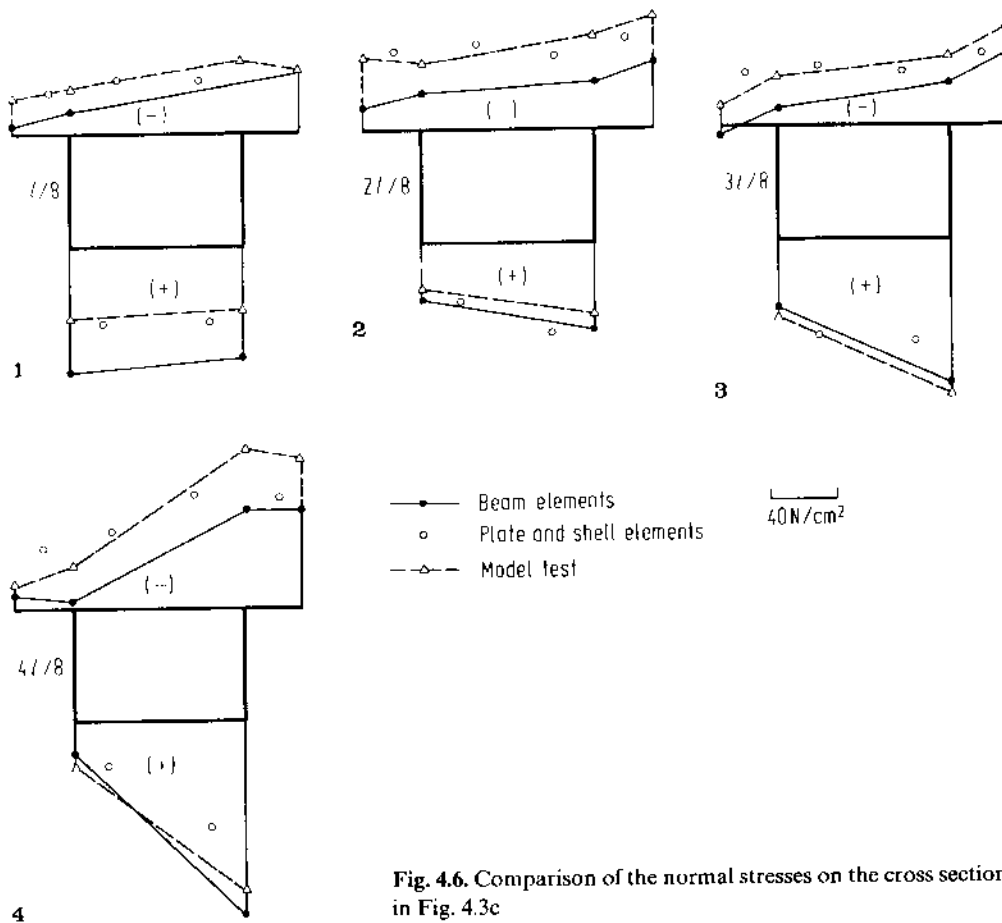


Fig. 4.6. Comparison of the normal stresses on the cross sections in Fig. 4.3c

### 4.3 Influence of Curvature on Normal Stresses

The influence of the curvature of a curved box girder on normal stresses is illustrated with a specific numerical example.

Figure 4.7 shows a cross-section of a steel box girder with the length of the curved axis being 24.0 m. The girder is simply supported at two ends and has diaphragms at the ends and mid-span. Under vertical loads uniformly distributed on the whole

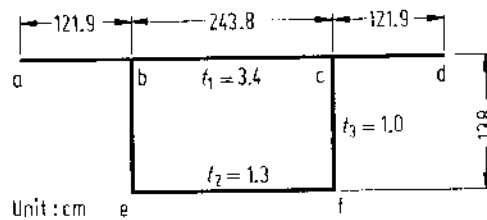
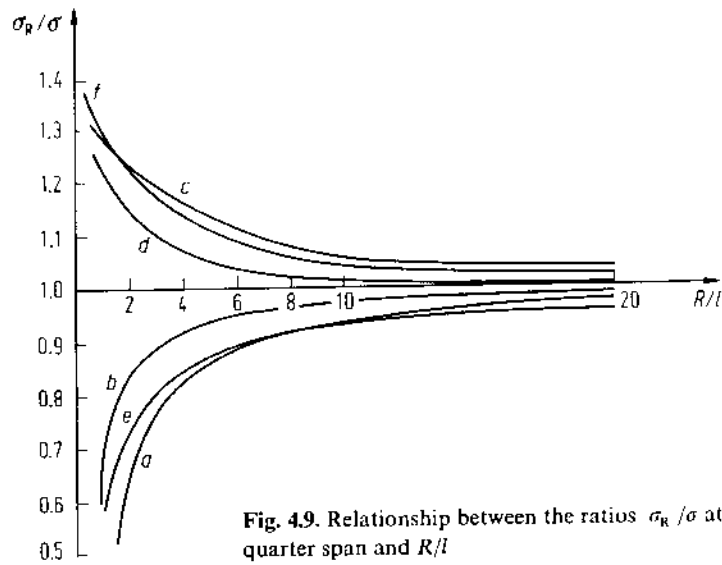
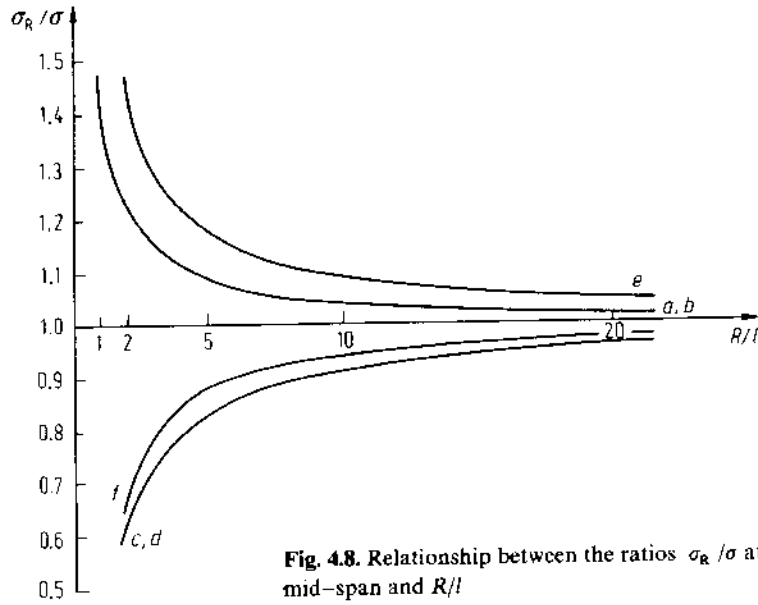


Fig. 4.7. Cross section of a steel box girder



girder, the normal stresses  $\sigma_R$  at the specified points on cross-sections at mid-span and quarter point with variation of the curvature are evaluated. Figures 4.8 and 4.9 show that relationship between  $\sigma_R/\sigma$ , the ratio of the whole normal stress  $\sigma_R$  in curved girders due to curvatures to the stress  $\sigma$  (bending only!) in corresponding straight girder ( $R \rightarrow \infty$ ), and  $R/l$ , the ratio of the radius  $R$  to the length  $l$  of the girder.

From Figs. 4.8 and 4.9 it can be observed that the normal stresses caused by warping torsion and cross-sectional distortion decrease with the curvature of the



box girder, and when  $R/l > 5$ ,  $|(\sigma_R - \sigma)/\sigma| < 20\%$ ; when  $R/l > 10$ ,  $|(\sigma_R - \sigma)/\sigma| < 10\%$ ; when  $R/l > 10$ ,  $|(\sigma_R - \sigma)/\sigma| < 5\%$ .

#### 4.4 Influence of the Number of Diaphragms

We assume that the girder of Fig. 4.7 has two more diaphragms placed at  $\frac{1}{4}l$  and  $\frac{3}{4}l$  and analyze the ratios of the normal stresses  $\sigma_R/\sigma$  as a function of  $R/l$ . The results are given in Figs. 4.10 and 4.11. It can be seen that when  $R/l \geq 2$ ,  $|(\sigma_R - \sigma)/\sigma| < 10\%$  and when  $R/l > 5$ ,  $(\sigma_R - \sigma)/\sigma \approx 1$ . The comparison of Figs. 4.10 and 4.11 with Figs. 4.8 and 4.9 reveals that for a steel box girder it is efficient to reduce the normal stresses due to distortion and warping torsion by suitably increasing the number of intermediate diaphragms.

To find out how many diaphragms should be set in a box girder, we have analyzed the girder, shown in Fig. 4.7, with seven intermediate diaphragms placed at equal intervals along the span in addition to the two end diaphragms.

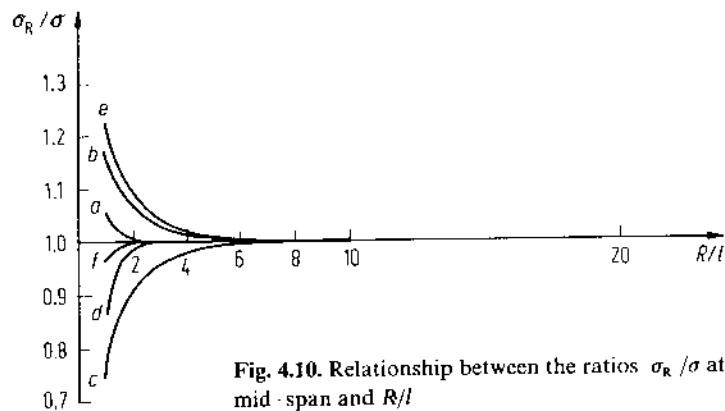


Fig. 4.10. Relationship between the ratios  $\sigma_R/\sigma$  at mid-span and  $R/l$

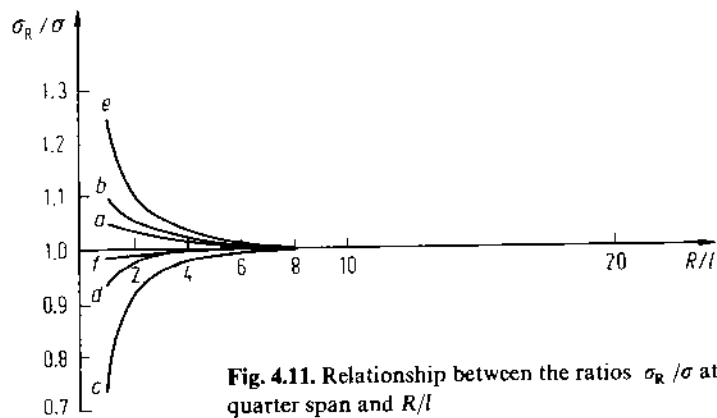


Fig. 4.11. Relationship between the ratios  $\sigma_R/\sigma$  at quarter span and  $R/l$

The results obtained are practically the same as those for the girder with three intermediate diaphragms. This fact shows that installing too many diaphragms is unnecessary.

#### 4.5 Influence of Thickness of Plates of Box Girders

Figure 4.12 shows a cross-section of a concrete box girder, which is identical with that of Fig. 4.7 except for the thicknesses of plates. For the same conditions as those in Sect. 4.3 the ratios of normal stresses  $\sigma_R / \sigma$  as a function of  $R/l$  are calculated and plotted in Figs. 4.13 and 4.14 for the cross-section at the mid-span and at quarter point, respectively.

From Figs. 4.13 and 4.14 it can be observed that for the concrete box girder in Fig. 4.12, with two end and one mid-span diaphragms and under uniform loads,  $|(\sigma_R - \sigma)/\sigma| < 10\%$ , when  $R/l > 5$ , and  $|(\sigma_R - \sigma)/\sigma| < 5\%$ , when  $R/l > 10$ ; they are

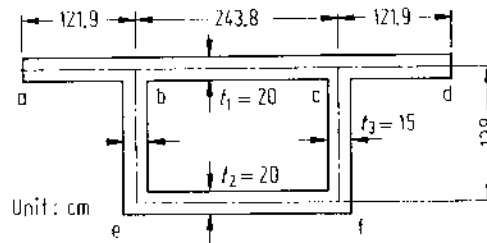


Fig. 4.12. Cross section of a concrete box girder

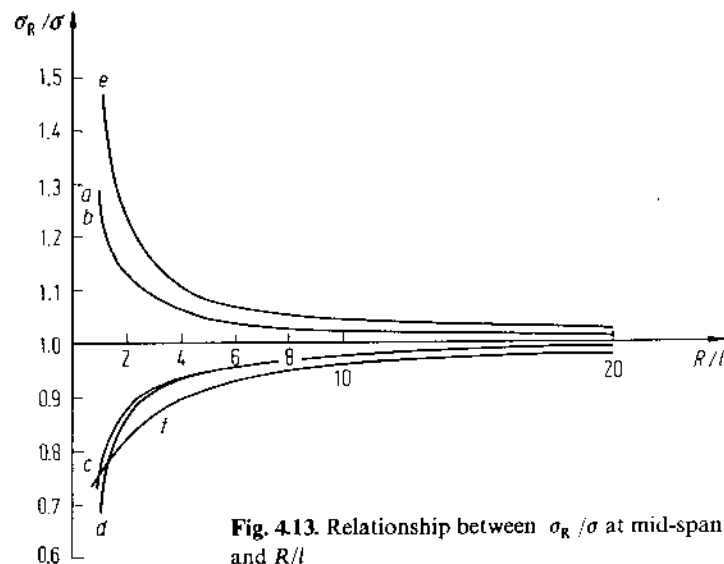


Fig. 4.13. Relationship between  $\sigma_R / \sigma$  at mid-span and  $R/l$

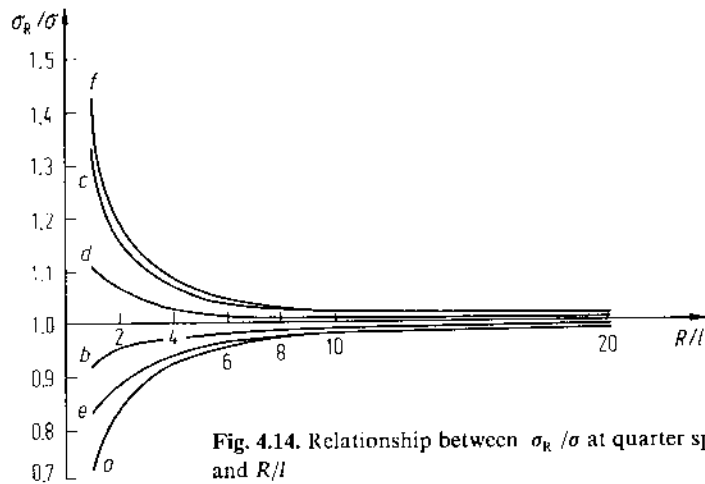


Fig. 4.14. Relationship between  $\sigma_R/\sigma$  at quarter span and  $R/l$

about half of those for the corresponding steel box girder (see Figs. 4.8 and 4.9). The reason for this is that owing to the increase in the thicknesses of plates of the box girder, the torsion and distortion rigidities of cross-section are increased and, consequently, the deformations and the normal stresses due to torsion and distortion of cross-section decrease.

#### 4.6 Effect of the Variation of $R$ Along the Width of Cross-section

The effects of the variation of  $R$  along the width on normal stresses is analyzed for the same box girder shown in Fig. 4.7 by considering  $R = R_0 = \text{const}$  and  $R(x)$  variable; the stresses obtained are  $\sigma_{RC}$  and  $\sigma_{RV}$ . The relationship between  $\sigma_{RC}/\sigma_{RV}$  and  $R_0/B$ , ratio of curvature  $R_0$  to the width of the bridge  $B$ , is shown in Fig. 4.15,

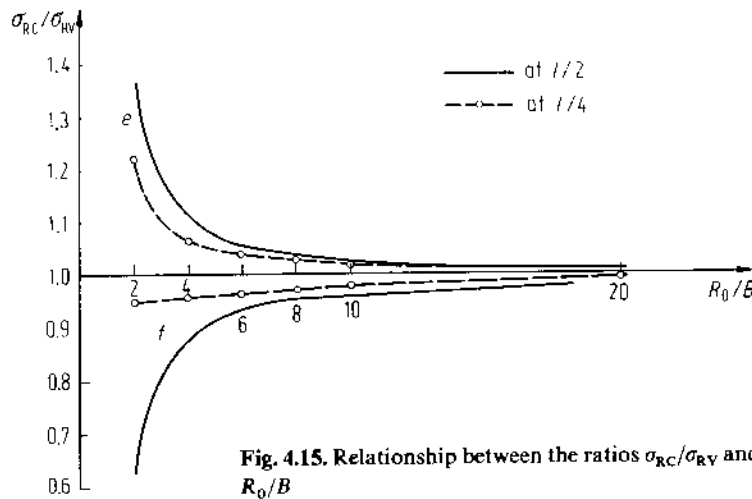


Fig. 4.15. Relationship between the ratios  $\sigma_{RC}/\sigma_{RV}$  and  $R_0/B$

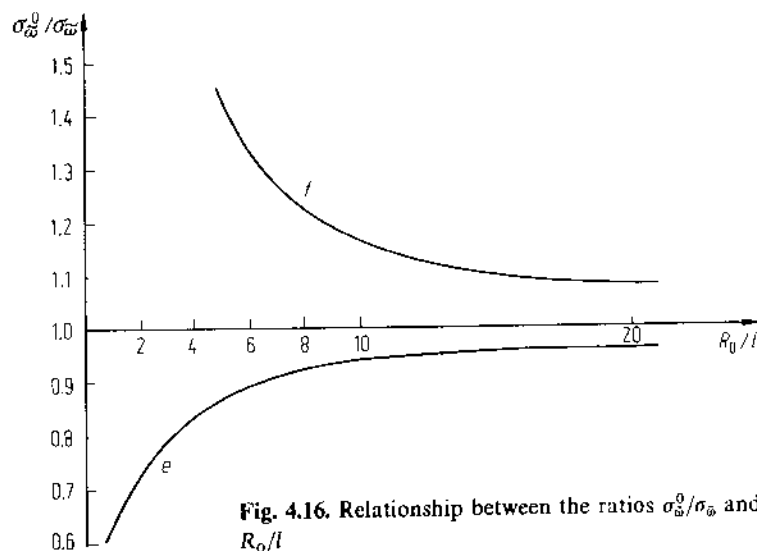
in which solid lines  $e$  and  $f$  refer to points  $e$  and  $f$  in the bottom flange of the cross-section at mid-span, and dotted lines  $e$  and  $f$  refer to the corresponding points at quarter span. From the figure it can be seen that when  $R_0/B > 10$ , the relative error caused by disregarding the variation of  $R$  along the width is less than 5 percent.

#### 4.7 Influence of Coupling on Distortion

For straight box girders, the error in distortional normal stress  $\sigma_{\bar{\omega}}$  caused by disregarding the coupling effect of distortion  $\tilde{\theta}$  of cross-section with angle of twist  $\theta$  is usually not greater than 5%, while for horizontally curved box girders the error is greater because the coupling is extended to other displacements owing to the initial curvature of girder, see Eq. (4.4). The same girder discussed in Sect. 4.3 under uniformly distributed load on a half bridge width along the span was investigated. Let  $\sigma_{\bar{\omega}}$  and  $\sigma_{\bar{\omega}}^0$  denote the distortional normal stresses obtained by considering and neglecting the effect of coupling of  $\tilde{\theta}$  with other displacements; the relationship between  $\sigma_{\bar{\omega}}^0/\sigma_{\bar{\omega}}$  and  $R_0/l$  is shown in Fig. 4.16. It can be seen that the errors in distortional normal stress  $\sigma_{\bar{\omega}}$  caused by neglecting the effect of coupling of  $\tilde{\theta}$  with other displacement components are < 20% when  $R_0/l > 10$ , and < 10%, when  $R/l > 20$ , i.e., they are greater than those for straight box girders.

#### 4.8 Effect of Shear Strain $\gamma_w$ on Warping Torsion

To assess the effect of shear strain  $\gamma_w$  on the warping torsion in a curved box girder, the stresses  $\sigma_{\omega}$  and  $\sigma_{\omega}^0$  for the two cases, with and without consideration of  $\gamma_w$ , in



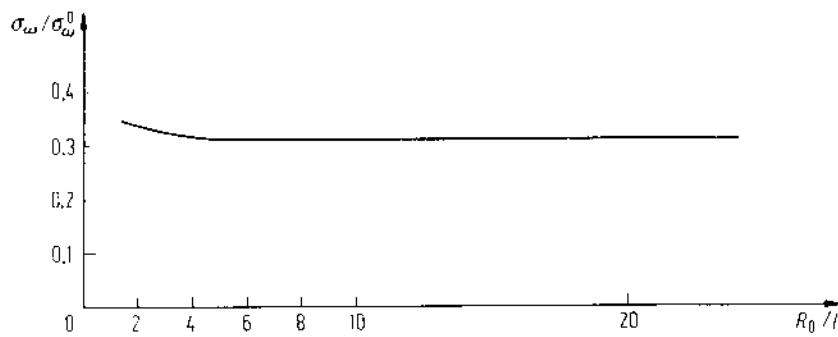


Fig. 4.17. Variation of  $\sigma_w/\sigma_w^0$  with  $R_0/l$

the numerical example in Sect. 4.3 with the assumption of rigid cross-section are evaluated under a concentrated torque applied at mid-span. The results shown in Fig. 4.17 reveal that, considering the effect of  $\gamma_w$ , the stresses  $\sigma_w$  due to warping torsion at mid-span are reduced close to that for a straight box girder, and the reduction is fundamentally independent of the curvature of girder.

## 5. Earthquake Response of Curved Box Girder Bridge

Earthquakes have caused bridge engineering professionals to reassess the design techniques that have been used for seismic design.

Culver (1967), Cheung and Cheung (1969), Heins (1979), and Rabizadeh and Shore (1975), have investigated the behavior of horizontally curved beams.

In this chapter, the formulation of the finite element and the method for the response of curved box girders, modeled as a one dimensional beam, will be presented. Consider first the original curved box girder bridge system, beam and columns, as in Fig. 5.1a, this system will be modeled as a combination of beam element connected with the pier element to form the entire structure, as shown in Fig. 5.1b. With this basic modeling, the dynamic response of the entire structure will be examined.

### 5.1 Finite Element Method

In developing the response of the curved bridge it is convenient to use curvilinear coordinates, shown in Fig. 5.2, where  $n, y$  is the vertical direction,  $r, x$  is the radial direction,  $z$  is the longitudinal direction, and  $u, v, w$  are displacements functions corresponding to  $r, n, z$  directions, and  $\theta$  is the transverse rotation function.

Assuming the box girder structure has a rigid internal diaphragm, and thus maintains its shape, the following displacement parameters  $\{\delta(z)\}$  can be used to describe the displacement model of the element;

$$\{\delta\} = \begin{Bmatrix} u \\ v \\ w \\ \theta \end{Bmatrix}. \quad (5.1)$$

#### 5.1.1 Stress-strain

The stresses induced on the curved element are represented by five actions or internal forces and can be described as follows:

$$\{\sigma\} = \begin{Bmatrix} M_y \\ M_x \\ N \\ T_c \\ M_\omega \end{Bmatrix}, \quad (5.2)$$

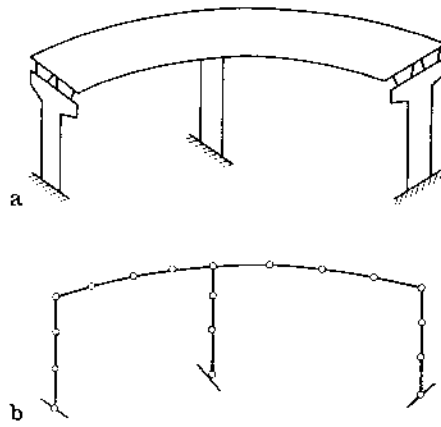


Fig. 5.1. a Original curved box girder system. b System idealization

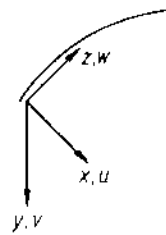


Fig. 5.2. Curvilinear coordinates

where  $M_y$  and  $M_x$  are the primary bending moments,  $N$  is the axial force,  $T_c$  is the pure torsional moment, and  $M_\omega$  is the bimoment. Neglecting the effect of nonlinear distribution of stresses due to curvature of girder, the strains related to deformation can be expressed as

$$\{\varepsilon\} = \begin{Bmatrix} u'' + \frac{w'}{R} \\ -v'' + \frac{\theta}{R} \\ -\frac{u}{R} + w' \\ \frac{v'}{R} + \theta' \\ -\frac{v''}{R} - \theta'' \end{Bmatrix} = \begin{bmatrix} d^2 & 0 & \frac{d}{R} & 0 \\ 0 & -d^2 & 0 & \frac{1}{R} \\ -\frac{1}{R} & 0 & d & 0 \\ 0 & \frac{d}{R} & 0 & d \\ 0 & -\frac{d^2}{R} & 0 & -d^2 \end{bmatrix} \begin{Bmatrix} u \\ v \\ w \\ \theta \end{Bmatrix} = [d] \{\delta\}, \quad (5.3)$$

where  $R$  is the radius of curvature and  $d = \partial/\partial z$ ,  $d^2 = \partial^2/\partial z^2$ . According to Hook's law, the stress-strain relationship for one-dimensional problems, is given by

$$\{\sigma\} [D] \{\varepsilon\}, \quad (5.4)$$

where  $\{\sigma\}$  and  $\{\varepsilon\}$  represent the induced internal forces and the corresponding strains, respectively; and  $[D]$  is rigidity matrix, given as

$$[D] = \begin{bmatrix} EF_{xx} & 0 & 0 & 0 & 0 \\ & EF_{yy} & 0 & 0 & 0 \\ & & EF & 0 & 0 \\ & & & GI_d & 0 \\ \text{symmetry} & & & & EF_{\omega\omega} \end{bmatrix}. \quad (5.5)$$

### 5.1.2 Displacement Functions

Normally, a beam element in space can be represented by six degrees of freedom — three translation displacements and three rotational displacements. However, additional degrees of freedom, for instance, due to warping, are required for curved bridge elements, which may be important and must be considered.

The expression for warping torsion of the nodal point displacements will include the parameter of variation of twist angle along the longitudinal direction of the beam, thus increasing the nodal point displacements to seven. However, in the following development displacements  $\delta_1, \delta_2, \dots, \delta_8$  will be used to express the joint  $i$  nodal displacement parameters, and  $\delta_9, \delta_{10}, \dots, \delta_{16}$  will be used to express joint  $j$  nodal point displacement parameters.

The nodal point displacements of the element can be given by

$$\{\delta\}^e = \begin{Bmatrix} \delta_i \\ \delta_j \end{Bmatrix}, \quad (5.6)$$

where

$$\{\delta_i\} = \begin{Bmatrix} \delta_1 \\ \delta_2 \\ \vdots \\ \delta_8 \end{Bmatrix}, \quad \{\delta_j\} = \begin{Bmatrix} \delta_9 \\ \delta_{10} \\ \vdots \\ \delta_{16} \end{Bmatrix},$$

where  $\delta_1, \delta_2, \delta_3, \delta_9, \delta_{10}$ , and  $\delta_{11}$  are translational displacements;  $\delta_4, \delta_5, \delta_6, \delta_{12}, \delta_{13}$ , and  $\delta_{14}$  are rotational displacements;  $\delta_8$  and  $\delta_{16}$  are the first derivatives of torsion angle along the longitudinal direction of the beam, which accounts for warping torsional influence;  $\delta_7$  and  $\delta_{15}$  are the curvature of the element. These nodal displacements are shown in Fig. 5.3.

Polynomials are assumed for the one-dimensional displacement model; a third and a fifth order polynomial are assumed for the displacement functions for  $\theta$  and  $u$ ; and a linear displacement function is assumed for  $w$ . Thus the following displacement matrix is obtained:

$$\{\delta\} = [N] \{\delta\}^e, \quad (5.7)$$

where



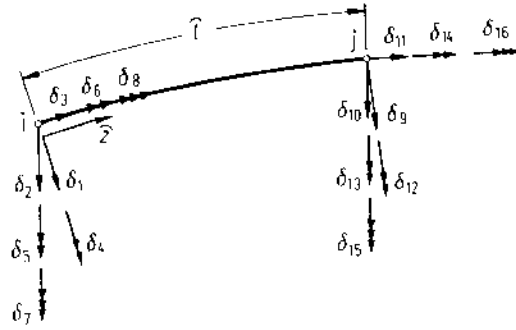


Fig. 5.3. Nodal displacements of the element

$$[N] = \begin{bmatrix} N_7 & 0 & 0 & 0 & N_8 & 0 & N_9 & 0 & N_{10} & 0 & 0 & 0 & N_{11} & 0 & N_{12} & 0 \\ 0 & N_1 & 0 & N_2 & 0 & 0 & 0 & 0 & 0 & N_3 & 0 & N_4 & 0 & 0 & 0 & 0 \\ 0 & 0 & N_5 & 0 & 0 & 0 & 0 & 0 & 0 & 0 & N_6 & 0 & 0 & 0 & 0 & 0 \\ 0 & 0 & 0 & 0 & 0 & N_1 & 0 & N_2 & 0 & 0 & 0 & 0 & 0 & N_3 & 0 & N_4 \end{bmatrix},$$

and

$$\left. \begin{aligned} N_1 &= 1 - 3z^2 + 2z^3, \\ N_2 &= (z - 2z^2 + z^3)\hat{l}, \\ N_3 &= (3z^2 - 2z^3), \\ N_4 &= (-z^2 + z^3)\hat{l}, \\ N_5 &= 1 - z, \\ N_6 &= z, \\ N_7 &= 1 - 10z^3 + 15z^4 - 6z^5, \\ N_8 &= (z - 6z^3 + 8z^4 - 3z^5)\hat{l}, \\ N_9 &= \frac{1}{2}(z^2 - 3z^3 + 3z^4 - z^5)\hat{l}^2, \\ N_{10} &= 10z^3 - 15z^4 + 6z^5, \\ N_{11} &= (-4z^3 + 7z^4 - 3z^5)\hat{l}, \\ N_{12} &= \frac{1}{2}(z^3 - 2z^4 + z^5)\hat{l}^2, \end{aligned} \right\} \quad (5.8)$$

where  $z = \hat{z}/\hat{l}$ ,  $\hat{l} = 2\hat{\lambda}$  = length of the element.

### 5.1.3 Nodal Forces and Element Stiffness Matrix

Assuming a uniform load  $p$  acts on the elements,

$$\{p\} = \begin{Bmatrix} p_x \\ p_y \\ p_z \\ m_z \end{Bmatrix}, \quad (5.9)$$

where  $p_x$ ,  $p_y$ , and  $p_z$  are the uniform loads in the  $x$ ,  $y$ , and  $z$  directions and  $m_z$  is the uniform torque. Assuming a virtual displacement  $\{\delta^*\}$  and a corresponding virtual strain  $\{\varepsilon^*\}$ , the total work done by the stress (internal work) and uniform load (external work) is computed as

$$W = \int \{\varepsilon^*\}^T \{\sigma\} dz - \int \{\delta^*\}^T \{p\} dz . \quad (5.10)$$

Using the nodal point displacements to express the preceding equation gives  $\{\delta^*\} = [N]\{\delta^*\}^e$ , and substituting in Eqs. (5.3) and (5.7) gives

$$\{\varepsilon\} = [d]\{\delta\} = [d][N]\{\delta\}^e , \quad (5.11)$$

or

$$\{\varepsilon^*\} = [B]\{\delta^*\}^e ,$$

where

$$[B] = [d][N] . \quad (5.12)$$

Substituting (5.11) into (5.4) gives

$$\{\sigma\} = [D][B]\{\delta\}^e \quad (5.13)$$

Substituting (5.13), (5.7), and (5.11) into (5.10) gives

$$W = \{\delta^*\}^{eT} \int [B]^T [D] [B] dz \{\delta\}^e - \{\delta^*\}^{eT} \int [N]^T \{p\} dz \quad (5.14)$$

The element stiffness matrix and equivalent nodal point load matrix are therefore

$$\{F\}^e = [K]\{\delta\}^e - \{p\}^e ,$$

where

$$[K]^e = \int [B]^T [D] [B] dZ , \quad (5.15)$$

and

$$\{p\}^e = \int [N]^T \{p\} dZ , \quad (5.16)$$

the element stiffness matrix is obtained by substituting  $[B]$  and  $[D]$  into Eq. (5.15) and integrating.

#### 5.1.4 Element Mass Matrix

The influence of earthquake loading, using Newton's second law and considering the eccentricity of centroidal axes and shear center, will now be calculated. These inertia loads include element vibration acceleration ( $q_v$ ) and earthquake acceleration ( $q_g$ ) loads and can be expressed as

$$\{p\} = \{q_v\} + \{q_g\} . \quad (5.17)$$

Consider first the element vibrations ( $q_v$ ). Examination of Fig. 5.4 shows the eccentricity  $e = y_M$  between the centroidal  $O$  and shear center  $M$ , where the radial

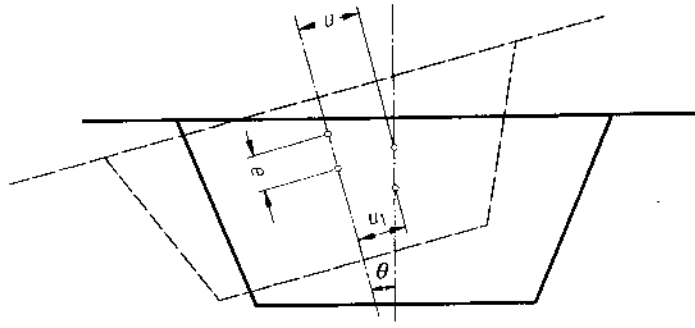


Fig. 5.4. Motions of a cross section

acceleration is given by  $\frac{\delta^2 u_1}{\delta t^2} = \frac{\delta^2 u}{\delta t^2} + \frac{\delta^2 \theta}{\delta t^2} e$ . The radial horizontal inertia force is therefore

$$q_{vx} = -\rho A_m \ddot{u}_1. \quad (5.18)$$

Similarly  $q_{vx}$  produces a torsion of  $-q_{vx} \cdot e$ ; therefore, the torsional inertia force is

$$q_{v\theta} = -(\rho I_m \ddot{\theta} + q_{vx} \cdot e). \quad (5.19)$$

The total acceleration of element vibration  $q_v$  is therefore

$$\{q_v\} = \begin{Bmatrix} q_{vx} \\ q_{vy} \\ q_{vz} \\ q_{v\theta} \end{Bmatrix} = -\rho [A] \{\ddot{\delta}\} = -\rho [A] [N] \{\ddot{\delta}\}^e, \quad (5.20)$$

where

$$[A] = -\rho \begin{bmatrix} A_m & 0 & 0 & -A_m e \\ 0 & A_m & 0 & 0 \\ 0 & 0 & A_m & 0 \\ -A_m e & 0 & 0 & I_m + A_m e \end{bmatrix},$$

where  $\rho$  = unit volume mass,  $A_m$  = cross section in calculating mass,  $I_m$  = mass moment of inertia. Substituting  $q_v$  into (5.17) and (5.16), the equivalent inertia force as a nodal point load is described as

$$\{p\}_v = -[m] \{\ddot{\delta}\}^e, \quad (5.21)$$

where

$$[m] = \int [N]^T \rho [A] [N] dz, \quad (5.22)$$

and  $[m]$  is element mass matrix.

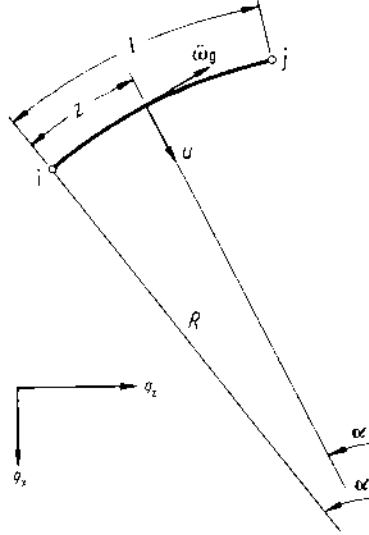


Fig. 5.5. Relationships between cartesian coordinates and curvilinear coordinates

### 5.1.5 Seismic Mass Matrix

In developing the seismic mass matrix in curvilinear coordinates, the earthquake accelerations  $\ddot{g}_x$  and  $\ddot{g}_z$  oriented in the cartesian coordinate system,  $x$  and  $z$ , must be transformed into radial and tangential directions. As shown in Fig. 5.5, the geometrical relationships can be written as:

$$\begin{aligned}\ddot{u}_g &= \ddot{g}_x \cos \alpha + \ddot{g}_z \sin \alpha, \\ \ddot{v}_g &= \ddot{g}_y, \\ \ddot{w}_g &= -\ddot{g}_x \sin \alpha + \ddot{g}_z \cos \alpha, \\ \ddot{\theta} &= 0.\end{aligned}\quad (5.23)$$

As given by Eq. (5.20), the ground acceleration load matrix  $q_g$  can similarly be written as

$$\begin{aligned}\{q_g\} &= \begin{Bmatrix} q_{gx} \\ q_{gy} \\ q_{gz} \\ q_{g\theta} \end{Bmatrix} = -\rho A_m \begin{bmatrix} \cos \alpha & 0 & \sin \alpha \\ 0 & 1 & 0 \\ -\sin \alpha & 0 & \cos \alpha \\ -e \cos \alpha & 0 & -e \sin \alpha \end{bmatrix} \begin{Bmatrix} \ddot{g}_x \\ \ddot{g}_y \\ \ddot{g}_z \end{Bmatrix} \\ &= -\rho A_m [T] \{\ddot{g}\}.\end{aligned}\quad (5.24)$$

Now, substituting Eq. (5.24) into Eq. (5.16) gives the equivalent earthquake inertia load:

$$\{p\}_g = -\rho A_m \int [N]^T [T] dz \{\ddot{g}\} = -[g_m] \{\ddot{g}\}, \quad (5.25)$$

where

$$[g_m] = \rho A_m \int [N]^T [T] dz .$$

### 5.1.6 Pier Element and Coordinate Transformation

The basic pier element is a straight element. Therefore, the basic curved beam element matrix can be used to develop the local stiffness matrix  $[K_p]$  and mass matrix  $[m_p]$  for the pier element by letting  $R \rightarrow \infty$ . However, the pier has to be transformed from the local coordinate into the global coordinate, by using the following formula:

$$\{\delta_p\}^e = [L] \{\delta\}^e , \quad (5.26)$$

where  $[L]$  is the coordinate transformation matrix:

$$[L] = \begin{bmatrix} L_i & 0 \\ 0 & L_j \end{bmatrix} , \quad (5.27)$$

$$[L_i] = [L_j] = \begin{bmatrix} 1 & 0 & 0 & 0 & 0 \\ 0 & 0 & -1 & 0 & 0 \\ 0 & 1 & 0 & 0 & 0 \\ 0 & 0 & 0 & 1 & 0 & 0 \\ 0 & 0 & 0 & 0 & -1 & 0 \\ 0 & 0 & 0 & 0 & 0 & 1 \end{bmatrix}$$

The stiffness and mass matrix for the global coordinate system, for the pier element, are, therefore,

$$[k_p]_g = [L]^T [k_p] [L] , \quad (5.28)$$

$$[m_p]_g = [L]^T [m_p] [L] . \quad (5.29)$$

The inertia force components of the pier due to earthquake acceleration can be calculated by using the following local coordinate system formula:

$$\{q\} = -\rho A_m \begin{bmatrix} \cos \alpha_1 & 0 & \sin \alpha_1 \\ \sin \alpha_1 & 0 & -\cos \alpha_1 \\ 0 & 1 & 0 \\ 0 & 0 & 0 \end{bmatrix} \{\bar{g}\} = -\rho A_m [T_p] \{\bar{g}\} , \quad (5.30)$$

where  $\alpha_1$  is a constant, as shown in Fig. 5.6.

Substituting Eq. (5.30) into Eq. (5.16) and integrating, gives the seismic mass matrix  $[g_{mp}]$  for the pier element. The local coordinate transformation into the global coordinate system is obtained from

$$[g_{mp}]_g = [L]^T [g_{mp}] . \quad (5.31)$$

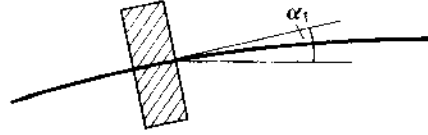


Fig. 5.6. Angle  $\alpha_1$  between the tangent direction and the z-direction

### 5.1.7 Dynamic Global Equations and Earthquake Response

By using the general dynamic equilibrium equation, assembling the stiffness, mass, and seismic matrices, and introducing the damping  $[C]$ , the following global equation is obtained:

$$[M]\{\ddot{\delta}\} + [C]\{\dot{\delta}\} + [K]\{\delta\} = -[G_m]\{\ddot{g}(t)\}, \quad (5.32)$$

when  $[M]$ ,  $[C]$ , and  $[K]$  are, respectively, the mass, damping, and stiffness matrices in global coordinate;  $[G_m]$  is the seismic mass matrix represented in the global coordinate system; and  $\{\ddot{g}(t)\}$  represents the three directional ground accelerations.

In solving the bridge problem, the following set of boundary conditions will be assumed;

1) beam: hinge:  $\delta_1 = 0, \delta_2 = 0, \delta_3 = 0, \delta_6 = 0,$  and  $\delta_7 = 0,$

roller:  $\delta_1 = 0, \delta_2 = 0, \delta_6 = 0,$  and  $\delta_7 = 0;$

2) beam and pier:

*fixed end:*  $\delta_1 = \delta_2 = \delta_3 = \delta_4 = \delta_5 = \delta_6 = 0.$

Now using the eigenvector matrix, as obtained from the free vibration equations, the earthquake responses of the structure in the elastic range can be determined by means of modal analysis. If the response to a specific earthquake record is required, Eq. (5.32) will be solved step by step for successive time intervals  $\Delta t$ .

## 5.2 Example

The bridge shown in Fig. 5.7 consists of a three-span continuous curved-beam bridge, with the end hinged and with all the other supports on rollers. The span lengths are 30.48 m, 30.48 m, 30.48 m; the radius is 182.88 m; and the pier height is 9.14 m.

The bridge was modeled with 16 nodes and 13 elements, as shown in Fig. 5.8, and investigated with the method presented here. It was also calculated as a space frame system with six degrees of freedom at each node by using the SAP IV program.

The results obtained by both methods agree well. For example, Figs. 5.9a-h illustrate the natural frequencies  $\omega_i$  (cps) and the mode shapes that occur in the radial direction (1, 4, 7), in the vertical direction (2, 3, 5, 8), and in the axial direction (6).

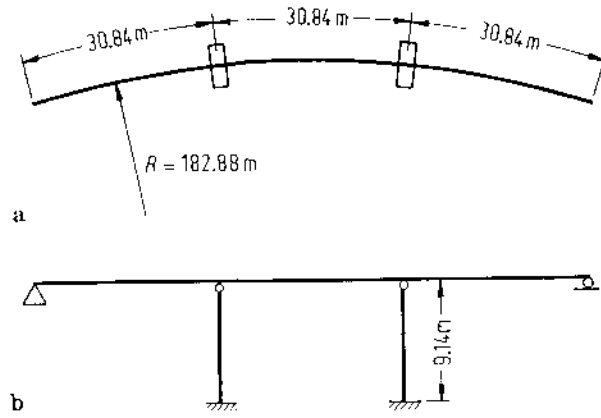


**Fig. 5.7a, b.** A three-span continuous curved-beam bridge. **a** Plan view. **b** Elevation

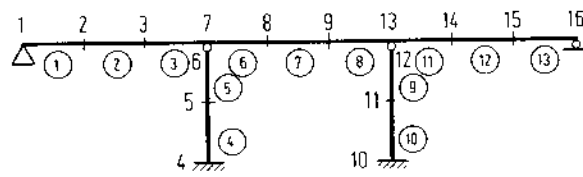


**Fig. 5.8.** Numbering of nodes and elements

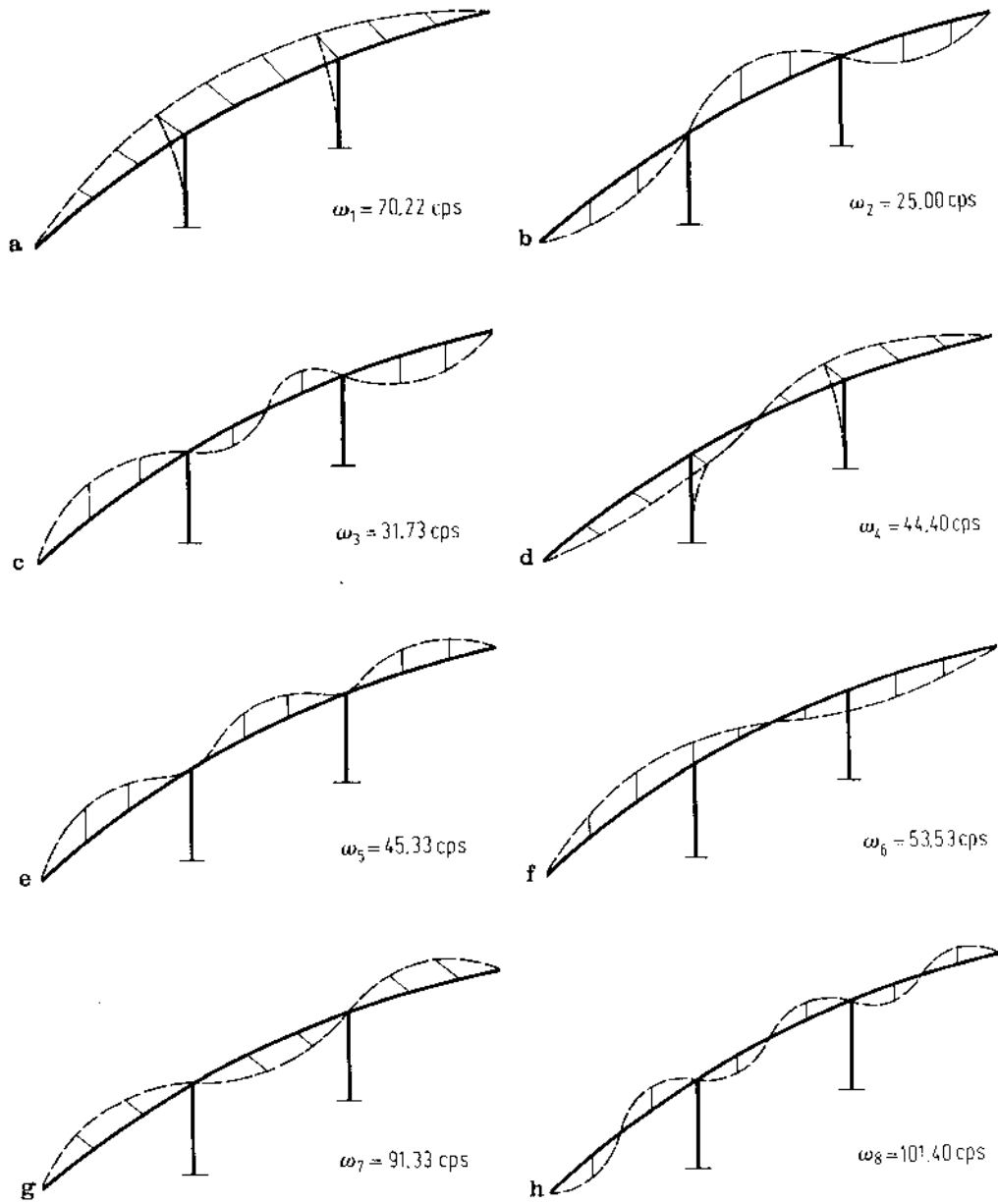


Fig. 5.9a-h. Nature frequencies  $\omega_i$  (cps) and the corresponding mode shapes



## 6. Bending and Torsion Theories of Truss Bridges

### 6.1 Introduction

The truss bridge, as shown in Fig. 6.1, is a spatial structure. When analyzing its bending and torsion according to classical structural theory, it is treated as a system consisting mainly of axially stressed members. This method, however, has its shortcomings. It involves a large amount of computation work and needs a large capacity computer, especially when performing the dynamic analysis; in addition, the method cannot show the influence of the constituent parts of a truss bridge, such as chord members, web members, lateral bracings, sway bracings, and portals, on the static and dynamic behavior of the structure as a whole. Furthermore, the method is not applicable to the truss bridges developed since the 1950s, which have steel deck plates as chords, see Fig. 6.2.

To overcome these shortcomings, Li (1975, 1978) extended the differential equation method developed for analyzing plane trusses (Li (Li) 1944, 1949) to the analysis of the spatial truss bridge structures. This approach is, in fact, an extension of the theory of the thin-walled box girder, the structural particularity of truss bridges being taken into account as will be shown in the following.

The basic idea is to convert the discrete structure of a truss bridge into a continuous model by transforming the web members into equivalent continuously distributed shear webs and the sway bracings into continuously distributed diaphragms. The portals are considered as elastic end supports. For inclined portals, the end parts of the truss may be considered as substructures.

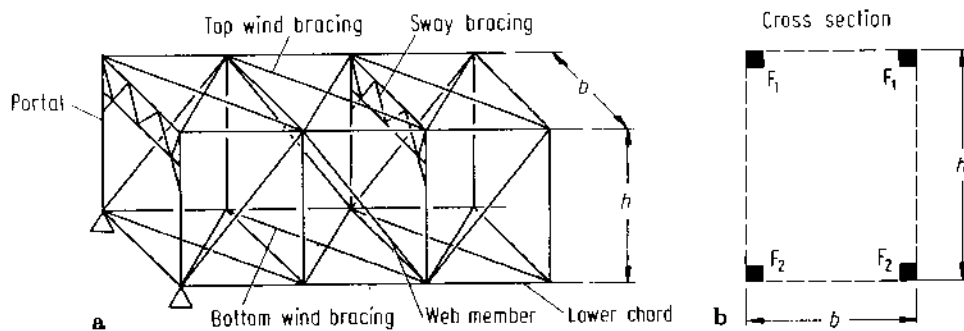


Fig. 6.1a,b. Constituent parts of a truss bridge

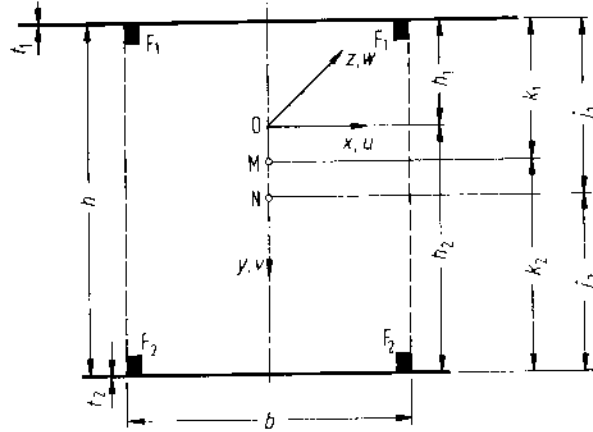


Fig. 6.2. A truss cross-section with steel deck plates

Because of their considerable magnitude and influence, the shear strains caused by the shear stresses due to bending and warping torsion in the webs of the truss must be taken into account. As mentioned and shown in Chap. 1, there are theories of bending and torsion established by introducing the shear deformations, in addition to other displacements or deformations, as new parameters. The influence of the shear strains is considered in another way given here (Li 1975) by using modification factors  $\mu$  for rigidities of bending and warping torsion, and thus without using additional displacement parameters.

Referring to Eqs. (1.49) and (1.83) for straight box girders, the differential equations of bending and torsion of the truss bridge, as shown in Figs. 6.1 and 6.2, can be given as follows:

$$(D_{xx}u_0'')'' = p_x + m_x', \quad (6.1a)$$

$$(D_{yy}v_0'')'' = p_y + m_y', \quad (6.1b)$$

$$(D_{\omega\omega}\theta'')'' - (C\theta')' + (D_{\omega\tilde{\omega}}\tilde{\theta}'')'' = m_z + m_\omega', \quad (6.1c)$$

$$(D_{\omega\tilde{\omega}}\theta'')'' + (D_{\tilde{\omega}\tilde{\omega}}\tilde{\theta}'')'' + \tilde{A}\tilde{\theta} = \tilde{m}_z + \tilde{m}_{\tilde{\omega}}', \quad (6.1d)$$

where  $u_0$ ,  $v_0$  are the horizontal and vertical deflections, respectively,  $\theta$ ,  $\tilde{\theta}$  are the angles of twist and distortion, respectively, and  $C$  is the rigidity of pure torsion.  $D_{xx}$ ,  $D_{yy}$ ,  $D_{\omega\omega}$ ,  $D_{\omega\tilde{\omega}}$ ,  $D_{\tilde{\omega}\tilde{\omega}}$  denote the rigidities of bending, warping torsion, and distortion, respectively, which have been modified by their corresponding  $\mu$ , as will be shown in the following section.

## 6.2 Influence of Webs of Truss

### 6.2.1 Shear Rigidity of Webs

The webs of a truss consisting of web members and the upper and lower bracings of the truss shown in Fig. 6.1 are meant to resist the shear forces and none of them

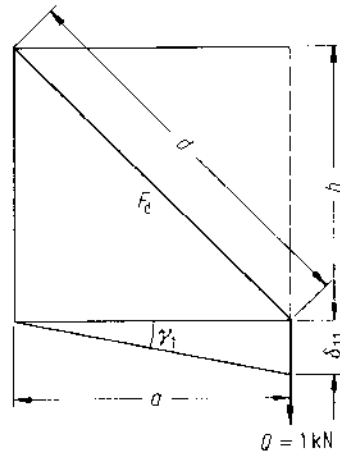


Fig. 6.3. Shear deformation of a truss panel

is capable of taking the normal stresses in the truss, whereas the upper and lower deck plates acting as chords and bracings of the truss bridge shown in Fig. 6.2 can resist both shear stresses and normal stresses. In comparison with the web plates, the webs consisting of members, especially the upper and lower bracings, have rather small shear rigidity.

Figure 6.3 shows a panel of a plane truss subject to a unit shear force  $Q$ . The shear strain induced is

$$\gamma_1 = \frac{1}{a} \delta_{11} = \frac{1}{a} \frac{d^3}{EF_d h^2}.$$

Imagine an equivalent shear web of thickness  $t^*$  having the shear rigidity

$$K = Ght^* \quad (6.2)$$

and yielding the same  $\gamma_1 = 1/K$ ; we have

$$t^* = \frac{E}{G} \frac{ah}{d^3} F_d. \quad (6.3)$$

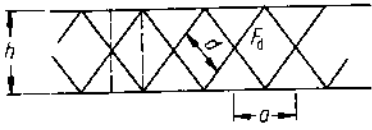
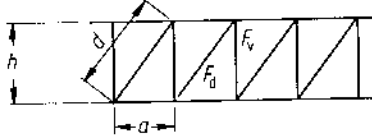
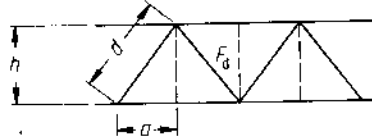
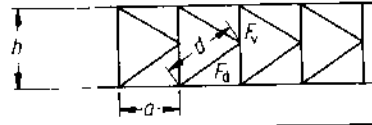
In Table 6.1 the thickness  $t^*$  of equivalent shear web of several web member systems are listed (Roik et al. 1972).

### 6.2.2 Influence of Shear Strain in Bending

Let us consider the bending of a plane truss, as shown in Fig. 6.4. The bending moment  $M_x$  will be held in equilibrium by the couple formed by the axial forces in both chords while the shear force  $Q_y$  is resisted by the web.

The deflection  $v$  consists of two parts:  $v_M$  produced by the bending moment  $M_x$  and  $v_Q$  caused by the shear force  $Q_y$ , which are obtained from

**Table 6.1.** The thickness  $t^*$  of equivalent shear web of several web member systems

System	The equivalent web plate thickness $t^*$
	$t^* = \frac{EhaF_d}{4Gd^3}$
	$t^* = \frac{E}{6} ah \frac{1}{\frac{a^3}{F_d} + \frac{h^3}{F_v}}$
	$t^* = \frac{E}{6} \frac{haF_d}{d^3}$
	$t^* = \frac{E}{6} ah \frac{1}{\frac{2d^3}{F_d} + \frac{h^3}{4F_v}}$

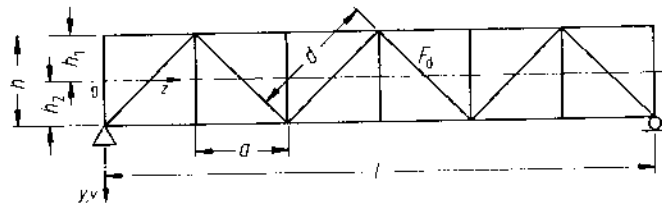


**Fig. 6.4.** A plane truss

$$\frac{d^2 v_M}{dz^2} = -\frac{M_x}{EF_{yy}}, \tag{6.4a}$$

$$\frac{dv_Q}{dz} = \frac{Q_y}{K_y} = \frac{1}{K_y} \frac{dM_x}{dz}. \tag{6.4b}$$

The total deflection is

$$v = v_M + v_Q, \tag{6.5}$$

or

$$v = \frac{1}{\mu_y} v_M,$$

where

$$\mu_y = \frac{1}{1 + (v_Q/v_M)}. \quad (6.6)$$

The factor  $\mu_y \leq 1$  represents the influence of the shear strain on the deflection. In general, it is not a constant, but a variable along the length of the truss. However, for a simply supported truss of constant cross section subject to a loading of  $\sin(n\pi z/l)$  ( $n = 1, 2, 3, \dots$ ) distribution  $\mu_y$  is a constant. In most cases of practical analysis of truss bridges such an assumption is possible. Thus, the differential equation of the total deflection can be written

$$\frac{d^2v}{dz^2} = -\frac{M_x}{D_{yy}}, \quad (6.7)$$

where

$$D_{yy} = \mu_y EF_{yy}.$$

The foregoing derivation shows that the effect of the shear strain on bending is approximately reflected in the magnification of the deflection induced by the bending moment or in the reduction of the bending rigidity by a factor  $\mu$ . The error caused by such an approximate treatment is in most cases insignificant, not only in analyzing stability (lateral buckling) and vibration, but also in determining the internal forces in truss bridges. The reason is that first for the stability and vibration we are working with eigenvalues, which are not sensitive to small variations of the rigidity or the shape of the deformation, and for the computation of internal forces, the rigidity acts first as a divider in finding the deformations from the loadings and then as a multiplier in determining the internal forces due to the deformations.

According to Eq. (6.6),  $\mu_y$  can be written in the following form:

$$\mu_y = \frac{1}{1 + \alpha \frac{EF_{yy}}{K_y l^2}}, \quad (6.8)$$

where the factor  $\alpha$  depends on the loading and support condition of the truss and is given as follows.

(1) Simply supported truss of constant cross section subjected to bending moment  $M(z) = M_c \sin(n\pi z/l)$  ( $n = 1, 2, 3, \dots$ ), which occurs in free bending vibration, and represents approximately the case of full load over the span, if  $n = 1$ . It can easily be verified that

$$\alpha = n^2 \pi^2 \quad (n = 1, 2, \dots). \quad (6.9)$$

(2) Truss as in case (1), subjected to a bending moment  $M_c$  acting at one end ( $\zeta = z/l = 1$ ),  $M(\zeta) = M_c \zeta$ . Integrating Eq. (6.4), we get

$$v_M = \frac{M_c l^2}{6EF_{yy}} \zeta^3 + A_1 \zeta + A_0,$$

$$v_Q = \frac{M_c}{K_y} \zeta + B_0.$$

**Table 6.2.**  $\alpha$  in Eq. (6.8) of cantilever truss

	Loading	Factor $\alpha$
1	Uniform load $p_c$	4
2	Variable load $p_c \zeta$	120/33
3	Variable load $p_c \zeta^2$	360/104
4	Single load $p(\zeta = 1)$	3

From the boundary condition  $[v = v_M + v_Q] = 0$ , it follows that

$$v = \frac{M_c I^2}{6EF_{yy}} (\zeta^3 - \zeta).$$

This equation means that the shear strain does not affect the deflection at all. Therefore,  $\mu_y$  for the continuous truss is the same as for the simple truss.

(3) Cantilever truss of constant cross section and length  $l$ . From the ratio  $v_Q/v_M$  at the free end and ( $\zeta = z/l = 1$ ) we obtain  $\alpha$  for different loadings as given in Table 6.2. For combined loading a reasonable value of  $\alpha$  can be taken from those values proportional to the corresponding loadings.

The foregoing investigation of the plane truss is also valid for the truss bridge shown in Fig. 6.1. In this case,  $F_{yy}$  and  $K_y$  in Eqs. (6.7) and (6.8) refer to the whole cross section of the truss.

For the bending in the horizontal plane we have analogously

$$D_{xx} = \mu_x EF_{xx},$$

$$\mu_x = \frac{1}{1 + \alpha \frac{EF_{xx}}{K_x l^2}} \quad (6.10)$$

### 6.2.3 Influence of Shear Strain in Warping Torsion and Distortion

During the warping torsion and the distortion of box section, the left and right trusses as well as the upper and lower trusses of the bridge, shown in Fig. 6.1, are bent in reverse direction, respectively, with each of the chord members belonging half to the vertical and half to the horizontal truss. Therefore, the effect of the shear strains may be given as

$$\bar{\mu}_x = \frac{1}{1 + \alpha \frac{EF_{xx}}{2K_x l^2}}, \quad \bar{\mu}_y = \frac{1}{1 + \alpha \frac{EF_{yy}}{2K_y l^2}}.$$

The average of  $\bar{\mu}_x$  and  $\bar{\mu}_y$  can approximately be considered as the factor  $\mu_\omega$ , representing the influence of shear strain in warping torsion and distortion. Using Eqs. (6.8) and (6.10), we obtain

$$\mu_{\omega} = \frac{\mu_x}{1 + \mu_x} + \frac{\mu_y}{1 + \mu_y}, \quad (6.11a)$$

and the rigidities in Eq. (6.1) will be

$$\begin{aligned} D_{\omega\omega} &= \mu_{\omega} E F_{\omega\omega}, \\ D_{\tilde{\omega}\tilde{\omega}} &= \mu_{\omega} E F_{\tilde{\omega}\tilde{\omega}}, \\ D_{\omega\tilde{\omega}} &= \mu_{\omega} E F_{\omega\tilde{\omega}}. \end{aligned} \quad (6.11b)$$

### 6.3 Boundary Conditions at Portal

Let us consider a simple supported truss bridge, as shown in Fig. 6.1. The portal acts here as an elastic support in the horizontal bending and torsion.

For the vertical bending, the conditions of a simple support are known:

$$[v_0] = 0, \quad [v_0''] = 0. \quad (6.12)$$

In torsion, the vertical displacements at both left and right supports are equal to zero, which gives

$$[v_0] \pm \frac{b}{2} [[\theta] - [\tilde{\theta}]] = 0.$$

Hence

$$[\theta] = [\tilde{\theta}]. \quad (6.13)$$

Furthermore, the horizontal displacement caused by the torsion and the horizontal bending at the supported end of the lower chords must be zero. Hence it follows according to Fig. 6.2 that

$$[u_2] = [u_0] - [k_2\theta] - [j_2\tilde{\theta}] = 0,$$

or

$$[u_0] = [(k_2 + j_2)\theta]. \quad (6.14)$$

At the end where the left or the right bearing can move freely in the longitudinal direction, no normal stresses are induced by the horizontal bending, warping torsion, and distortion; that is,

$$[u_0''] = 0, \quad (6.15a)$$

$$[\theta''] = 0, \quad (6.15b)$$

$$[\tilde{\theta}''] = 0. \quad (6.15c)$$

If both the left and the right bearings at one end are fixed in the longitudinal direction, there can be no rotation for the lower truss, which gives

$$[u_2'] = [u_0' - k_2\theta' - j_2\tilde{\theta}'] = 0, \quad (6.16)$$

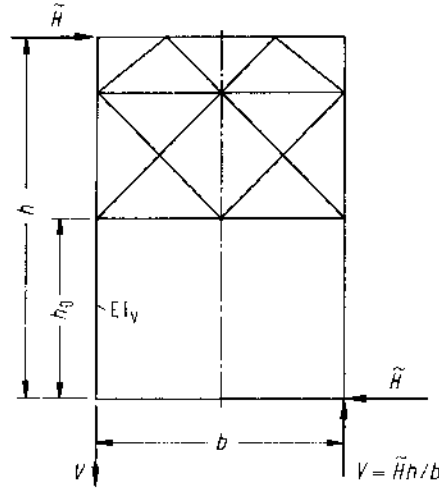


Fig. 6.5. A portal

i.e.,

$$[u'_0] = [k_2 \theta'] + [j_2 \tilde{\theta}'] .$$

Finally, the distortion or the shear angle of the portal  $[\tilde{\gamma}_N] = 2[\tilde{\theta}]$  must be proportional to the transverse horizontal shear force acting on it. The latter consists of three parts:  $Q_1(u_0)$ ,  $H(\theta)$ , and  $\tilde{H}(\tilde{\theta})$  produced by the horizontal bending  $u_0$ , the torsion  $\theta$ , and the distortion  $\tilde{\theta}$ , respectively. Denoting the shear rigidity of the portal by  $\tilde{R}_0$ , we have at  $z = 0$ :

$$2\tilde{R}_0[\tilde{\theta}] = Q_1(u_0) + H(\theta) + \tilde{H}(\tilde{\theta}) .$$

Hence it follows that after both sides are multiplied by  $2h$

$$\tilde{A}_0[\tilde{\theta}] = [C\tilde{\theta}' - 2k_2 D_{xx} u_0''' - (D_{\omega\omega} + D_{\omega\tilde{\theta}})\theta''' - (D_{\omega\tilde{\theta}} + D_{\tilde{\theta}\omega})\tilde{\theta}'''] , \quad (6.17)$$

where  $\tilde{A}_0 = 4h\tilde{R}_0$ .

For  $z = l$  we have to put a negative sign before the bracket on the right side of the above equation.

For reference, the shear rigidity  $\tilde{R}_0$  of the portal shown in Fig. 6.5 can approximately be given as

$$\tilde{R}_0 = \tilde{H}(\tilde{\gamma}_N = 1) = (10 \sim 14)EI_y \frac{h}{h_0^3} . \quad (6.18)$$

#### 6.4 Determination of Internal Forces

The theory given in the preceding sections can be applied directly to the analysis of the lateral buckling and bending and torsional vibrations of truss bridges. But,



in determining the internal forces, we must transform these from the continuous model truss into the real discrete truss, by means of integration.

In the real truss, the force of a chord member is determined by the bending moment or bimoment of the cross section at the opposite joint  $z_1$ , and the force of a diagonal, by the shear force at the center  $z_2$  of the panel. Investigations show that the mean over the panel in the model truss well represents the corresponding value just mentioned in the real truss and can be given as follows:

$$\begin{aligned}\bar{M}(z_1) &= \frac{1}{a_1} \int_{z_1-\lambda_1}^{z_1+\lambda_1} M(z) dz, \\ \bar{Q}(z_2) &= \frac{1}{a_2} \int_{z_2-\lambda_2}^{z_2+\lambda_2} Q(z) dz,\end{aligned}\tag{6.19}$$

where  $2\lambda_1 = a_1$  and  $2\lambda_2 = a_2$  denote the panel lengths referring to the chord member and the diagonal, respectively, which can be equal.

The horizontal shear force of a sway bracing in spacing  $a_3 = 2\lambda_3$  is analogously

$$\bar{H}(z_3) = \frac{2\tilde{R}}{a_3} \int_{z_3-\lambda_3}^{z_3+\lambda_3} \tilde{\theta}(z) dz,\tag{6.20}$$

where  $\tilde{R}$  is the shear rigidity of a sway bracing.

## 7. Spatial Stress Analysis of Truss Bridges

Based on the theories of bending and torsion of trusses presented in the preceding chapter, in this chapter two methods — the finite beam element method and the analytical method — for calculating the spatial internal forces in truss bridges are derived and then, as an example, simply supported steel truss bridges used in railway applications are analyzed with emphasis on the shearing forces in portals and sway bracings as well as in lateral bracings and main trusses owing to wind force and eccentric live load. Therefore, we consider mainly the lateral bending and torsion of the truss bridge. In order to verify the reliability of the finite beam element method, the results obtained are compared with those obtained by the classical method for space bar systems and those from a model test. The comparison reveals that this method can be applied in engineering with sufficient accuracy.

### 7.1 Finite Beam Element Method for Stress Analysis

The finite beam element method derived for torsion of straight box girders with deformable cross-sections in Chap. 2 is thoroughly applicable to truss bridges. It is only necessary to supplement the method with the lateral bending, for which the element deflection function  $u_0(z)$  can be expressed in polynomial of third order.

Hence, the nodal displacement parameters of a typical element are defined by

$$\{\delta\}^e = \begin{Bmatrix} \delta_i \\ \delta_j \end{Bmatrix},$$

where

$$\{\delta_i\} = (u_{0i} \ u'_{0i} \ \theta_i \ \theta'_i \ \theta''_i \ \tilde{\theta}_i \ \tilde{\theta}'_i \ \tilde{\theta}''_i)^T,$$

and

$$\{\delta_j\} = (u_{0j} \ u'_{0j} \ \theta_j \ \theta'_j \ \theta''_j \ \tilde{\theta}_j \ \tilde{\theta}'_j \ \tilde{\theta}''_j)^T.$$

(7.1)

For further derivation of the method see Sect. 2.1.

### 7.2 End Beam Element for Inclined Portal

The boundary conditions for truss bridges with vertical portals are discussed in Sect. 6.3.

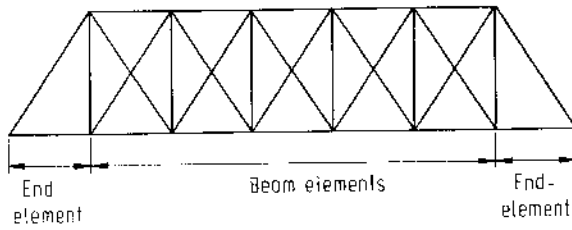


Fig. 7.1. Trapezoidal main truss

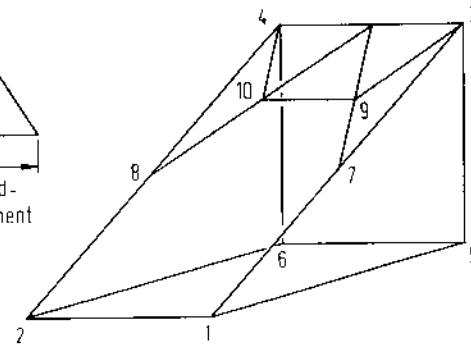


Fig. 7.2. Inclined portal substructure

In many cases the forms of the main trusses of bridges are trapezoidal. To apply the general finite beam element method to such truss bridges, we have to deal with the inclined portal as a special truss end beam element.

We regard the triangular element of an inclined portal (shown in Fig. 7.1) as an end beam element, i.e., a substructure element, which is composed of beam members. The procedure in detail is described as below.

Figure 7.2 shows the general shape of the substructure element. The substructure is made up of  $m$  members and  $n$  nodes. In each node there are six displacement parameters — three translations and three rotations. The nodal displacement vector of the substructure is

$$\{\delta^*\} = \begin{Bmatrix} \delta_b \\ \delta_c \end{Bmatrix}, \quad (7.2)$$

in which subscript b indicates the boundary nodes, subscript c the interior nodes. Hence, the relationship between the internal forces and the displacements can be defined by

$$\begin{bmatrix} K_{bb} & K_{bc} \\ K_{cb} & K_{cc} \end{bmatrix} \begin{Bmatrix} \delta_b \\ \delta_c \end{Bmatrix} = \begin{Bmatrix} F_b \\ F_c \end{Bmatrix}. \quad (7.3)$$

From the second equation we have

$$\{\delta_c\} = [K_{cc}]^{-1}(\{F_c\} - [K_{cb}]\{\delta_b\}). \quad (7.4)$$

Substituting the above relation into the first equation and denoting

$$\begin{aligned} [\bar{K}] &= [K_{bb}] - [K_{bc}][K_{cc}]^{-1}[K_{cb}], \\ \{\bar{F}\} &= \{F_b\} - [K_{bc}][K_{cc}]^{-1}\{F_c\}, \end{aligned} \quad (7.5)$$

we obtain

$$[\bar{K}]\{\delta_b\} = \{\bar{F}\}. \quad (7.6)$$

According to the formula in (7.5), we can evaluate the condensed stiffness matrix and load vector of the inclined portal substructure element.

From the geometric relationship we can derive the transformation of the boundary node displacements of the substructure into those of the truss beam element, and correspondingly for the element stiffness matrix.

### 7.3 Analysis of Shear Forces in Portals and Sway Bracings

In this section attention is focused on the analysis of the shearing forces carried by portals and sway bracings.

The numerical analysis reveals that the forces of portals and sway bracings are primarily related to the deformation of cross-sections of trusses and can be determined by a parameter — the shearing force  $\tilde{H}$  in a sway bracing — shown in Fig. 7.3. The calculation procedure is convenient and consistent with that we used before.

The results of numerical calculation show further that the shear force  $\tilde{H}_0$  in a portal and the shear force  $\tilde{H}_c$  in the sway bracing at the mid-span or  $\tilde{H}_1$  in the sway bracings adjacent to a portal govern the practical design of portals and sway bracings.

In order to obtain the practical calculation formulas for the shear forces  $\tilde{H}_0$  and  $\tilde{H}_c$ , or  $\tilde{H}_1$ , we assessed the influences of the cross-sectional areas of chord members, the areas of the diagonal members in lateral bracings, the span length, and the ratio of the shearing rigidity of portal to that of sway bracing, on the shear forces. To make the analysis practical, the dimensions of double tracks steel truss bridges (shown in Fig. 7.4,  $l = 80$  m) and a single track one (shown in Fig. 7.5,  $l = 112$  m) used in railway applications are taken as the basic data of the bridges to be analyzed. The winds considered are shown in the figures.

The results of analysis show that when the areas of chord members and the diagonal members in lateral bracings vary within the practical range, they have very little influences on the shear forces in portals and sway bracings, and, in general, do not exceed 10%. The primary factors affecting the shear forces are the span length  $l$  and the ratio of the shear rigidity of portal to that of sway bracing, i.e.  $\tilde{R}_0/\tilde{R}$ . From the numerical result, and applying the least squares method, we obtain the following formulas:

1. For double-track railway truss bridges, when  $60 \text{ m} \leq l \leq 100 \text{ m}$  and  $0.5 \leq \tilde{R}_0/\tilde{R} \leq 2.0$ . The shear force in a portal is

$$\tilde{H}_0(\text{KN}) = W[0.2997 + 0.9585r - 0.1982r^2 + 0.0095(l - 80)], \quad (7.7)$$

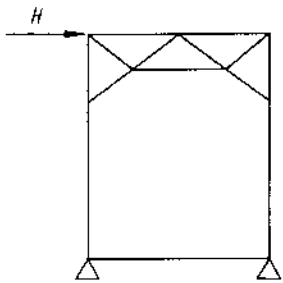


Fig. 7.3. Mechanical model of portals and sway bracings

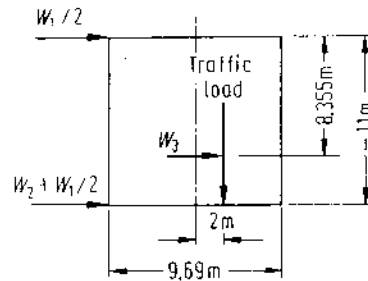


Fig. 7.4. Cross-section of a double-track bridge

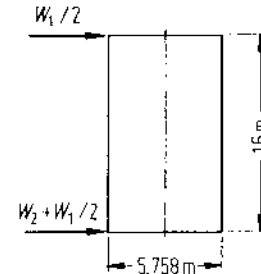


Fig. 7.5. Cross-section of a single-track bridge

where  $r = \bar{R}_0/\bar{R}$  and  $W(\text{KN}) = 7.0934W_1 + 2.9071W_2 + 40.2462W_3$ .  $W_1$ ,  $W_2$ , and  $W_3$  denote the wind forces on the main truss, the deck system, and the train, respectively;  $\bar{R}_0$  is the shearing rigidity of portal,  $\bar{R}$  is the shearing rigidity of sway bracing; if the number of panels  $n$  is not equal to 10,  $\bar{R}$  should be multiplied by  $n/10$ ;  $l$  is the span length (m). The shear force in the sway bracing (at the mid-span) is

$$\bar{H}_c = W[1.5662 - 0.8429r + 0.2360r^2 + 0.0049(l - 80)], \quad (7.8)$$

where  $W = -(1.4786W_1 + 2.9929W_2 + 39.8040W_3)$ .

2. For single-track railway truss bridges, when  $80 \text{ m} \leq l \leq 140 \text{ m}$  and  $0.8 \leq \bar{R}_0/\bar{R} \leq 4.0$ . The shear force in a portal is

$$\bar{H}_0 = W[0.5249 + 0.3093r - 0.0427r^2 + 0.0098(l - 112)], \quad (7.9)$$

where  $W = 15.7130W_1 + 7.2842W_2$ .

The shearing force in the sway bracing (adjacent to a portal) is

$$\bar{H}_1 = W[2.2249 - 0.7953r + 0.1092r^2 + 0.0099(l - 112)], \quad (7.10)$$

where  $W = 5.0329W_1 + 1.3343W_2$ .

## 7.4 Comparison of Theoretical and Experimental Results

In order to verify the accuracy of the results by the finite beam element method, we performed an experiment on a truss bridge model made of Perspex with  $l = 119.5 \text{ cm}$  and panel length  $l_1 = l/10$ , as shown in Figs. 7.6 and 7.7.

The shear forces in trusses obtained from the experiment and by the finite beam element method as well as by the classical method for a space bar system are shown in Fig. 7.8. From the figures it can be seen that the results by the finite beam element method agree well with model test results, but are a little larger than those obtained by the finite element method of the space bar system. This is because in the latter method the joints of the model are considered to be absolutely rigidly jointed. However, the maximum difference is not greater than 15%.

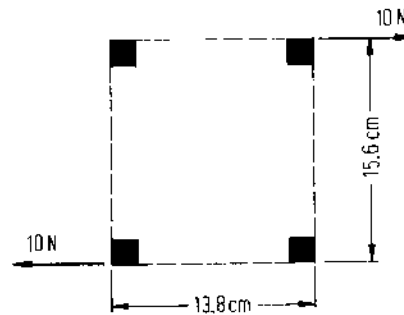


Fig. 7.6. Cross-section and loads at mid-span

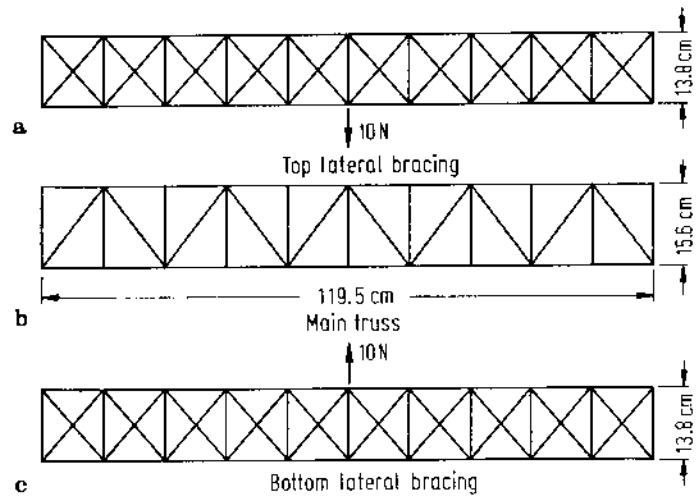


Fig. 7.7a-c. Dimensions of the model

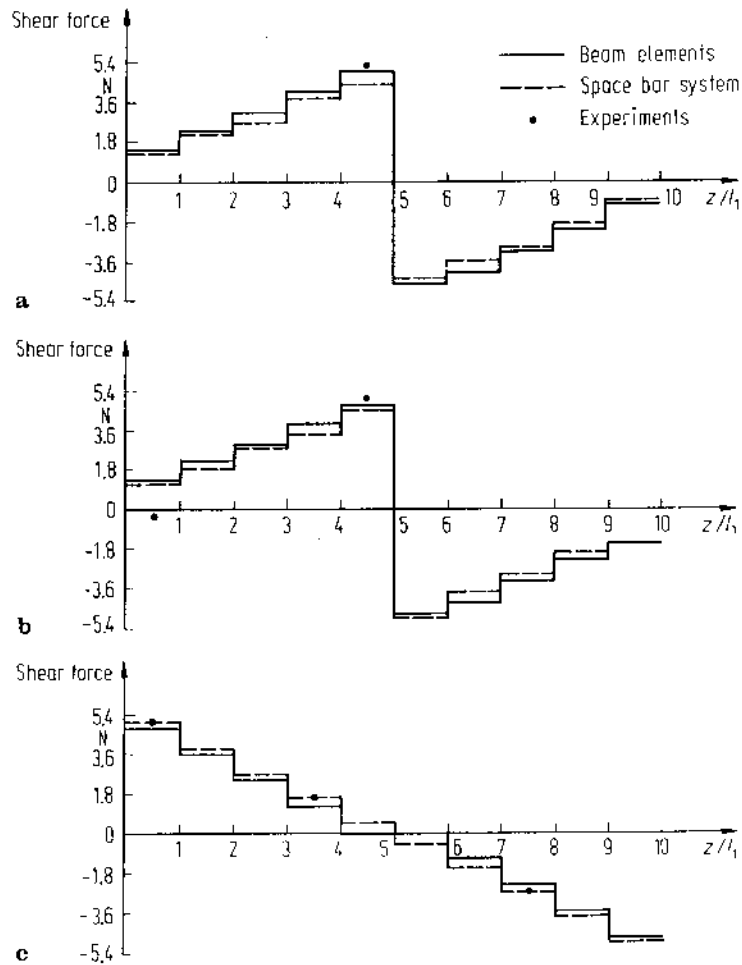


Fig. 7.8. Shear forces in (a) the top lateral bracing, (b) the bottom lateral bracing, and (c) the main truss

## 7.5 Analytical Solution of the Internal Forces

In the previous sections we presented the finite beam element method for analyzing the internal forces of truss bridges and verified the reliability of the method. In practical design some simpler formulas easily calculated by hand are required. Hence, based on the simplifications of the differential equations of bending and torsion of trusses, an analytical solution is derived. Formulas for calculating the internal forces and the shear forces in sway bracings are given in this section.

### 7.5.1 Simplification of the Differential Equations

The following simplifications of the differential equations are carried out.

#### 7.5.1.1 Neglect the Effect of the Warping Torsion

Pure torsion is dominant in torsion for a beam with closed cross-section. Results from calculation reveal that consideration of the effect will increase the torsional rigidity of cross-section by about 4% only (Li 1975).

#### 7.5.1.2 Neglect the Coupling of Warping Torsion and Distortion of Cross-section as Discussed in Chaps. 1 and 2

Thus, from Eq. (6.1) we obtain simplified differential equations of lateral bending, torsion, and distortion as follows:

$$\begin{aligned} D_{xx}u_0^{(4)} &= p_x, \\ -C\theta'' &= m_z, \\ D_{\omega\omega}\tilde{\theta}^{(4)} + \tilde{A}\tilde{\theta} &= \tilde{m}_z. \end{aligned} \quad (7.11)$$

The symbols are given in Chap. 1.

The boundary conditions discussed in Sect. 6.3 can be simplified accordingly.

### 7.5.2 Solution of the Differential Equations

The solution of the differential equation (7.11) will be composed of the homogeneous solution and particular solution. For simply supported truss bridges the loads and the particular solution of displacements can be represented in the general form of Fourier series so that we obtain general formulas for the integration constants in the homogeneous solution. Consequently, the complete solution has the general form.

The homogeneous solution of Eq. (7.11) is

$$\begin{aligned}
u_0 &= A_1 z^3 + A_2 z^2 + A_3 z + A_4, \\
\bar{\theta} &= B_1 z + B_2, \\
\bar{\theta} &= \cos \alpha z (C_1 \sinh \alpha z + C_2 \cosh \alpha z) + \sin \alpha z (C_3 \sinh \alpha z + C_4 \cosh \alpha z),
\end{aligned} \tag{7.12}$$

where  $\alpha = \sqrt[4]{A/4D_{\bar{\omega}\bar{\omega}}}$ , and  $A_i$  ( $i = 1, \dots, 4$ ),  $B_i$  ( $i = 1, 2$ ) and  $C_i$  ( $i = 1, \dots, 4$ ) are integration constants.

The particular solution can be given as follows:

$$\begin{aligned}
u_0^* &= \frac{1}{D_{xx}} \sum_{n=1}^{\infty} \left(\frac{1}{\zeta_n}\right)^4 P_{xn} \sin \zeta_n z, \\
\theta^* &= \frac{1}{C} \sum_{n=1}^{\infty} \left(\frac{1}{\zeta_n}\right)^2 m_{zn} \sin \zeta_n z, \\
\bar{\theta}^* &= \frac{1}{D_{\bar{\omega}\bar{\omega}}} \sum_{n=1}^{\infty} \left(\frac{1}{\zeta_n}\right)^4 \frac{\tilde{m}_{zn}}{1 + \frac{\bar{A}}{D_{\bar{\omega}\bar{\omega}}} \left(\frac{1}{\zeta_n}\right)^4} \sin \zeta_n z,
\end{aligned} \tag{7.13}$$

$\zeta_n = \frac{n\pi}{l};$

They correspond to the loading

$$\begin{aligned}
p_x(z) &= \sum_{n=1}^{\infty} p_{xn} \sin \zeta_n z, \\
m_z(z) &= \sum_{n=1}^{\infty} m_{zn} \sin \zeta_n z, \\
\tilde{m}_z(z) &= \sum_{n=1}^{\infty} \tilde{m}_{zn} \sin \zeta_n z,
\end{aligned} \tag{7.14}$$

where  $p_{xn}$ ,  $m_{zn}$ , and  $\tilde{m}_{zn}$  are load factors. For instance, for a concentrated load,  $P$  applied at  $z = a$  is

$$p_n = \frac{2P}{l} \sin \zeta_n a.$$

Adding Eqs. (7.12) and (7.13), we can evaluate the integration constants to satisfy the boundary conditions of a simply supported truss bridge.

Denoting

$$\begin{aligned}
c &= \cos \alpha l, & s &= \sin \alpha l; \\
\bar{c} &= \cosh \alpha l, & \bar{s} &= \sinh \alpha l,
\end{aligned}$$

we have

$$\begin{aligned}
A_1 &= A_2 = 0, \\
A_3 &= \frac{1}{l} (k_2 + j_2) [(C_1 \bar{s} + C_2 \bar{c})c + C_4 \bar{c}s - C_2], \\
A_4 &= (k_2 + j_2) C_2,
\end{aligned}$$



$$B_1 = \frac{1}{l} [(C_1 \bar{s} + C_2 \bar{c})c + C_4 \bar{c}s - C_2],$$

$$B_2 = C_2,$$

$$C_1 = \frac{\bar{s}}{\bar{c}s} (C_4 c - C_2 s),$$

$$C_3 = 0,$$

$$C_2 = \frac{P_1 G_{22} - P_2 G_{12}}{G_{11} G_{22} - G_{12} G_{21}},$$

and

$$C_4 = \frac{P_2 G_{11} - P_1 G_{21}}{G_{11} G_{22} - G_{12} G_{21}},$$

in which

$$G_{11} = \frac{\tilde{A}_0}{2} - \frac{1}{\bar{c}} \left[ \frac{C}{2l} (c - \bar{c}) - \bar{s} D_{\bar{\omega}\bar{\omega}} \alpha^3 \right],$$

$$G_{12} = \frac{-1}{\bar{c}s} \left[ \frac{C}{2l} (s^2 + \bar{s}^2) - D_{\bar{\omega}\bar{\omega}} \alpha^3 (cs - \bar{c}\bar{s}) \right],$$

$$G_{21} = \frac{-1}{\bar{c}} \left[ \frac{\tilde{A}}{2} c + \frac{C}{2l} (c - \bar{c}) + D_{\bar{\omega}\bar{\omega}} \alpha^3 s \right],$$

$$G_{22} = \frac{1}{\bar{c}s} \left[ - \left( \frac{\tilde{A}_0}{2} - \frac{C}{2l} \right) (s^2 + \bar{s}^2) + D_{\bar{\omega}\bar{\omega}} \alpha^3 (cs - \bar{c}\bar{s}) \right],$$

$$P_1 = \sum_{n=1}^{\infty} \frac{1}{\zeta_n} \left[ k_2 p_{xn} + \frac{1}{2} m_{zn} + \frac{1}{2} \frac{\tilde{m}_{zn}}{1 + \frac{\tilde{A}}{D_{\bar{\omega}\bar{\omega}}} \left( \frac{1}{\zeta_n} \right)^4} \right],$$

and

$$P_2 = \sum_{n=1}^{\infty} \frac{1}{\zeta_n} (-1)^n \left[ k_2 p_{xn} + \frac{1}{2} m_{zn} + \frac{1}{2} \frac{\tilde{m}_{zn}}{1 + \frac{\tilde{A}}{D_{\bar{\omega}\bar{\omega}}} \left( \frac{1}{\zeta_n} \right)^4} \right].$$

## 7.6 Examples

Consider the simply supported truss bridge model in Sect. 7.4.

For horizontal uniform loading 1 N/cm acting on the upper chord, the shear forces obtained from the finite beam element method and the analytical solution are shown in Fig. 7.9. It can be seen that the analytical solution is fairly accurate.

For the loading of the model test as shown in Fig. 7.7, the results of calculations are given in Fig. 7.10.

The efficiency of the analytical method presented here can readily be seen from the figures.

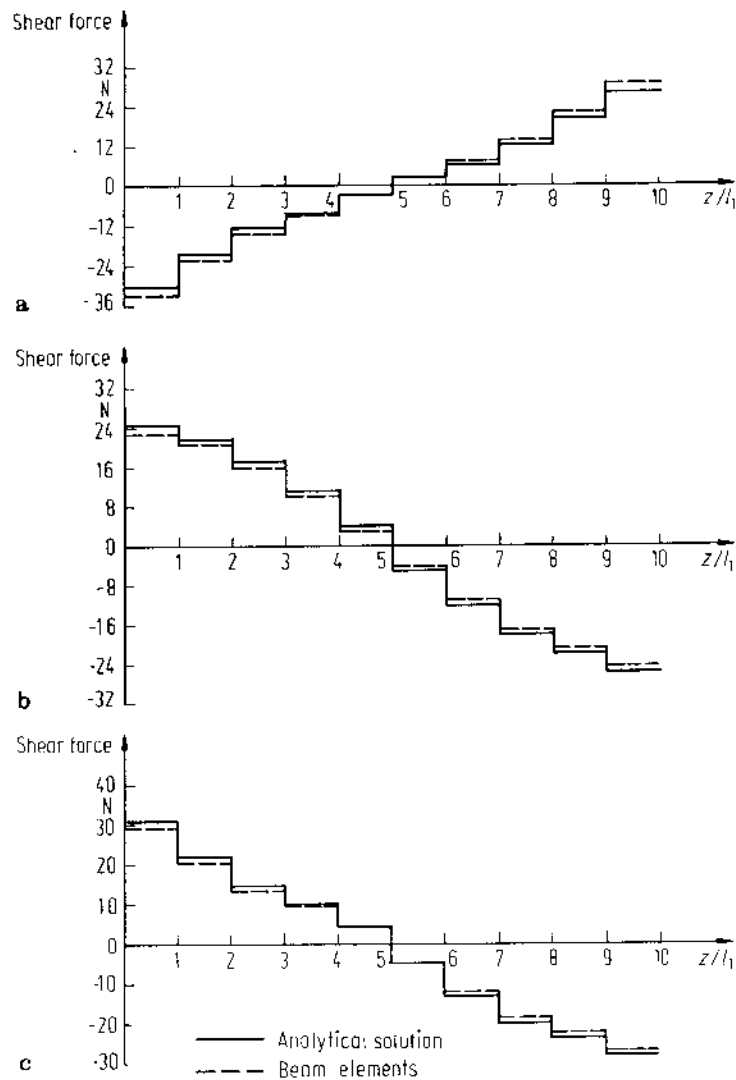
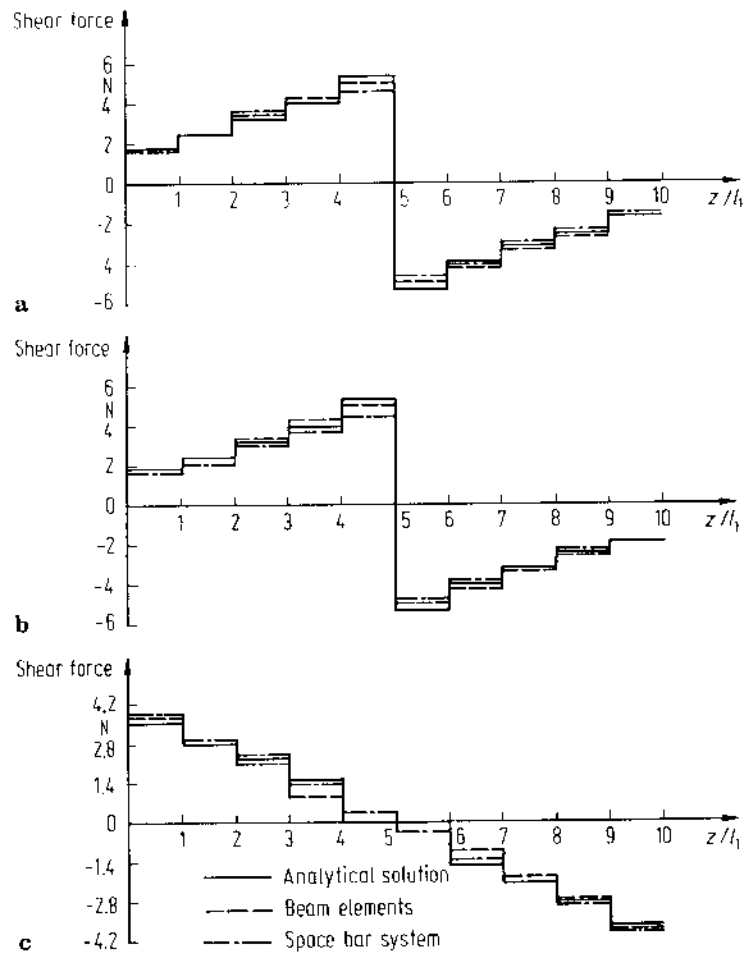


Fig. 7.9. Shear forces in (a) the top lateral bracing, (b) the bottom lateral bracing, and (c) the main truss



**Fig. 7.10.** Shear forces in (a) the top lateral bracing, (b) the bottom lateral bracing, and (c) the main truss

## 8. Lateral Stability of Truss Bridges

Since the study of lateral buckling of beams was made in 1899 by L. Prandtl and A.G.M. Michell, there have been many developments. A thorough investigation of the lateral stability of truss bridges with deformable cross-sections was made by Li (1975) and useful practical results were obtained. This chapter deals with the lateral buckling of truss bridge based on the theories presented in Chaps. 1 and 6. It begins with the derivation of the differential equations of lateral buckling. Then an analytical method and a finite element method to solve these equations are considered. At the end of this chapter, a numerical example, a simple approximate method for analyzing lateral stability of truss bridges, and the model test results are given.

### 8.1 Derivation of Differential Equations of Lateral Buckling

#### 8.1.1 Basic Principle

The cross-section of the truss bridge investigated is shown in Fig. 8.1, in which the solid lines represent the chord members and steel deck plate, and the dotted lines represent the web members. The bridge has a constant cross-section and a vertical axis of symmetry. The  $x$  axis and  $y$  axis are the principal axes.  $M$  and  $N$  denote the center of twist and the center of shearing deformation of the cross-section, respectively. Let  $r_1$  and  $r_2$  denote the height measured from the acting point of the resultant force  $q$ , which is the sum of dead load  $g$  and live load  $p$  acting on the top deck and the lower one, to  $M$  and  $N$ , respectively. We refer to  $r_1$  and  $r_2$  as the over-centers of load  $q$ .

A truss loaded with uniform vertical load  $q$  undergoes vertical displacements. Lateral buckling will appear when  $q$  reaches a certain critical load, and the lateral displacement  $u_0$ , the angle of twist  $\theta$ , and the angle of distortion  $\tilde{\theta}$  will occur. According to the principle of elastic potential, the elastic equilibrium of the truss in the lateral buckling state can be expressed as follows:

$$\delta U = \delta U_e + \delta U_s + \delta U_q = 0, \quad (8.1)$$

where

$\delta U_e$  = variation of elastic strain energy due to the lateral buckling deformations  $u_0$ ,  $\theta$ ,  $\tilde{\theta}$ ;

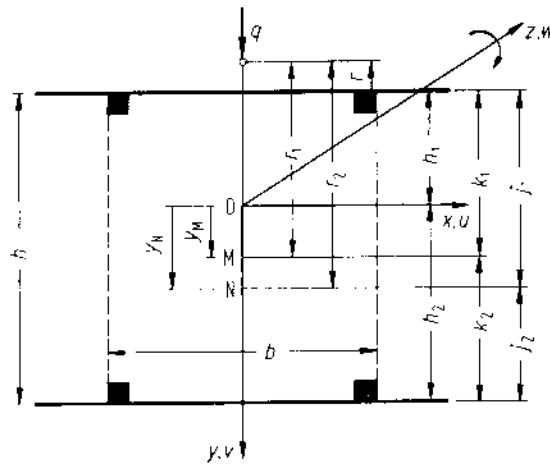


Fig. 8.1. Typical cross section of a truss bridge

$\delta U_s$  = variation of the potential energy of internal force  $S(M, Q)$  caused by bending in the vertical plane due to  $u_0, \theta, \tilde{\theta}$ ;

$\delta U_q$  = variation of the potential energy of load  $q$  due to  $u_0, \theta, \tilde{\theta}$ .

The first term  $\delta U_s$  can be found in Chaps. 1 and 6. It is only necessary to calculate  $\delta U_s$  and  $\delta U_q$ .

### 8.1.2 Potential of Existing Internal Forces Due to Lateral Buckling

The variation of the potential energy of the forces  $S(M, Q)$  in the vertical plane induced by  $u_0, \theta, \tilde{\theta}$  can be expressed in the following form:

$$\delta U_s = - \int_V (\sigma_z \delta \epsilon_z + \tau_{yz} \delta \gamma_{yz}) dF dz. \quad (8.2)$$

When lateral buckling occurs, the lateral and vertical displacements of an arbitrary point on the cross-section can be written as follows:

$$\begin{aligned} u(x, y, z) &= u_0(z) - y_1 \theta - y_2 \tilde{\theta}, \\ v(x, y, z) &= x \theta - x \tilde{\theta}, \end{aligned} \quad (8.3)$$

with  $y_1 = y - y_M, y_2 = y - y_N$ .

The strains caused by those displacements can be expressed as follows:

$$\begin{aligned} \epsilon_z &= -\frac{1}{2} \left( \frac{\partial u}{\partial z} \right)^2 - \frac{1}{2} \left( \frac{\partial v}{\partial z} \right)^2, \\ \gamma_{yz} &= -\frac{\partial u}{\partial y} \frac{\partial u}{\partial z} - \frac{\partial v}{\partial y} \frac{\partial v}{\partial z}. \end{aligned} \quad (8.4)$$

The substitution of Eq. (8.3) into Eq. (8.4) leads to

$$\begin{aligned}
\delta\varepsilon_z &= -(u'_0 - y_1\theta' - y_2\tilde{\theta}')(\delta u'_0 - y_1\delta\theta' - y_2\delta\tilde{\theta}') \\
&\quad - x^2(\theta' - \tilde{\theta}')(\delta\theta' - \delta\tilde{\theta}'), \\
\delta\gamma_{yz} &= (u'_0 - y_1\theta' - y_2\tilde{\theta}')(\delta\theta + \delta\tilde{\theta}) \\
&\quad + (\theta + \tilde{\theta})(\delta u'_0 - y_1\delta\theta' - y_2\delta\tilde{\theta}') \\
&\quad \text{"'"} = d/dz = d.
\end{aligned} \tag{8.5}$$

The formulas for calculating the vertical bending stresses  $\sigma$ ,  $\tau$  and their integrations are

$$\begin{aligned}
\sigma_z &= \frac{M}{F_{yy}} y, \quad \int_F \sigma_z dF = 0, \\
\int_F y \sigma_z dF &= M, \quad \int_{F^*} \tau_{yz} dF = \int_{F^*} \tau dF = Q = M',
\end{aligned} \tag{8.6}$$

where  $F^*$  = area of the cross-section of the equivalent web plate of the web member that resists the shear deformation.

Introducing Eqs. (8.5) and (8.6) into Eq. (8.2) and transforming  $\delta u'_0$ ,  $\delta\theta'$ ,  $\delta\tilde{\theta}'$  into  $\delta u_0$ ,  $\delta\theta$ ,  $\delta\tilde{\theta}$  by means of integration by parts, and setting

$$\begin{aligned}
\int_{F^*} \tau y_1 dF &= e_1 M, \\
\int_{F^*} \tau y_2 dF &= e_2 M, \\
e_1 &= \frac{1}{2}(h_2 - h_1) - y_M, \\
e_2 &= \frac{1}{2}(h_2 - h_1) - y_N, \\
e_3 &= e_1 - e_2 = y_N - y_M, \\
n_1 &= \frac{F_{y3}}{F_{y2}} + \frac{F_{x2y}}{F_{y2}} - 2y_M, \\
n_2 &= \frac{F_{y3}}{F_{y2}} + \frac{F_{x2y}}{F_{y2}} - 2y_N, \\
n_3 &= \frac{F_{y3}}{F_{y2}} - \frac{F_{x2y}}{F_{y2}} - (y_M + y_N),
\end{aligned} \tag{8.7}$$

we find

$$\begin{aligned}
\delta U_s &= \int \{ M(\theta + \tilde{\theta})'' \delta v_0 + (Mu''_0 - m_{11} - m_{12})\delta\theta \\
&\quad + M(u''_0 - m_{21} - m_{22})\delta\tilde{\theta} \} dz + [\text{boundary values}],
\end{aligned} \tag{8.8}$$

where

$$\begin{Bmatrix} m_{11} \\ m_{12} \\ m_{21} \\ m_{22} \end{Bmatrix} = \begin{Bmatrix} n_1(M\theta'Y + e_1M''\theta) \\ n_3(M\tilde{\theta}'Y + e_3M'\tilde{\theta}' + e_1M''\tilde{\theta}) \\ n_3(M\theta'Y - e_3M'\theta' + e_2M''\theta) \\ n_2(M\tilde{\theta}'Y + e_2M''\tilde{\theta}) \end{Bmatrix}. \tag{8.9}$$

### 8.1.3 Potential of Vertical Loads Due to Lateral Buckling

The variation of the potential of the vertical load  $q$  due to the displacements of lateral buckling  $\delta U_q$  can be written as follows:

$$\delta U_q = - \int q \delta v dz, \quad (8.10)$$

where  $\delta v$  is the variation of the displacement at points of load application. It is

$$\begin{aligned} v &= \frac{1}{2}(r_1 \theta - r_2 \tilde{\theta})(\theta + \tilde{\theta}), \\ \delta v &= r_1 \theta \delta \theta + r_2 \tilde{\theta} \delta \tilde{\theta} + r_3(\theta \delta \tilde{\theta} + \tilde{\theta} \delta \theta), \end{aligned} \quad (8.11)$$

where  $r_3 = \frac{1}{2}(r_1 + r_2)$ .

Substituting Eq. (8.11) into Eq. (8.10) we obtain:

$$\delta U_q = - \int q [r_1 \theta \delta \theta + r_2 \tilde{\theta} \delta \tilde{\theta} + r_3(\theta \delta \tilde{\theta} + \tilde{\theta} \delta \theta)] dz. \quad (8.12)$$

### 8.1.4 Differential Equations of Lateral Buckling

Substituting  $\delta U_e$  (referring to Chaps. 1 and 6) Eqs. (8.8) and (8.12) into Eq. (8.1), we obtain the differential equations of lateral buckling as follows:

$$([DL] + [G]) \begin{Bmatrix} u_0 \\ \theta \\ \tilde{\theta} \end{Bmatrix} = 0, \quad (8.13)$$

where

$$\begin{aligned} [DL] &= \begin{bmatrix} D_{xx}d^4 & 0 & 0 \\ 0 & (D_{\omega\omega}d^4 - Cd^2) & D_{\omega\tilde{\omega}}d^4 \\ 0 & D_{\omega\tilde{\omega}}d^4 & (D_{\tilde{\omega}\tilde{\omega}}d^4 + \tilde{A}) \end{bmatrix}, \\ [G] &= \begin{bmatrix} 0 & d^2M & d^2M \\ Md^2 & -(n_1dMd + e_1M'' + qr_1) & -(n_3dMd + e_3M'd \\ & & + e_1M'' + qr_3) \\ Md^2 & -(n_3dMd - e_3M'd & -(n_2dMd + e_2M'' + qr_2) \\ & + e_2M'' + qr_3) & \end{bmatrix}. \end{aligned} \quad (8.15)$$

All the boundary values from integration by parts must vanish, which yields the boundary conditions.

The matrix  $[DL]$  in Eq. (8.14) is deduced from  $\delta U_e$ , which represents small internal forces of bending and twisting of cross-section due to lateral buckling, and is symmetrical. The matrix  $[G]$  in Eq. (8.15) is deduced from  $\delta U_s$  and  $\delta U_q$ , which represents the small lateral load and twisting load due to lateral buckling deformations. The matrix  $[G]$  is asymmetrical, but it can be transformed into a symmetrical matrix when using Galerkin's method and finite element method.

As the cross-section of truss is asymmetrical about the horizontal axis and has a wide upper deck plate and/or a lower one, generally, the centroid of the cross-section does not coincide with the centers  $M, N$  of  $\theta, \tilde{\theta}$  and the leading terms containing  $n_i$  ( $i = 1, 2, 3$ ) will appear in matrix  $[G]$ . If both the upper and lower chord members have steel deck plates acting with them, or have both lateral bracings instead of steel plates,  $n_i$  and  $e_i$  are generally very small and the terms related to them also have little influence on lateral buckling. If only the upper chord is provided with the steel deck plate and the lateral bracing is used at the lower chord, or, conversely, the point  $M$  is very close to the steel deck plate (for its shear rigidity is significantly larger than that of the lateral bracing) but the centroid of the cross-section is still close to the midheight of the cross-section. In this case the terms  $n_i, e_i$  and the load terms related with them will have considerable influence on the lateral buckling.

If the cross-section of the truss has two axes of symmetry, then  $e_i = n_i = 0$ , and all the load terms containing  $e_i$  and  $n_i$  are equal to zero as well.

## 8.2 Approximate Analytical Solution of the Lateral Buckling

We consider simply supported truss bridges having vertical portals. When the portal is deformable, even for single-span truss bridges, it is very difficult to obtain the lateral critical load by integrating Eq. (8.13) exactly. For this reason, we present in this section Galerkin's method for calculating the critical load. For a continuous truss and the truss with varying cross-sectional rigidity, the finite beam element method can be used and will be shown in the next section.

The truss bridge is assumed to be subjected to a uniform load  $q$  (dead load plus equivalent live loads). The bending moment curve can be expressed approximately as follows:

$$M(z) = M_c \sin \zeta z, \quad \zeta = \pi/l, \quad (8.16)$$

where  $M_c$  = the moment at mid-span.

It is assumed that the lateral buckling displacements can be approximated by the relations

$$\begin{aligned} u_0(z) &= (k_2 + j_2)\alpha_0 + \frac{h}{2}\alpha \sin \zeta z, \\ \theta(z) &= \alpha_0 + \alpha_1 \sin \zeta z, \\ \tilde{\theta}(z) &= \alpha_0 + \alpha_2 \sin \zeta z. \end{aligned} \quad (8.17)$$

Those expressions can satisfy the following boundary conditions (refer to Chap. 6):

$$\left. \begin{aligned} z = 0 \\ z = l \end{aligned} \right\} : \begin{aligned} [\theta] = [\tilde{\theta}] = \alpha_0, \quad [u_2] = [u_0 - (k_2 + j_2)\alpha_0] = 0 \\ [u_0''] = 0, \quad [\tilde{\theta}''] = 0, \quad [\tilde{\theta}'''] = 0. \end{aligned} \quad (8.18)$$



However, Eq. (8.17) cannot satisfy the differential equation (8.13). As an approximate solution, it is required that the total virtual work done by the summation  $F(z)$  of internal force and loads on the left-hand side of Eq. (8.13) be equal to zero for any arbitrary virtual displacement  $\delta \xi$  (Galerkin's method), i.e.

$$\int_0^L F(z) \delta \xi dz = 0. \quad (8.19)$$

Substituting Eqs. (8.16) and (8.17) into Eq. (8.13), taking virtual displacement functions  $\delta \xi = \delta \alpha \sin \zeta z$ ,  $\delta \alpha_1 \sin \zeta z$ ,  $\delta \alpha_2 \sin \zeta z$ , respectively, and integrating Eq. (8.19), we obtain three equations for coefficients  $\alpha$ ,  $\alpha_0$ ,  $\alpha_1$ ,  $\alpha_2$ . The fourth one is the compatibility condition of portal deformation, referring to Eq. (6.17).

The four equations can be written in the following form:

$$\begin{bmatrix} -a_0 & 2\bar{k}_2 & c + d_1 + d_2 & d_{12} + d_2 \\ -\frac{3\pi}{2}w & 1 & -2w & -2w \\ -\bar{r}_{01}w & -2w & c + d_1 + \bar{r}_{11}w & d_{12} + \bar{r}_{12}w \\ \frac{4a}{\pi} - \bar{r}_{02}w & -2w & d_{12} + \bar{r}_{12}w & d_2 + a + \bar{r}_{22}w \end{bmatrix} \begin{Bmatrix} \alpha_0 \\ \alpha \\ \alpha_1 \\ \alpha_2 \end{Bmatrix} = 0, \quad (8.20)$$

where

$$\begin{bmatrix} \bar{r}_{12} \\ \bar{r}_{01} \\ \bar{r}_{ii} \end{bmatrix} = \begin{bmatrix} \bar{n}_3 + \bar{e}_1 + \bar{e}_2 - \frac{3}{8}\pi n \bar{r}_3 \\ -\frac{3}{2}\pi \bar{e}_i + 3n \bar{r}_i - \frac{3}{2}n \bar{r}_3 \\ \bar{n}_i + 2\bar{e}_i - \frac{3}{4}\pi n \bar{r}_i \end{bmatrix}, \quad (8.21)$$

$$[\bar{k}_2 \quad \bar{e}_i \quad \bar{n}_i \quad \bar{r}_i] = \frac{2}{h} [k_i \quad e_i \quad n_i \quad r_i],$$

$$\begin{bmatrix} d_1 & d_{12} & d_2 \\ a_0 & a & c \end{bmatrix} = \frac{4}{h^2 D_{xx}} \begin{bmatrix} D_{\omega\omega} & D_{\omega\bar{\omega}} & D_{\bar{\omega}\bar{\omega}} \\ \bar{A}_0 & \bar{A} & C \\ \zeta^3 & \zeta^4 & \zeta^2 \end{bmatrix}, \quad (8.22)$$

$$w = \frac{4}{3\pi} s, \quad s = \frac{2M_c}{hD_{xx}\zeta^2} = \frac{S_k}{P_E} \quad (8.23)$$

$$n = \frac{q}{M_c \zeta^2}.$$

In order to solve Eq. (8.20) conveniently, we can eliminate  $\alpha_0$  and  $\alpha$  by means of the first and second equations and obtain two equations for coefficients  $\alpha_1$  and  $\alpha_2$ .

The obvious solution to Eq. (8.20) is that  $\alpha_0$ ,  $\alpha$ ,  $\alpha_1$ , and  $\alpha_2$  are equal to zero, which means that the truss is in a vertical bending state without lateral deformation. As the lateral buckling occurs,  $\alpha_0$ ,  $\alpha$ ,  $\alpha_1$ , and  $\alpha_2$  are not equal to zero, and it is required that the denominator determinant be equal to zero,

$$|N| = 0, \quad (8.24)$$

from which, we can obtain the lateral buckling equation.

After solving the lateral buckling equation and obtaining the value of  $w$ , the critical moment  $M_{ck}$  at mid-span and the critical load  $q_k$  are obtained as follows, see Eq. (8.23):

$$M_{ck} = \frac{s \cdot h \cdot D_{xx} \cdot \zeta^2}{2} = w \frac{3\pi^3 h}{8l^2} D_{xx}, \quad (8.25a)$$

$$q_k = \frac{8M_{ck}}{l^2} = w \frac{3n\pi^5 h}{8l^4} D_{xx}. \quad (8.25b)$$

Substituting  $w$  into Eq. (8.20), the corresponding lateral buckling deformation coefficients  $\alpha_i$  can be obtained. Then the  $u_0$ ,  $\theta$ ,  $\bar{\theta}$  can be calculated from Eqs. (8.17). Since Eq. (8.20) is homogeneous, only the deformation shapes, i.e. the proportion between the coefficients  $\alpha_i$ , can be determined.

The factor  $s$  in Eq. (8.23) can be considered as the ratio of the critical compression force  $S_k$  of the upper chord members (two chord members and the steel deck plate acting with them), when lateral buckling occurs, to the Euler's buckling load  $P_E$  of an axially loaded compression member, consisting of the upper chord members and having the bending rigidity  $\frac{1}{2}D_{xx}$  and both ends hinged.

In Eqs. (8.23) and (8.25b)  $n$  is equal to  $8/\pi^2$  for a simply supported beam, and we can approximately take  $n = 1$  when the lateral stability of the sidespan of a continuous beam is analyzed.

### 8.3 Determination of Lateral Buckling Safety Factor

In the investigation presented previously the stresses in the truss are assumed to be below the elastic limit  $\sigma_E$ , i.e.

$$\max \sigma_k = \frac{1}{h \cdot F_c} M_{ck} \leq \sigma_E, \quad (8.26)$$

where  $F_c$  represents the cross-section of upper or lower chord member, whichever is the smaller, including the steel deck plate acting with them.

In truss bridges, generally  $\max \sigma_k > \sigma_E$ , i.e. the lateral buckling of truss occurs in the range of elasto-plastic deformation of the material. In this case the elastic theory for analyzing the lateral stability is not valid. As an approximation, we treat it using the method for calculating the critical stress of an axially loaded compression member at elasto-plastic buckling.

#### 8.3.1 Approximate Modification of Safety Factor for Plastic Deformation

Consider an axially loaded compression member made of the same material as that of the truss. Assume that it has the same critical compressive stresses  $\max \sigma_k$ , which

are calculated according to the elastic theory as that of Eq. (8.26), then its slenderness ratio is

$$\lambda = \pi \sqrt{\frac{E}{\max \sigma_k}} \quad (8.27)$$

The real elasto-plastic buckling critical stress  $\sigma_k^*$  corresponding to the slenderness ratio  $\lambda$  can be obtained approximately according to the related references. If we take a quartic parabola to express the  $\sigma_k - \lambda$  curve approximately, the  $\sigma_k^*$  can be written as follows:

$$\sigma_k^* = \sigma_F [1 - (1 - m)\bar{\lambda}^4], \quad (8.28)$$

where  $m = \sigma_E/\sigma_F$ ,  $\sigma_F =$  yield point,  $\lambda = \lambda/\lambda_E$ ,  $\lambda_E = \pi\sqrt{E/\sigma_F}$ . For steel, we can take  $m = 0.8$ .

The modification factor for the elastic critical stresses is

$$\mu_p = \frac{\sigma_k^*}{\max \sigma_k} \quad (8.29)$$

The lateral buckling critical load and bending moment are also to be modified according to the coefficient  $\mu_p$ . Therefore, the lateral buckling safety factor will be

$$v = \mu_p \frac{q_k}{q} = \mu_p \frac{M_{ck}}{M_c} \quad (8.30)$$

where  $q$  and  $M_c$  represent the design load and the peak value of moment, respectively.

### 8.3.2 Example (Li 1983)

Figure 8.2 shows a continuous three-span truss bridge. We take its sidespan as a simply supported truss bridge for an approximate analysis. The bridge has an upper steel deck plate and a lower one, acting together with the upper and lower chord members, respectively.

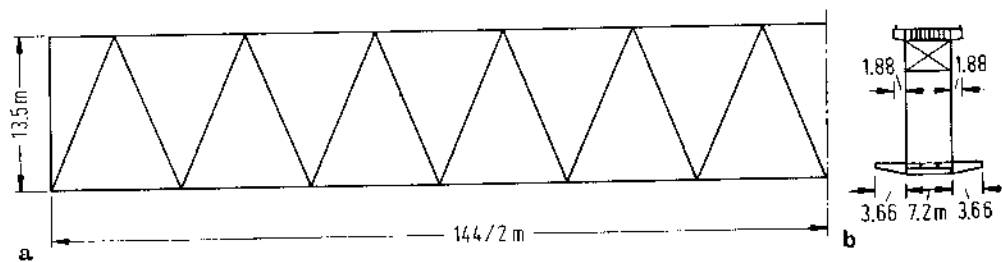


Fig. 8.2a,b. Elevation and cross section of a truss bridge

Basic data:  $q = 172.5 \text{ KN/m}$

$$\begin{aligned} \begin{Bmatrix} h_1 \\ k_1 \\ j_1 \end{Bmatrix} &= \begin{Bmatrix} 6.54 \\ 7.44 \\ 7.46 \end{Bmatrix} \text{ (m)}, \\ \begin{Bmatrix} D_{\omega\omega} \\ D_{\omega\bar{\omega}} \\ D_{\bar{\omega}\bar{\omega}} \end{Bmatrix} &= \begin{Bmatrix} 4.831 \\ 5.615 \\ 6.537 \end{Bmatrix} \times 10^{10} \text{ (KN - m}^4\text{)}, \\ \begin{Bmatrix} D_{xx} \\ C \end{Bmatrix} &= \begin{Bmatrix} 1.823 \\ 0.200 \end{Bmatrix} \times 10^9 \text{ (KN - m}^2\text{)}, \\ \begin{Bmatrix} R_0 \\ R \end{Bmatrix} &= \begin{Bmatrix} 2.117 \\ 4.586 \end{Bmatrix} \times 10^5 \text{ (KN)}. \end{aligned}$$

According to Eq. (8.24), the lateral buckling equation is

$$6.6469w^3 + 859.519w^2 + 280.971w - 643.639 = 0.$$

The smallest root is  $w = 0.716$ . It follows that:

$$\begin{aligned} M_{ck} &= w \frac{3\pi h D_{xx} \zeta^2}{8} = 9.867 \times 10^6 \text{ (KN - m)}, \\ q_k &= 3807 \text{ (KN/m)}, \\ \max \sigma_k &= \frac{M_{ck}}{h \cdot F_c} = 2.193 \times 10^3 \text{ (MPa)}, \\ \lambda &= \pi \sqrt{\frac{E}{\max \sigma_k}} = 30.43, \\ \sigma_k^* &= \sigma_T [1 - (1 - m)\bar{\lambda}^4] = 3.707 \times 10^2 \text{ (MPa)}, \\ \mu_p &= \frac{\sigma_k^*}{\max \sigma_k} = 0.169. \end{aligned}$$

Finally, the lateral buckling safety factor

$$v = \mu_p \frac{q_k}{q} = 3.731.$$

#### 8.4 Finite Beam Element Method for Analyzing Lateral Buckling

In cases of more complicated bridge structure such as a continuous truss or the truss with varying cross-sectional rigidity, it is difficult to obtain the solution that satisfies the required accuracy by Galerkin's method. For this reason, this section presents the finite beam element method for evaluating the lateral buckling critical load.

### 8.4.1 Basic Principle

Stability analysis is a problem of solving for the eigenvalue. In Chaps. 2, 4, 7, the quintic parabolas were taken to express the displacement functions  $\theta$ ,  $\tilde{\theta}$  of the element for analyzing stresses of truss. Here, we can reduce the requirements for element displacement functions, and they all can be taken in the form of cubic parabolas to ensure the continuity of the displacements  $u$ ,  $\theta$ ,  $\tilde{\theta}$  and their first derivatives. The nodal displacement parameters of an element are as follows:

$$\begin{aligned} \{\delta\}^e &= \begin{Bmatrix} \delta_i \\ \delta_j \end{Bmatrix}, \\ \{\delta_i\} &= [u_i \ u'_i \ \theta_i \ \theta'_i \ \tilde{\theta}_i \ \tilde{\theta}'_i]^T, \\ \{\delta_j\} &= [u_j \ u'_j \ \theta_j \ \theta'_j \ \tilde{\theta}_j \ \tilde{\theta}'_j]^T. \end{aligned} \quad (8.31a)$$

The element displacements are

$$\{\delta\} = \begin{Bmatrix} u \\ \theta \\ \tilde{\theta} \end{Bmatrix} = [N] \{\delta\}^e, \quad (8.31b)$$

where  $[N]$  is a matrix of polynomials of third order. Here, we substitute  $u$  for  $u_0$  for convenience in writing.

The small lateral bending and torsional displacements  $\{\delta\}$  of lateral buckling induce the elastic nodal forces of the element:

$$\{F\}^e = [k] \{\delta\}^e, \quad (8.32)$$

where  $[k]$  denotes element stiffness matrix.

The additional nodal forces of the element induced by in-plane internal forces  $S$  and the displacements are

$$\{n\}^e = [k_g] \{\delta\}^e, \quad (8.33)$$

where  $[k_g]$  is the element geometric matrix.

Equating the elastic nodal forces  $\{F\}^e$  to the additional nodal loads at all nodes, i.e. the indifferent equilibrium, the global lateral buckling equations are obtained as follows:

$$([K] - [G])\{\delta\} = 0, \quad (8.34)$$

where  $[K]$  = global stiffness matrix,  $[G]$  = global geometric matrix,  $\{\delta\}$  = global column vector of nodal displacements.

After imposing the boundary conditions, we solve Eq. (8.34) by setting its denominator determinant equal to zero:

$$|[K] - [G]| = 0, \quad (8.35)$$

from which we obtain the critical load of elastic lateral buckling.

In the following it will suffice to calculate the element geometric matrix, because the calculation of the element stiffness matrix has been shown in preceding chapters.

### 8.4.2 Element Geometric Matrix

For convenience of calculation, Eq. (8.15) is rewritten as follows:

$$\begin{aligned}
 [G] &= M \begin{bmatrix} 0 & 1 & 1 \\ 1 & -n_1 & -n_3 \\ 1 & -n_3 & -n_2 \end{bmatrix} d^2 + M' \begin{bmatrix} 0 & 2 & 2 \\ 0 & -n_1 & -n_3 - e_3 \\ 0 & -n_3 + e_3 & -n_2 \end{bmatrix} d \\
 &+ M'' \begin{bmatrix} 0 & 1 & 1 \\ 0 & -e_1 & -e_1 \\ 0 & -e_2 & -e_2 \end{bmatrix} + q \begin{bmatrix} 0 & 0 & 0 \\ 0 & -r_1 & -r_3 \\ 0 & -r_3 & -r_2 \end{bmatrix} \\
 &= [S_M]d^2 + [S'_Q]d + [S''_{q_1}] + [S_{q_2}]. \quad (8.36)
 \end{aligned}$$

The element geometric matrix is

$$\begin{aligned}
 [k_g] &= \int_{\xi} [N]^T [G] [N] dz \\
 &= \int_{\xi} [N]^T [S_M] [N''] dz + \int_{\xi} [N]^T [S'_Q] [N'] dz \\
 &\quad + \int_{\xi} [N]^T [S''_{q_1}] [N] dz + \int_{\xi} [N]^T [S_{q_2}] [N] dz.
 \end{aligned}$$

After integrating by parts and grouping, the expression for the symmetrical geometric matrix is obtained as follows:

$$\begin{aligned}
 [k_g] &= - \int_{\xi} [N']^T M [g_1] [N'] dz - \int_{\xi} [N]^T M' [g_2] [N'] dz \\
 &\quad - \int_{\xi} [N']^T M' [g_2]^T [N] dz + \int_{\xi} [N]^T M'' [g_3] [N] dz, \quad (8.37)
 \end{aligned}$$

where

$$\begin{aligned}
 [g_1] &= \begin{bmatrix} 0 & 1 & 1 \\ 1 & -n_1 & -n_3 \\ 1 & -n_3 & -n_2 \end{bmatrix}, \\
 [g_2] &= \begin{bmatrix} 0 & 0 & 0 \\ 1 & 0 & -e_2 \\ 1 & -e_1 & 0 \end{bmatrix}, \\
 [g_3] &= \begin{bmatrix} 0 & 0 & 0 \\ 0 & (r_1 + e_1) & r_3 \\ 0 & r_3 & r_2 + e_2 \end{bmatrix}. \quad (8.38)
 \end{aligned}$$

### 8.4.3 Example

We take the same example in Sect. 8.3.2 and calculate the lateral buckling safety factor by the finite beam element method previously described.

Writing the program according to the equations described in Sect. 8.4.2, we obtain from the computation of the following results. As single span truss:

$$q_k = 3976 \text{ (KN/m)}$$

$$\text{modified safety factor } \nu = 3.74 .$$

As continuous three-span truss:

$$q_k = 4072 \text{ (KN/m)}$$

$$\text{modified safety factor } \nu = 4.97 .$$

The results indicate that there is not much difference between the solutions obtained by Galerkin's method and by the finite beam element method for a single-span truss. Taking the sidespan of the continuous truss as a single span and in Eq. (8.25b) setting  $n = 1$  instead of  $8/\pi^2$ , we obtained  $\nu = 4.67$ , which is only 6% smaller than  $\nu = 4.97$  of the continuous three-span truss, i.e. it is a good approximation.

## 8.5 Practical Method for Determining Critical Load

Li (1975) investigated the influences of the cross-sectional rigidities and load over-centers on the lateral buckling critical load and proposed a practical, simple method as follows:

In Eq. (8.23) the coefficient  $s = S_k/P_E$ , which marks the lateral buckling critical load, can be approximately calculated by the following formula:

$$s = s_0(1 - \delta_0 - \delta \cdot e), \quad (8.39)$$

where  $s_0$  is the value of  $s$  when the portal is assumed to be rigid. It can be approximately given by following formula:

$$s_0 = \frac{2}{3} \sqrt{3} \sqrt{\frac{(1+a)c}{1+a+c}} \mu, \quad (8.40)$$

where  $\mu = \mu_a/\mu_x$  (refer to Chap. 6) and  $a, c$  according to Eq. (8.22).  $\delta_0$  represents the influence of the portal deformation.  $\delta \cdot e$  represents the influence of load over-centers, where  $\delta$  is approximately constant and  $e = 2r/h$ ,  $r$  is the over-center of load  $q$ .

The curves representing the relation between  $s_0/\sqrt{\mu}$  and  $a, c$  according to Eq. (8.40) are shown in Figs. 8.3 and 8.4, respectively.

The figures show that  $s_0$  increases with increasing  $a$  and  $c$ . Hence, it is reasonable to increase  $a$  and  $c$  simultaneously if a large lateral buckling critical load is needed.

The effect of the deformation of portals on the lateral stability is mainly related to the ratio of the shearing rigidity of portal  $a_0$  and not to the ratios  $a$  and  $c$ . The curve representing the relation between  $1 - \delta_0$  and  $1/a_0$  is shown in the upper part of Fig. 8.5, from which it can be seen that the deformation of the portal has a large effect on the lateral stability.

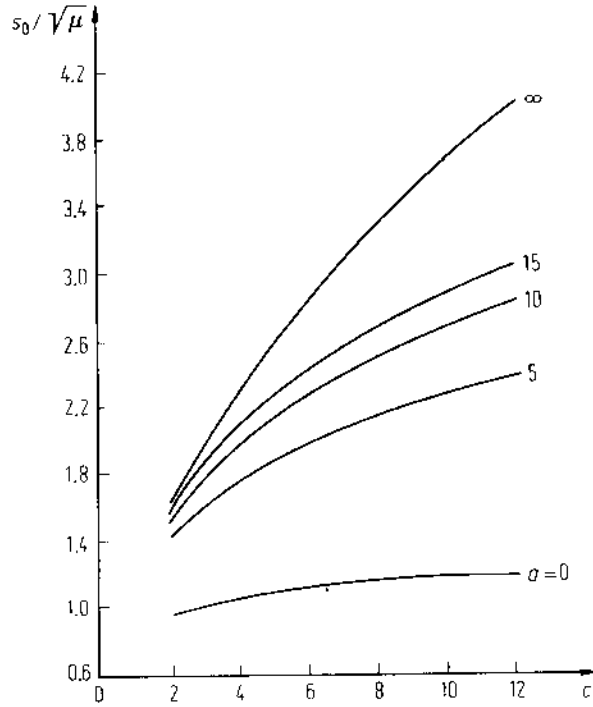


Fig. 8.3.  $s_0/\sqrt{\mu}$  vs.  $c$  curves in parameter  $a$

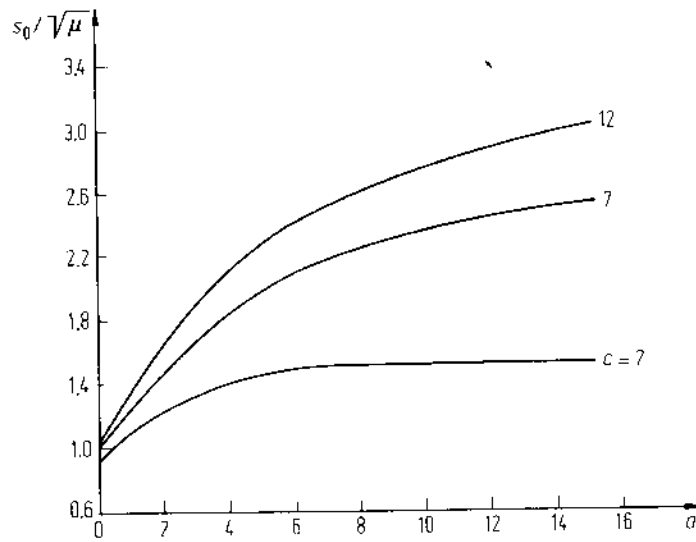


Fig. 8.4.  $s_0/\sqrt{\mu}$  vs.  $a$  curves in parameter  $c$



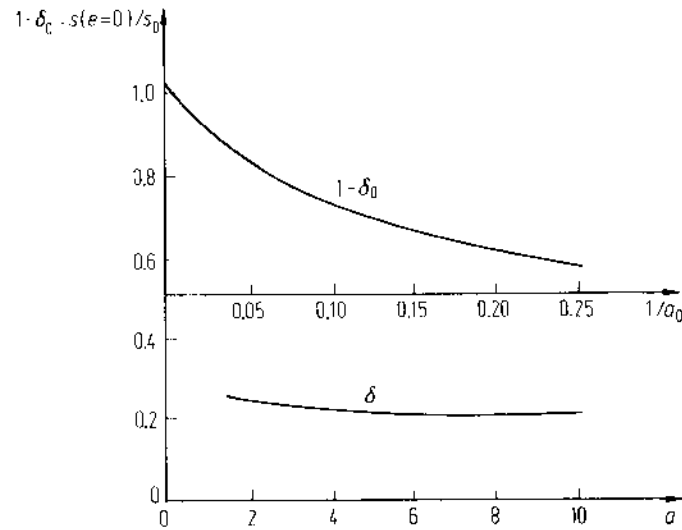


Fig. 8.5. Variation of  $1 - \delta_0$  with  $1/a_0$ , and  $\delta$  with  $a$

The weak interrelationship between the load over-center ratios and  $a$  is shown in the lower part of Fig. 8.5. The relationship between  $\delta$  and  $c$  is weaker than that between  $\delta$  and  $a$ . Practically,  $\delta \approx 0.20 \sim 0.25$ .

The preceding results indicate that in order to calculate the lateral buckling safety factor of truss approximately, we can first calculate the value of  $s$  using Eqs. (8.39) and (8.40) and curves in Fig. 8.5, and then the critical load  $q_k$ .

*Example.* The example shown in Sect. 8.3.2 is examined once again. From Eq. (8.40), we obtain

$$s_0 = 2.09 .$$

With the values of  $a_0$  and  $a$  in Sect. 8.3.2 we can obtain from Fig. 8.5

$$1 - \delta_0 = 0.78 ,$$

$$\delta = 0.2 ,$$

with  $e = 0.05$  we obtain

$$s = 1.62 .$$

According to Eq. (8.25b),

$$q_k = 3658 \text{ KN/m} .$$

The result differs from that obtained by Galerkin's method by only 4%.

## 8.6 Influence of the Slope of Inclined Portals

In all preceding calculations we have considered truss bridges having vertical portals. The influence of the slope  $\beta$  of an inclined portal frame of the trapezoidal

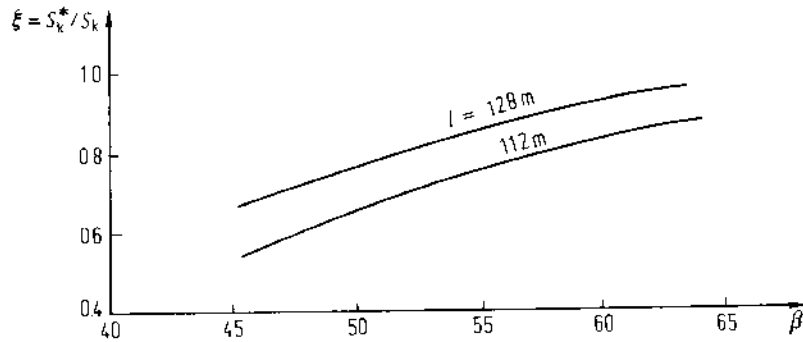


Fig. 8.6. The influence of the slope  $\beta$  of inclined portal

truss bridge on the lateral buckling has been investigated (Cao 1982) and the result is shown in Fig. 8.6, where  $\xi$  denotes the ratio of the lateral buckling load of the trapezoidal truss bridge to that of the corresponding truss bridge with vertical portals. It can be seen that the slope of portal has a great effect on the critical load  $S_k^*$  of lateral buckling. With increasing  $\beta$ ,  $S_k^*$  increases significantly. The value of  $S_k^*$  at  $\beta = 60^\circ$  almost doubles that at  $\beta = 45^\circ$  and is close to the value of  $S_k$ . It can also be seen that the influence of  $\beta$  on  $\xi$  decreases greatly with increasing of span length  $l$ .

## 8.7 Model Tests

To examine the reliability of the theory presented, two Plexiglass models of truss bridges were made and tested.

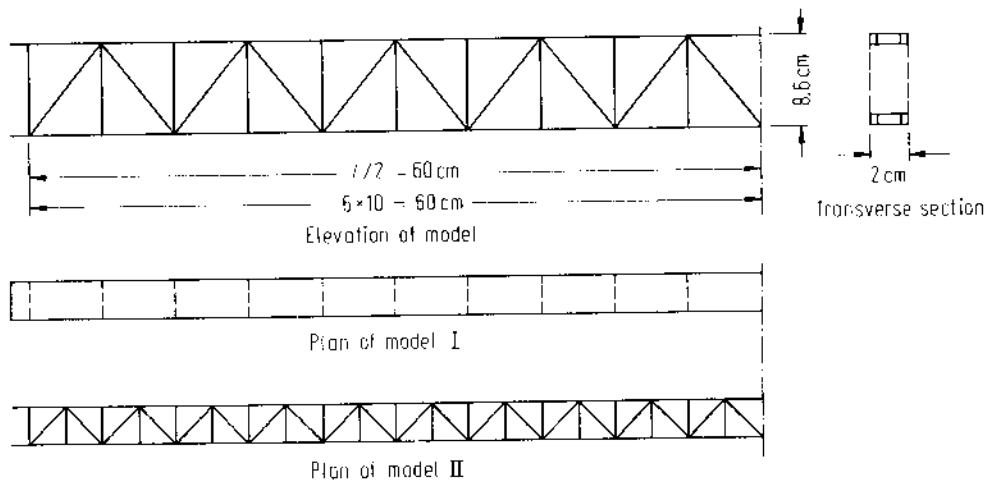


Fig. 8.7. The dimensions of the models

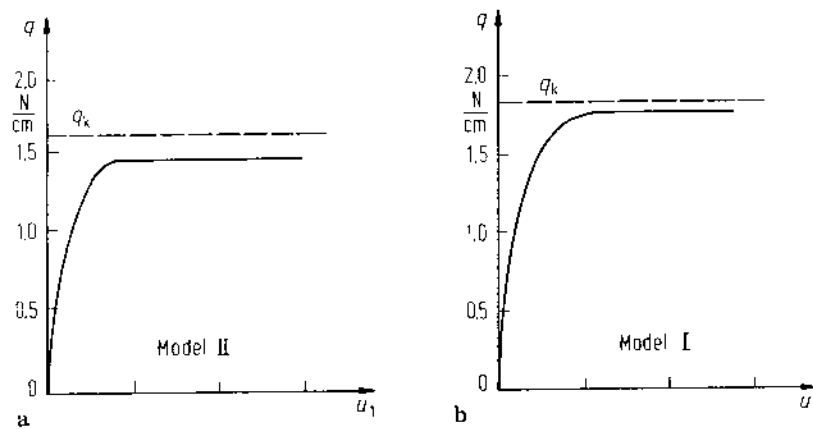


Fig. 8.8a,b. The test results

The dimensions of the models are shown in Fig. 8.7. Model I has an upper deck plate and a lower one acting together with the chord members. Model II has a top and a bottom lateral bracing.

The relations between the load and the lateral displacement  $u_1$  at the midspan of upper chord are shown in Fig. 8.8, in which it can be seen that owing to the unavoidable effect of initial eccentricity of the load, etc.,  $u_1$  occurs as soon as the load is applied.

The lateral buckling critical loads obtained by the model test and by the finite beam element method with ten elements in a span are given in Table 8.1.

It can be seen that the theoretical and experimental results agree well, but the test results are a little smaller than the theoretical ones owing to the initial eccentricity of loading and the imperfection of the construction of the models.

Table 8.1. Lateral buckling critical load  $q_k$ 

Name	Model	
	I	II
Test results (N/cm)	1.758	1.411
Theoretical results (N/cm)	1.839	1.631
Relative errors	4.6%	13.7%

## 9. Bending and Torsional Vibrations of Truss Bridges

In this chapter we will consider the bending and torsional vibrations of truss beam bridges and introduce two methods of analysis (Li 1975, 1978) based on the theory presented in Chap. 6.

An analytical method for simple truss bridges by applying the energy principle is given first. It follows the finite beam element method for single- and multiple-span continuous truss bridges.

### 9.1 Energy Method

#### 9.1.1 Basic Principle

For simply supported truss bridges having rigid vertical portals, an exact solution to the bending and torsional vibration can be obtained easily from differential Eq. (6.1) by using Fourier series to describe the vibrational displacements,  $u_0(z, t)$ ,  $\theta(z, t)$ ,  $\dot{\theta}(z, t)$ , and  $v_0(z, t)$  (Li 1975). But the portals of through truss bridges are deformable and have great influence on the bridge's behavior. It is difficult to get an exact solution from the differential equation, and approximate solution methods are desirable, such as energy method given in this chapter.

The bridge studied is simply supported with constant cross-section and vertical portals. In order that the study can be concentrated on the lateral bending and torsional vibrations, we assume that the mass of the bridge is symmetrically distributed with respect to the center line of the cross-section. Thus, the vertical bending vibration can be treated separately as a plane truss.

As is well known, Lagrange's equation without considering damping is

$$\frac{d}{dt} \frac{\partial T}{\partial \dot{q}_k} + \frac{\partial U}{\partial q_k} = 0, \quad (9.1)$$

in which

$T(\dot{q}_k, t)$  --- kinetic energy of the system in vibration,

$U(q_k, t)$  --- potential energy of the system,

$q_k$  --- general coordinate,

$\dot{q}_k = \frac{\partial q_k}{\partial t}$  --- corresponding velocity.

If  $T = 0$ , the preceding equation represents the static equilibrium of the system. In the following section, calculations of  $T$  and  $U$  will be given for the lateral bending and torsional vibrations of truss bridge.

### 9.1.2 Energy in Lateral Bending and Torsional Vibrations

The kinetic energy in the lateral bending and torsional vibrations of a truss bridge is

$$T = \frac{1}{2} \int_1 dz \int_F (\dot{u}^2 + \dot{v}^2) \rho dF,$$

or

$$T = \frac{1}{2} \int_1 dz \int_F [(\dot{u}_0 - y_2 \dot{\theta} - y_3 \dot{\tilde{\theta}})^2 + x^2 (\dot{\theta} - \dot{\tilde{\theta}})^2] \rho dF, \quad (9.2)$$

where  $\rho$  represents the mass density, and

$$y_2 = y - y_M, \quad y_3 = y - y_N.$$

The strain energy in the lateral bending and torsional vibrations can be expressed as

$$U_e = \frac{1}{2} \int_1 [D_{xx}(u_0'')^2 + C(\theta')^2 + D_{\omega\omega}(\theta'')^2 + 2D_{\omega\tilde{\omega}}\theta''\tilde{\theta}'' + D_{\tilde{\omega}\tilde{\omega}}(\tilde{\theta}'')^2 + \tilde{A}\tilde{\theta}^2] dz + \frac{1}{2} \cdot 2 \cdot 2\tilde{A}_0\tilde{\theta}_0^2, \quad (9.3)$$

in which the term outside the integral denotes the strain energy of deformation ( $2\tilde{\theta}_0$ ) of the portals at the two ends.

The potential energy of the dynamic loads  $p_x$ ,  $m_z$ ,  $\tilde{m}_z$ , corresponding to  $u_0$ ,  $\theta$ ,  $\tilde{\theta}$ , respectively, is

$$U_p = - \int_1 (p_x u_0 + m_z \theta + \tilde{m}_z \tilde{\theta}) dz. \quad (9.4)$$

The sum of  $U_e$  and  $U_p$  is the potential energy  $U$  in equation (9.1)

$$U = U_e + U_p. \quad (9.5)$$

### 9.1.3 Equation of Bending and Torsional Vibrations

In the following we consider in detail the case of a half-wave symmetrical vibration that has great practical significance. With reference to Fig. 6.2, the following approximate functions that satisfy the boundary conditions of a simply supported truss (see Chap. 6) are adopted:

$$\begin{aligned}
 u_0(z, t) &= (k_2 + j_2)q_0(t) + \lambda_c q_1(t) \sin \zeta z, \\
 \theta(z, t) &= q_0(t) + q_2(t) \sin \zeta z, \\
 \tilde{\theta}(z, t) &= q_0(t) + q_3(t) \sin \zeta z, \\
 \zeta &= \pi/l,
 \end{aligned} \tag{9.6}$$

in which  $\lambda_c$  is a constant, length being its unit, i.e.  $\lambda_c = h/2$ ;  $q_0$  represents the displacement of the portal; and  $q_1, q_2, q_3$  represent the amounts of increment at mid-span. They are the general coordinates in Eq. (9.1). The preceding expressions can be written as:

$$\begin{aligned}
 \{\delta\} &= [L] \{q\}, \\
 [L] &= \begin{bmatrix} (k_2 + j_2) & \lambda_c \sin \zeta z & 0 & 0 \\ 1 & 0 & \sin \zeta z & 0 \\ 1 & 0 & 0 & \sin \zeta z \end{bmatrix}, \\
 \{q\} &= [q]^T = [q_0 \ q_1 \ q_2 \ q_3]^T
 \end{aligned} \tag{9.7}$$

Substituting Eq. (9.7) into Eq. (9.2) and (9.3), we obtain

$$T = \frac{l}{4} \{\dot{q}\}^T [M] \{\dot{q}\}, \tag{9.8}$$

$$U_e = \frac{l}{4} \{q\}^T [K] \{q\}, \tag{9.9}$$

where  $[M]$  is the mass matrix,  $[K]$  is the stiffness matrix. Substituting Eq. (9.7) into Eq. (9.4), we have

$$U_p = -\frac{l}{2} \{q\}^T \{P\},$$

where

$$\begin{aligned}
 \{P\} &= \frac{2}{l} \int [L]^T \{p\} dz, \\
 \{p\} &= [p]^T = [p_x \ m_z \ \tilde{m}_z]^T.
 \end{aligned} \tag{9.10}$$

Substituting  $T, U_e, U_p$  from Eq. (9.8), (9.9), (9.10) into Eq. (9.1), we obtain the following equation of vibration:

$$\left( [K] + [M] \frac{d^2}{dt^2} \right) \{q(t)\} = \{p(t)\}. \tag{9.11}$$

$[K]$  and  $[M]$  in the above equation are matrices of fourth order. To make the calculation easier, they may be transformed to third order. The procedure is as follows: Using the deformation compatibility Eq. (6.17) for the bridge portal,  $q_0$  can be expressed as a function of  $q_1, q_2, q_3$  —  $q_0 = f(q_1, q_2, q_3)$ . Hence Lagrange's equation will have this function as an additional requirement:

$$\frac{d}{dt} \frac{\partial T}{\partial \dot{q}} + \frac{\partial U}{\partial q_k} + \left( \frac{d}{dt} \frac{\partial T}{\partial \dot{q}_0} + \frac{\partial U}{\partial q_0} \right) \frac{\partial f}{\partial q_k} = 0, \quad (9.1a)$$

$$k = 1, 2, 3.$$

The vibration equation (9.11) derived by using the preceding expression contains three general coordinates  $q_1, q_2, q_3$ , and the corresponding stiffness matrix  $K$  and mass matrix  $M$  are of third order. The result is as follows: Let

$$\begin{bmatrix} a_0 & a & c \\ d_2 & d_3 & d_{23} \end{bmatrix} = \frac{1}{D_{xx} \lambda_c^2 \zeta^4} \begin{bmatrix} \tilde{A}_0 \zeta & \tilde{A} & C \zeta^2 \\ D_{\omega\omega} \zeta^4 & D_{\omega\omega} \zeta^4 & D_{\omega\omega} \zeta^4 \end{bmatrix}. \quad (9.12)$$

The function  $q_0$  can be written

$$q_0 = [n_k] \{q_k\}, \quad k = 1, 2, 3, \quad (9.13)$$

$$[n_k] = \frac{1}{a_0} [2\bar{k}_2 (c + d_2 + d_{23}) (d_{23} + d_3)].$$

The stiffness matrix is

$$[K] = D_{xx} \lambda_c^2 \zeta^4 [k], \quad (9.14)$$

$$[k] = \begin{bmatrix} 1 & 0 & 0 \\ (c + d_2) & d_{23} & \\ \text{symmetry} & (a + d_{33}) & \end{bmatrix} + \begin{bmatrix} n_1 & 0 \\ n_2 & 0 \\ n_3 & \alpha \end{bmatrix} \times \begin{bmatrix} n_1 \alpha_0 & n_2 \alpha_0 & (n_3 \alpha_0 + \alpha) \\ n_1 & n_2 & n_3 \end{bmatrix}, \quad (9.15)$$

where

$$[\alpha_0 \ \alpha] = \left[ \left( \frac{4}{\pi} a_0 + 2a \right) \frac{4}{\pi} a \right].$$

For the case of uniform distribution of mass, the mass matrix is

$$[M] = \tilde{M} \lambda_c^2 [v], \quad (9.16)$$

where

$$[v] = \begin{bmatrix} 1 & -v_2 & -v_3 \\ (v_{22} + v_{11}) & (v_{23} - v_{11}) & \\ \text{symmetry} & (v_{33} + v_{11}) & \end{bmatrix} + \begin{bmatrix} n_1 & (\mu_1 + n_1 \mu_0) \\ n_2 & (\mu_2 + n_2 \mu_0) \\ n_3 & (\mu_3 + n_3 \mu_0) \end{bmatrix} \begin{bmatrix} \mu_1 & \mu_2 & \mu_3 \\ n_1 & n_2 & n_3 \end{bmatrix},$$

$$[\mu_0 \ \mu_1 \ \mu_2 \ \mu_3] = \left[ 8v_{00} \quad -\frac{8}{\pi} v_0 \quad \frac{8}{\pi} v_{20} \quad \frac{8}{\pi} v_{30} \right],$$

$$v_i = \frac{1}{\lambda_c \tilde{M}} \int_F \xi_i \rho dF,$$

$$v_{ik} = \frac{1}{\lambda_c^2 \tilde{M}} \int_F \xi_i \xi_k \rho dF,$$

$$\tilde{M} = \int_F \rho dF,$$

$$[\xi_1 \ \xi_2 \ \xi_3 \ \xi_0] = [x \ y_2 \ y_3 \ (y - h_2)].$$

The second matrices on the right-hand sides of Eqs. (9.15) and (9.17) represent the influence of the deformation of the bridge portals on the stiffness and mass matrices.

#### 9.1.4 Lateral Bending and Torsional Free Vibrations

For free vibration, the dynamic load term on the right-hand side of Eq. (9.11) is zero and  $q(t)$  has the following form:

$$q_i(t) = A \cos \omega t + B \sin \omega t ,$$

in which  $\omega$  is the circular frequency of free vibration,  $A$  and  $B$  are constants of integration. Damping, which can usually be neglected in the calculation of  $\omega$ , is not considered here.

The equation of free vibration can be found by substituting the preceding expression into Eq. (9.11):

$$([K] - \omega^2[M])\{q\} = 0 . \quad (9.17)$$

In the case of uniform mass  $\bar{M}$  over the whole bridge, this equation can be written as

$$([k] - w^2[v])\{q\} = 0 , \quad (9.18)$$

where

$$w^2 = \frac{\omega^2}{\omega_y^2} , \quad \omega_y^2 = \frac{\bar{M}}{D_{xx}l^4} .$$

Only when the denominator determinant is equal to zero, does  $\{q\}$  have a nonzero solution, where the frequency equation for finding  $\omega$  can be obtained:

$$|[K] - \omega^2[M]| = 0 , \quad (9.19)$$

or

$$|[k] - w^2[v]| = 0 . \quad (9.20)$$

By substituting  $\omega_i$  or  $w_i$  ( $i = 1, 2, 3$ ) obtained into Eqs. (9.17) or (9.18), the mode of vibration, i.e., the relative proportion of  $q_{ik}$  ( $k = 0, 1, 2, 3$ ) can be found.

After the determination of the free vibration, the forced vibration of a truss bridge can be analyzed by the resolution of vibration modes and is omitted here.

## 9.2 Finite Beam Element Method

For multiple-span continuous truss bridges, or for variable sectional rigidity and mass distribution along the span of the bridge, it will be difficult to solve the bending and torsional vibration problems analytically. In the following, the application of the finite beam element method will be briefly introduced. Emphasis is put on the



calculation of free vibration, since the solution for forced vibration can be found by the method of modal analysis.

### 9.2.1 Mass Matrix of Truss Beam Element

The required stiffness and mass matrices of a truss beam element can be calculated from the differential Eq. (6.1). The derivation of element stiffness matrix has been shown in the preceding chapters. The mass matrix will be derived below.

The nodal displacement parameters and the element displacement function for the truss beam element are given by Eqs. (8.31a) and (8.31b).

The displacements at any point on the truss beam section can be expressed in terms of matrix as follows:

$$\begin{Bmatrix} u \\ v \end{Bmatrix} = \begin{bmatrix} 1 & -\xi_2 & -\xi_3 \\ 0 & \xi_1 & -\xi_1 \end{bmatrix} \begin{Bmatrix} u \\ \theta \\ \hat{\theta} \end{Bmatrix},$$

i.e.,

$$\begin{Bmatrix} u \\ v \end{Bmatrix} = [A] \{\delta\} = [A][N] \{\delta\}^e.$$

In the case of free vibration the force of inertia is

$$\{q_M\} = -\rho \begin{Bmatrix} \ddot{u} \\ \ddot{v} \end{Bmatrix} = \rho \omega^2 [A][N] \{\delta\}^e.$$

This produces the nodal force of inertia

$$\{F_M\}^e = \omega^2 [m]^e \{\delta\}^e,$$

where the element mass matrix has following form:

$$\begin{aligned} [m]^e &= \int_0^e \rho [N]^T [A]^T [A] [N] dz \\ &= \int_0^e [N]^T [S] [N] dz, \end{aligned} \quad (9.21)$$

in which

$$[S] = \begin{bmatrix} s_{11} & s_{12} & s_{13} \\ & s_{22} & s_{23} \\ \text{symmetry} & & s_{33} \end{bmatrix}$$

$$s_{11} = \iint_F \rho dF = \tilde{M},$$

$$s_{12} = -S_x + y_M \tilde{M},$$

$$s_{13} = -S_x + y_N \tilde{M},$$

$$s_{22} = J_x + J_y - 2y_M S_x + y_M^2 \tilde{M},$$

$$S_{23} = J_x - J_y - (y_M + y_N)S_x + y_M y_N \tilde{M},$$

$$S_{33} = J_x + J_y - 2y_N S_x + y_N^2 \tilde{M},$$

$\tilde{M}$  — overall mass of the section,

$S_x$  — static moment of mass about x-axis,

$J_x, J_y$  — moment of inertia of section mass about x and y-axis, respectively.

Assembling the element stiffness and mass matrices, we have the global stiffness matrix  $[K]$  and global mass matrix  $[M]$ . Then the frequency of free vibration can be calculated from Eqs. (9.17) to (9.20).

### 9.3 Example (Li 1975, 1978)

Taking the Wuhan Bridge over the Yangzi River as an example, the characteristics of lateral bending and torsional vibrations of truss bridges are investigated.

The Wuhan Bridge as shown in Fig. 9.1 is a three-span continuous truss bridge. The upper deck is for highway and pedestrian traffic, while the lower one is for a two-track railway.

In order to investigate the forced vibration possibly induced by pedestrian loading, the upper deck with full pedestrian loading is taken as the object of analysis. The distribution of the loads upon the cross section is shown in Fig. 9.2. The free vibration of a corresponding single-span bridge is calculated by using the analytical method as well as the finite element, while the three-span continuous bridge is calculated only by the finite element method.

In the calculation by the finite element method, two cases, four and eight elements for a span, are considered. The shear stiffness  $R$  of the sway bracing is also taken for two cases:  $R_1$  and  $6R_1$ . The natural circular frequencies ( $\text{Hz}/2\pi$  s) and corresponding vibration modes can be seen from Figs. 9.3 and 9.4.

The calculation result shows that the values of  $\omega$  from the finite beam element method and the analytical method are quite close, especially for the first and second

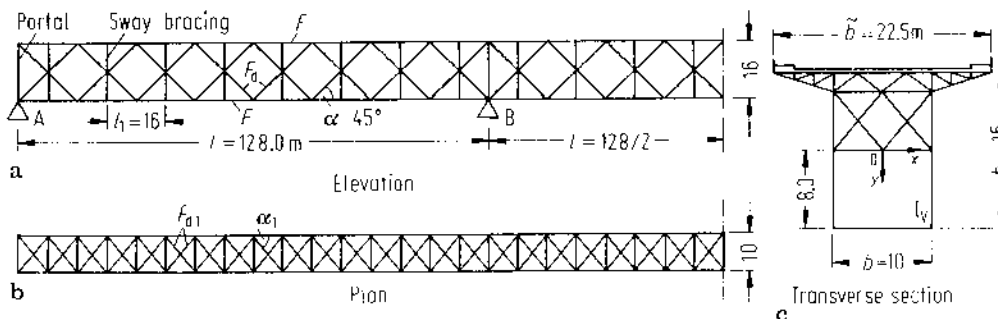


Fig. 9.1a-c. The dimension of the Wuhan Bridge

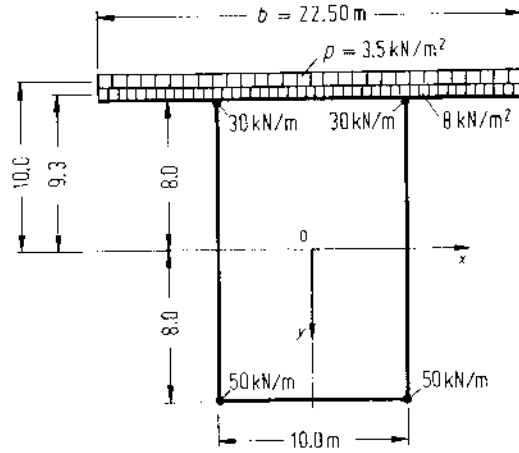


Fig. 9.2. The distribution of loads

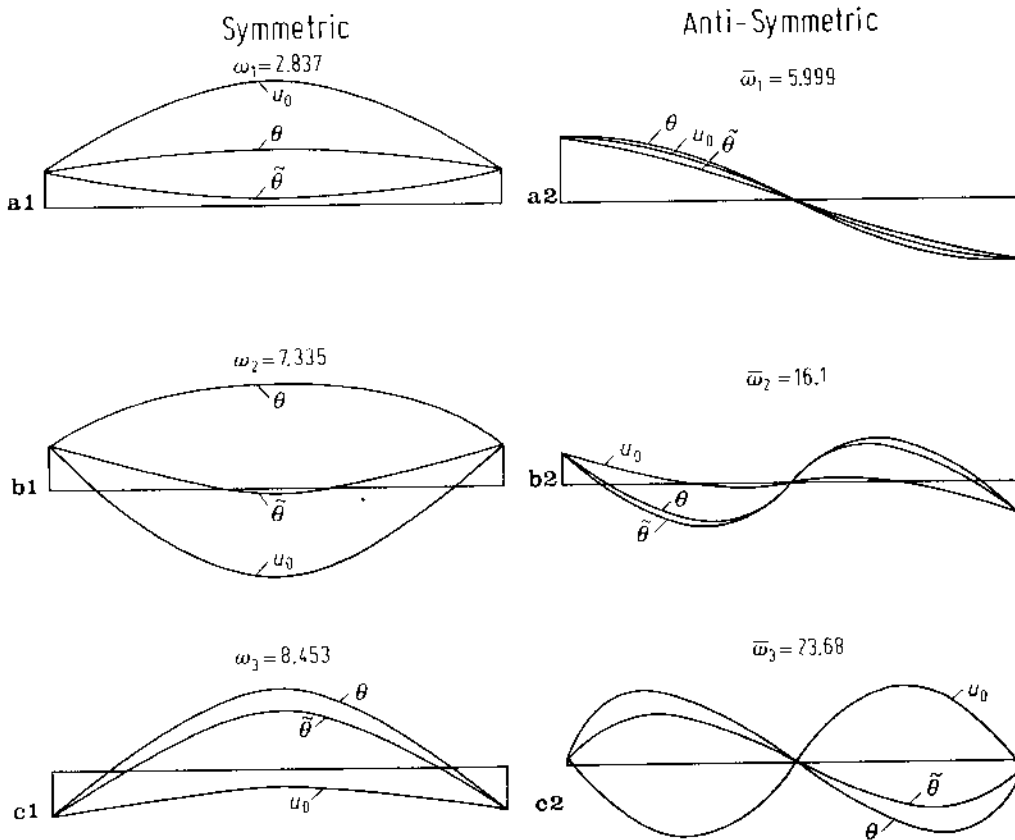


Fig. 9.3a-c. Lateral bending-torsional free vibrations of a single span truss bridge ( $R = R_1$ )

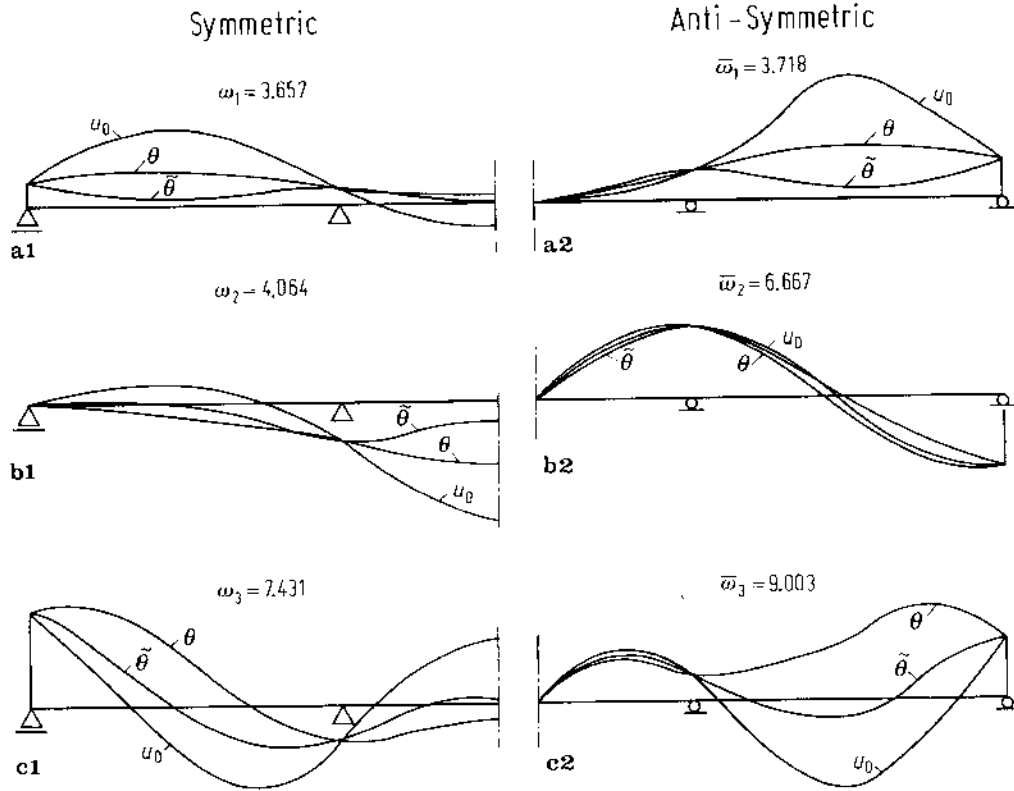


Fig. 9.4a-c. Lateral bending-torsional free vibrations of a continuous three-span truss bridge ( $R = 6R_1$ )

frequencies. The difference between the frequencies, when a span is divided into four and eight elements, is smaller than 1%. Therefore, in engineering practice, it is sufficiently accurate to use four elements for one span in the calculation.

By increasing the shear stiffness of the sway bracing  $R_1$  by six times, the increase in the first and second frequencies is only about 10%, its influence being small. However, the influence of the deformation of the bridge portal is significant. For instance, the fundamental frequency  $\omega_1$  increases by 30% when the bridge portal is assumed to be rigid.

In a single-span truss bridge the free vibration  $\omega_1$  as shown in Fig. 9.3 is mainly in lateral bending ( $u_0$ ), while the rest are all dominated by torsion and warping ( $\theta, \tilde{\theta}$ ). However, for the three-equal-span continuous truss bridge the free vibrations shown in Fig. 9.4 are mainly dominated by bending.

It can be seen further that  $\omega_1, \bar{\omega}_1, \omega_2$  for the single-span truss are comparable with to  $\omega_1, \bar{\omega}_2, \omega_3$  for the three-equal-span truss, and the corresponding vibration modes are similar in the side or middle span.

Therefore, for approximate vibration calculation, the three-equal-span truss beam can be replaced by a single-span one.

Based on this idea, the forced vibration possibly induced by pedestrian loading on the bridge was analyzed (Li 1975). Assume the overall width of the bridge deck

$b = 22.5$  m, and full pedestrian loading  $p_y = 3.5$  kN/m<sup>2</sup>. The moment on the left and right side with respect to the center of the cross section is

$$m_z = -\tilde{m}_z = m = \pm \frac{p_y b^2}{8} = \pm 221.5 \text{ kN/m}.$$

If it is in a state of rest without any disturbance, the moment on both sides is balanced. It would occur a disturbance moment  $\varepsilon m$ , if there is a small disturbance  $\varepsilon$ . Assume  $\varepsilon m$  to be approximately distributed along the whole span, the calculation reveals that the symmetrical second mode for the single span is dominant, and that  $\varepsilon = 5\%$  would suffice to induce the complete amplitude of the lateral displacements  $u$  of remarkable magnitude: 8 mm at the top of the end portal, 11 mm at the bottom chord at midspan, and 3 mm at the upper chord at midspan. They are close to the result of observation when the bridge swayed under the load of crowded people during its opening, and the period of this vibration mode is also very close to that (0.9 s) observed.

## 10. Spatial Analysis of Arch-Truss Bridges

An Arch and truss combined system, as shown in Fig. 10.1, is often used for long-span bridges. For this kind of structure the analysis of stresses due to wind loads and the calculation of lateral stability are related to lateral bending and torsion. A finite arch-beam element method based on the theory given in Chap. 6 has been developed (Li and Shi 1978; Li et al. 1983) and is presented in this chapter.

### 10.1 Finite Elements of the Arch-Truss

A part of an arch-truss is shown in Fig. 10.2. It is assumed that the hanger, the horizontal strut of arch, and that of the top lateral bracing of truss form a cross-frame. If the arch is subjected to lateral loads (such as wind loads), a part of the load is transmitted by the wind bracing of the arch to the supports. The rest of it is transmitted by the cross-frames to the truss, and then to the supports. Therefore, the behavior of the arch-truss bridge, when subjected to lateral loads, is related to the lateral bending, torsional rigidities of truss and arch, as well as the shear rigidity of the cross-frame.

First, the truss and arch are transformed into a continuous structural model, and the rigidity of the cross-frame is distributed over its spacing. Then the bridge

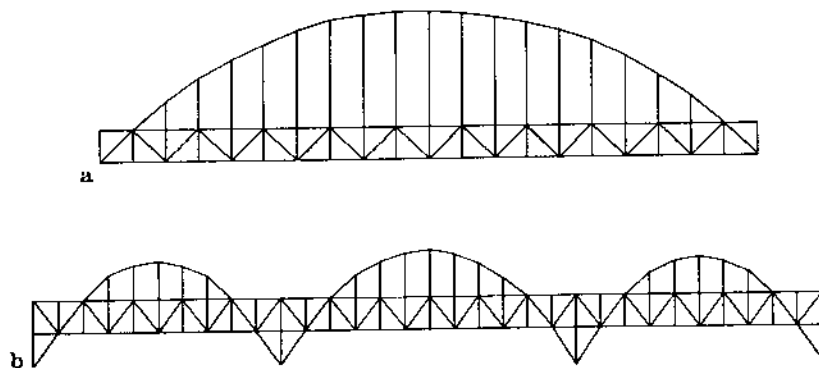
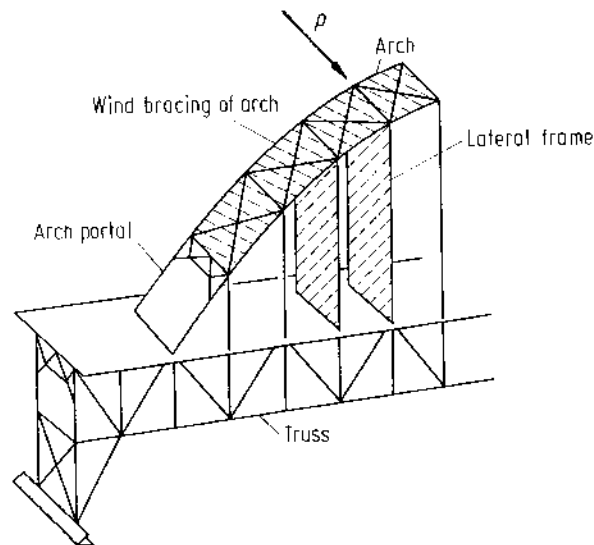
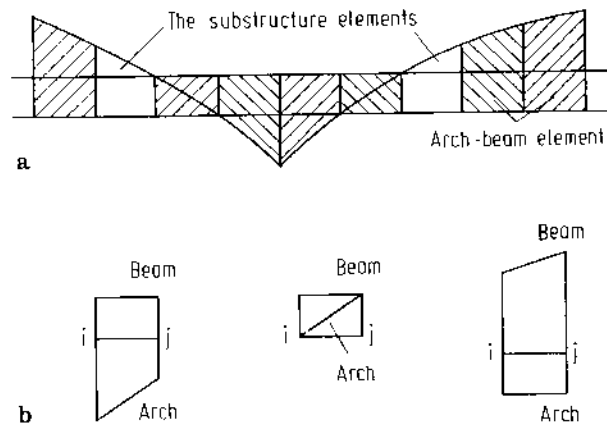


Fig. 10.1a,b. Typical arch-truss bridges



**Fig. 10.2.** Constituent parts of an arch-truss bridge



**Fig. 10.3a,b.** Types of arch-beam element

is divided into arch-beam elements along the longitudinal axis of the bridge, as shown in Fig. 10.3a.

There are three types of arch-beam element and a substructure element at arch portal as shown in Fig. 10.3. For the stress analysis, one panel can be taken as an arch-beam element, and for the lateral buckling and vibration analysis, the length of elements may not be divided according to the panels.

The elements at the arch portals, being different from the other part of arch, are considered as the substructural element, similar to the end truss beam element for inclined portals in Chap. 7.

As the cross-section of the bridge is generally symmetrical about the center line of the cross-section, the vertical bending can be treated separately, thus we consider in the following only the lateral bending and torsion.

## 10.2 Nodal Displacements of the Arch-Beam Element in Lateral Bending and Torsion

For the analysis of the stresses caused by lateral bending and torsion, the number of the nodal displacements of the truss is eight, i.e. the lateral displacement  $u$  and its derivative  $u'$ , the angle of twist  $\theta$  and the distortion  $\tilde{\theta}$  of the cross-section, and their first and second derivatives (see Chap. 8).

The displacements of arch are the lateral translation  $\hat{u}$  and its derivative  $\hat{u}' = d\hat{u}/dz$ , and the torsion angle  $\hat{\theta}$ . Since the axial deformation and displacement of the hangers are very small, we can consider that the rotation of the arch  $\hat{\psi}$  is equal to that of the truss  $\psi = \theta - \nu\tilde{\theta}$ , where for rectangular cross-section of truss,  $\nu = 1$ ; see Fig. 10.8. Thus, the nodal displacement parameters of the arch-beam element are as follows (Fig. 10.4):

$$\{\delta\}^e = \begin{Bmatrix} \delta_i \\ \delta_j \end{Bmatrix},$$

$$\{\delta_i\} = [\hat{u}_i \ \hat{u}'_i \ u_i \ u'_i \ \theta_i \ \theta'_i \ \theta''_i \ \tilde{\theta}_i \ \tilde{\theta}'_i \ \tilde{\theta}''_i]^T, \quad (10.1)$$

$$\{\delta_j\} = [\hat{u}_j \ \hat{u}'_j \ u_j \ u'_j \ \theta_j \ \theta'_j \ \theta''_j \ \tilde{\theta}_j \ \tilde{\theta}'_j \ \tilde{\theta}''_j]^T.$$

## 10.3 Stiffness Matrix of Arch-Beam Element

The stiffness matrix of the arch-beam element can be written as follows:

$$[k] = [k]_T + [k]_A + [k]_F, \quad (10.2)$$

where  $[k]_T$ ,  $[k]_A$ ,  $[k]_F$  are the element stiffness matrix of the truss, of the arch, and of the cross-frame, respectively, and will be deduced separately as follows.

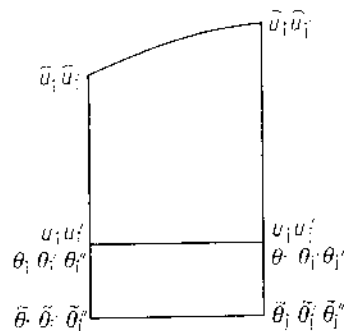


Fig. 10.4. The nodal displacement parameters of an arch-beam element



### 10.3.1 Element Stiffness Matrix of Truss $[k]_T$

The element stiffness matrix of truss can be written as follows:

$$[k]_T = [L]_T^T [\bar{k}]_T [L]_T, \tag{10.3}$$

where  $[\bar{k}]_T$  is that referred to local coordinates and  $[L]_T$  is the transformation matrix

$$[L]_T = \begin{bmatrix} L_{T1} & 0 \\ 0 & L_{T3} \end{bmatrix},$$

$$[L_{Ti}] = [L_{Tj}] = \begin{bmatrix} 0 & 0 & 1 & & & 0 \\ & & & 1 & & \\ & & & & 1 & \\ & & & & & 1 \\ & & & & & & 1 \\ & & & & & & & 1 \\ & 0 & & & & & & & 1 \end{bmatrix}.$$

### 10.3.2 Element Stiffness Matrix of Arch $[k]_A$

It is assumed that the built-up arch has an open cross-section or a closed cross-section, as shown in Fig. 10.5. In elevation, the arch has a shape of a broken line or a continuous curve. Considering that one arch-beam element may include several panels, we treat the arch as a curve in deducing the element stiffness matrix.

The coordinate axes of arch are shown in Fig. 10.6. The nodal displacement parameters of arch element (Fig. 10.7) are defined by

$$\{\hat{\delta}\}^e = \begin{Bmatrix} \hat{\delta}_i \\ \hat{\delta}_j \end{Bmatrix}, \quad \{\hat{\delta}_i\} = \begin{Bmatrix} \hat{u}_{0i} \\ \hat{u}'_{0i} \\ \hat{\theta}_i \\ \hat{\theta}'_i \end{Bmatrix}, \quad \{\hat{\delta}_j\} = \begin{Bmatrix} \hat{u}_{0j} \\ \hat{u}'_{0j} \\ \hat{\theta}_j \\ \hat{\theta}'_j \end{Bmatrix}. \tag{10.4}$$

For the displacement functions  $\hat{u}$  and  $\hat{\theta}$  of the element we take the polynomials of third order. They can be given as follows:

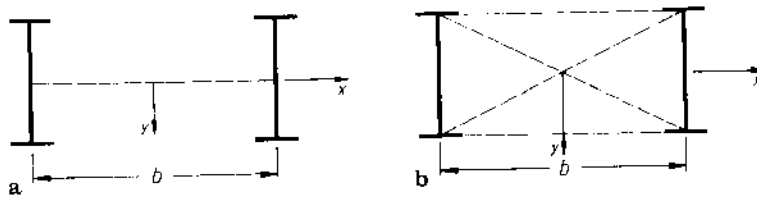


Fig. 10.5a,b. Sections of built-up arches

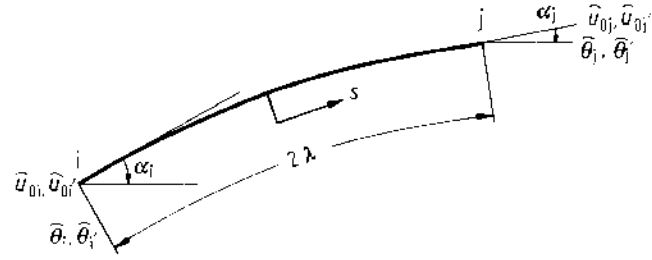
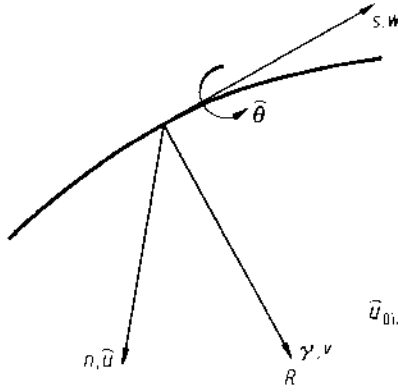


Fig. 10.6. Coordinate system of arch Fig. 10.7. The nodal displacement parameters of arch element

$$\begin{aligned} \begin{Bmatrix} \hat{u} \\ \hat{\theta} \end{Bmatrix} &= \begin{bmatrix} N_1 & N_2 & 0 & 0 & N_3 & N_4 & 0 & 0 \\ 0 & 0 & N_1 & N_2 & 0 & 0 & N_3 & N_4 \end{bmatrix} \{\hat{\delta}\}^e \\ &= \begin{Bmatrix} N_u \\ N_\theta \end{Bmatrix} \{\hat{\delta}\}^e = [N]_2 \{\hat{\delta}\}^e, \end{aligned} \quad (10.5)$$

where  $N_i$  is polynomial of third order. We can calculate the element stiffness matrix of the arch from its physical equations. According to Fig. 10.6, the lateral deflection curvature  $\chi_r$ , torsional curvature  $\chi_s$ , and its derivative  $\chi'_s$  are as follows:

$$\{\chi\}_A = \begin{Bmatrix} \chi_r \\ \chi_s \\ -\chi'_s \end{Bmatrix} = [\hat{B}]_A \{\hat{\delta}\}^e, \quad (10.6)$$

where

$$[\hat{B}]_A = \begin{Bmatrix} \left( -N_u'' + \frac{1}{R} N_\theta \right) \\ \left( \frac{N_u'}{R} + N_\theta' \right) \\ \left( -\frac{N_u''}{R} - N_\theta'' \right) \end{Bmatrix}, \quad (10.7)$$

where  $R$  = the radius of curvature.

The bending moment, torsional moment, and the bimoment are

$$\{\hat{S}\}_A = \begin{Bmatrix} M_r \\ M_s \\ M_\omega \end{Bmatrix} = \begin{bmatrix} \hat{B}_y & 0 & 0 \\ 0 & \hat{C} & 0 \\ 0 & 0 & \hat{D}_\omega \end{bmatrix} \begin{Bmatrix} \chi_r \\ \chi_s \\ -\chi'_s \end{Bmatrix} = [\hat{D}]_A \{\chi\}_A, \quad (10.8)$$

or

$$\{\hat{S}\} = [\hat{D}]_A [\hat{B}]_A \{\hat{\delta}\}^e, \quad (10.9)$$

where according to Fig. 10.5  $\hat{B}_y = EI_y \cdot \mu_y$ ,  $I_y = \frac{\hat{F}}{2} b^2$ ,  $\mu_y$  is the modification factor of the lateral bending rigidity of the arch, considering the influence of the shearing deformation see Chap. 6.

$\hat{C} = \frac{G}{3} \sum h \delta^3$  — The rigidity of free torsion of arch.

$\hat{D}_\omega$  — The rigidity of warping torsion of the cross-section of arch.

Assume that the cross-section of arch is rigid, we have  $\hat{D}_\omega = \frac{1}{4} \hat{B}_x b^2$ , where  $\hat{B}_x = EI_x$ .

The element stiffness matrix of arch in local coordinates can be obtained by using Eqs. (10.6) and (10.9). That is

$$[\hat{k}]_A = \int [\hat{B}]_A^T [\hat{D}] [\hat{B}]_A ds. \quad (10.10)$$

The relations between the nodal displacement parameter of arch element in the local coordinates  $\{\hat{\delta}\}^e$  and those of arch-beam element  $\{\delta\}^e$  are

$$\begin{aligned} \hat{u}'_{0i} &= \hat{u}'_i \cos \alpha_i + (\theta_i - \hat{\theta}_i) \sin \alpha_i, \\ \hat{\theta}'_i &= -\hat{u}'_i \sin \alpha_i + (\theta_i - \hat{\theta}_i) \cos \alpha_i. \end{aligned}$$

Taking  $\hat{\theta}'_i = (\theta_i - \hat{\theta}_i)/\cos \alpha_i$  and

$$[\hat{L}_i] = \begin{bmatrix} 1 & 0 & 0 & 0 & 0 & 0 & 0 & 0 & 0 & 0 \\ 0 & \cos \alpha_i & 0 & 0 & \sin \alpha_i & 0 & 0 & -\sin \alpha_i & 0 & 0 \\ 0 & -\sin \alpha_i & 0 & 0 & \cos \alpha_i & 0 & 0 & -\cos \alpha_i & 0 & 0 \\ 0 & 0 & 0 & 0 & 0 & 1/\cos \alpha_i & 0 & 0 & -1/\cos \alpha_i & 0 \end{bmatrix},$$

we get

$$\{\hat{\delta}_i\} = \begin{Bmatrix} \hat{u}_{0i} \\ \hat{u}'_{0i} \\ \hat{\theta}_i \\ \hat{\theta}'_i \end{Bmatrix} = [\hat{L}_i] \{\delta_i\}.$$

Similarly,

$$\{\hat{\delta}_j\} = [\hat{L}_j] \{\delta_j\}.$$

Combining the two equations above, we obtain

$$\{\hat{\delta}\}^e = \begin{bmatrix} \hat{L}_i & 0 \\ 0 & \hat{L}_j \end{bmatrix} \{\delta\}^e = [\hat{L}] \{\delta\}^e, \quad (10.11)$$

where  $[\hat{L}]$  = the transformation matrix. Then the arch element stiffness matrix of the arch-beam element can be written as follows:

$$[k]_A = [L]^T [\hat{k}_A] [L]. \quad (10.12)$$

### 10.3.3 Element Stiffness Matrix of the Cross-frame $[k]_F$

The cross-frames may be arranged at nodes of element. Its shearing rigidities can be equally divided by two adjacent elements at the node.

The undeformed and deformed states of cross-frame are shown in Fig. 10.8. The shear deformation can be written as follows:

$$\gamma_i = \hat{\phi}_i - \psi_i = \frac{\hat{u}_i - u_i}{\hat{h}_i} - \theta_i + \tilde{\theta}_i, \quad (10.13)$$

where  $u_1 = u_i + k_{1i}\theta_i + j_{1i}\tilde{\theta}_i$  (see Fig. 6.2). Setting  $\eta_{1i} = k_{1i} + \hat{k}_i$ ,  $\tilde{\eta}_{1i} = j_{1i} - \hat{h}_i$ , we get

$$\begin{aligned} \gamma_i &= \frac{1}{\hat{h}_i} [1 \ 0 \ -1 \ 0 \ -\eta_{1i} \ 0 \ 0 \ -\tilde{\eta}_{1i} \ 0 \ 0] \{\delta_i\} \\ &= [B_i] \{\delta_i\}. \end{aligned} \quad (10.14a)$$

Similarly,

$$\gamma_j = [B_j] \{\delta_j\}. \quad (10.14b)$$

Then, we obtain

$$\{\gamma\}_F = \begin{Bmatrix} \gamma_i \\ \gamma_j \end{Bmatrix} = \begin{bmatrix} B_i & 0 \\ 0 & B_j \end{bmatrix} \begin{Bmatrix} \delta_i \\ \delta_j \end{Bmatrix} = [B]_F \{\delta\}^e. \quad (10.15)$$

The physical equations can be written as follows:

$$\{S\}_F = \begin{Bmatrix} S_i \\ S_j \end{Bmatrix} = \begin{bmatrix} \bar{R}_i/2 & 0 \\ 0 & \bar{R}_j/2 \end{bmatrix} \begin{Bmatrix} \gamma_i \\ \gamma_j \end{Bmatrix} = [D]_F \{\gamma\}_F.$$

From the preceding equation, the element stiffness matrix of the cross frame can be calculated:

$$[k]_F = \int_{\hat{h}} [B]_F^T [D]_F [B]_F d\hat{h}. \quad (10.16)$$

There is no cross-frame at the nodes where the arch is connected with truss beam, and here  $[k]_F$  vanishes.

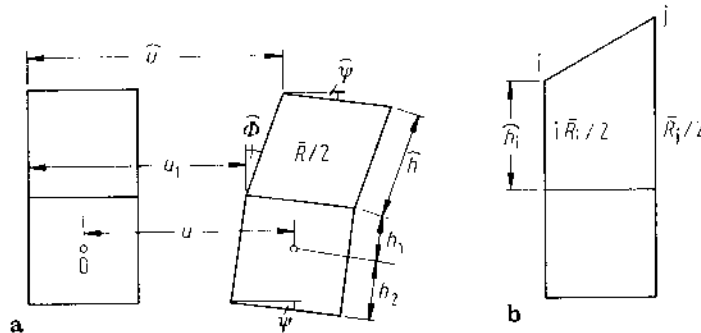


Fig. 10.8a,b. The undeformed and deformed states of the cross-section

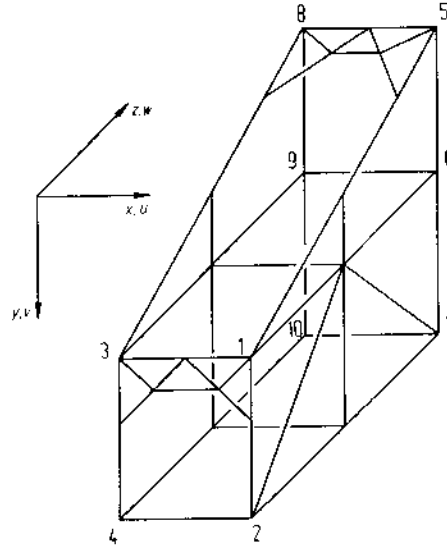


Fig. 10.9. A typical substructure element

### 10.4 Substructure Element at the Arch Portal

A substructure element at arch portal is shown in Fig. 10.9. It has ten boundary nodes. In the way described in Sect. 7.2, we can get the condensed stiffness matrix and load vector matrix of the substructure element as well as its transformation matrix.

### 10.5 Boundary Conditions

For the bridge having arch ribs directly connected to the fixed supports (shown in Figs. 10.1 and 10.2), the boundary conditions are

$$[\bar{u}] = 0, \quad [\bar{u}'] = 0, \quad [\bar{\theta}] = [\tilde{\theta}]. \quad (10.17)$$

When the arch is connected with truss, its displacements are the same as those of the chords. For instance, when the connection is at the lower chord, the continuous conditions are

$$\begin{aligned} \hat{u} &= u_2 = u_0 - k_2 \theta - j_2 \tilde{\theta}, \\ \frac{d\hat{u}}{ds} &= \frac{du_2}{dx} \cos \alpha + (\theta - \tilde{\theta}) \sin \alpha. \end{aligned} \quad (10.18)$$

That is

$$\hat{u}' = u_0' - k_2 \theta' - j_2 \tilde{\theta}' + (\theta - \tilde{\theta}) \tan \alpha,$$

where  $\alpha$  is given in Fig. 10.7.

If the truss, instead of the arch, is connected to the support, the boundary conditions can be found in Chap. 6.

## 10.6 Calculation of Internal Forces

After obtaining the nodal displacement parameters of arch-beam elements, the internal forces of truss can be calculated as shown in Chap. 6. The forces of arch can be calculated according to Eq. (10.8), and taking the average along the arch panel.

## 10.7 Comparison Between the Model Test and the Theory

(Li and Shi 1978)

A steel bridge model, made to scale 1:20 according to a single truck railway steel bridge with a span of 112 m, is shown in Fig. 10.10. The stress and deformation tests have been made for wind loads, which are simulated by static horizontal lateral loads at nodes. The model bridge was computed by the proposed method and by the method of spatial bar system.

In the calculation by the finite arch-beam element method described in this chapter one panel was taken as an element except the substructure element at arch portal.

The lateral deflections  $u$  and the axial forces  $S$  in the members are shown in Figs. 10.11 and 10.12. The efficiency of the method presented here can be seen from the figures.

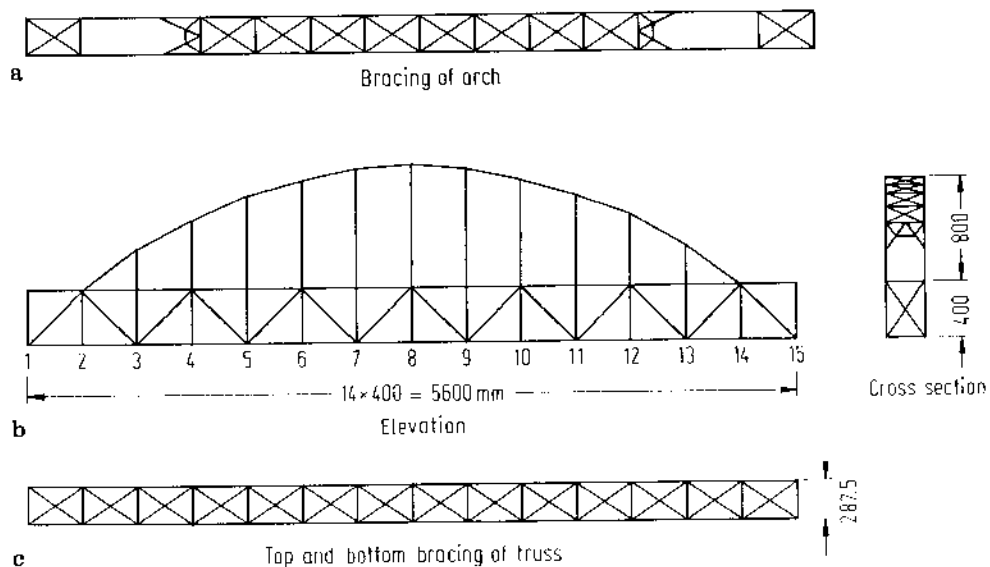


Fig. 10.10a-c. The dimensions of a steel bridge model

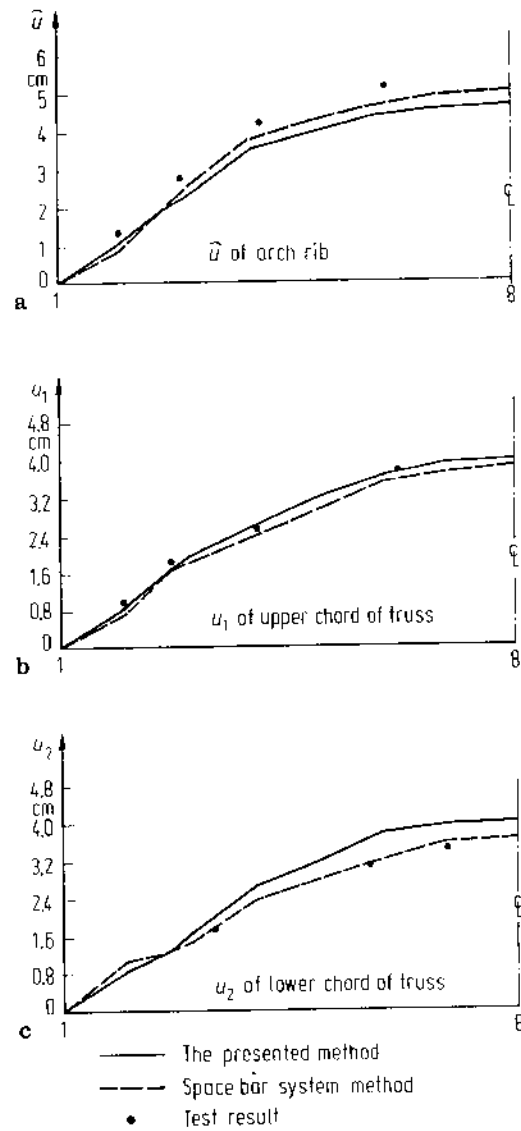


Fig. 10.11a-c. The comparisons of lateral deflections

## 10.8 Finite Element Method for the Lateral Buckling Analysis of Arch-Truss

The lateral stability of the arch-truss bridge has been analyzed according to the principle presented in Sects. 8.4 and 10.1 (Li et al. 1983). Here we can take all the displacement functions of element  $u$ ,  $\theta$ ,  $\tilde{\theta}$  in the form of cubic parabolas.

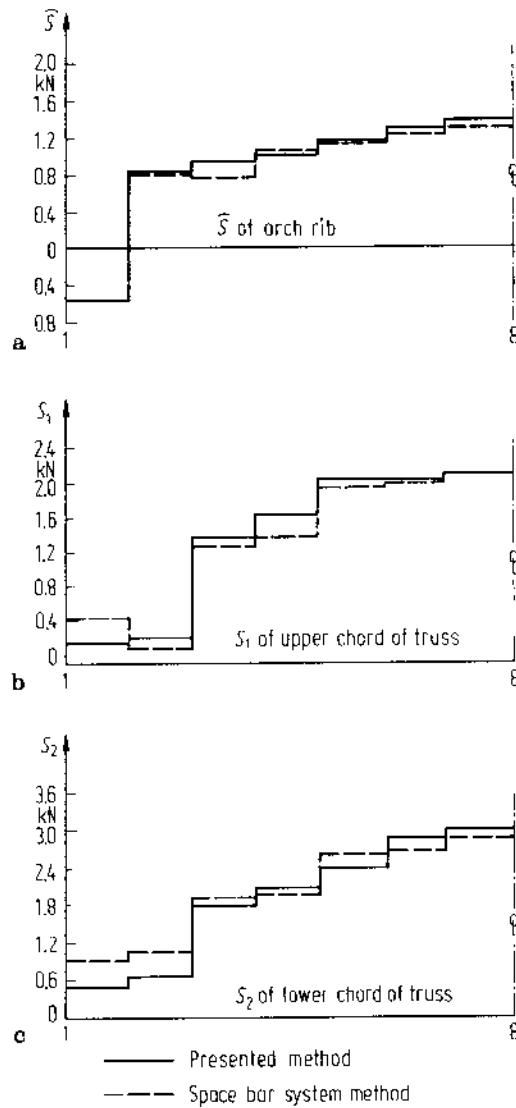


Fig. 10.12a-c. The comparisons of the axial forces

If the bridge is subjected to vertical design load  $q$ , only the forces in plane  $\{S\}$ , i.e. the bending moment  $M$  of truss, the arch thrust  $H$ , and the tension  $V$  of hanger will be induced.

When the lateral elastic buckling occurs, small lateral bending-torsional displacements  $\{\delta\}$  will be induced in the bridge, which induces the elastic nodal forces:

$$\{F\}_k^e = [k]\{\delta\}^e = ([k]_T + [k]_A + [k]_F)\{\delta\}^e. \quad (10.19)$$

The indices T, A, F, denote the truss, arch, and cross-frame, respectively.

Assuming the critical load is  $\nu$  times as large as the design load, where  $\nu$  is the safety factor of elastic lateral buckling, then the additional nodal forces induced by



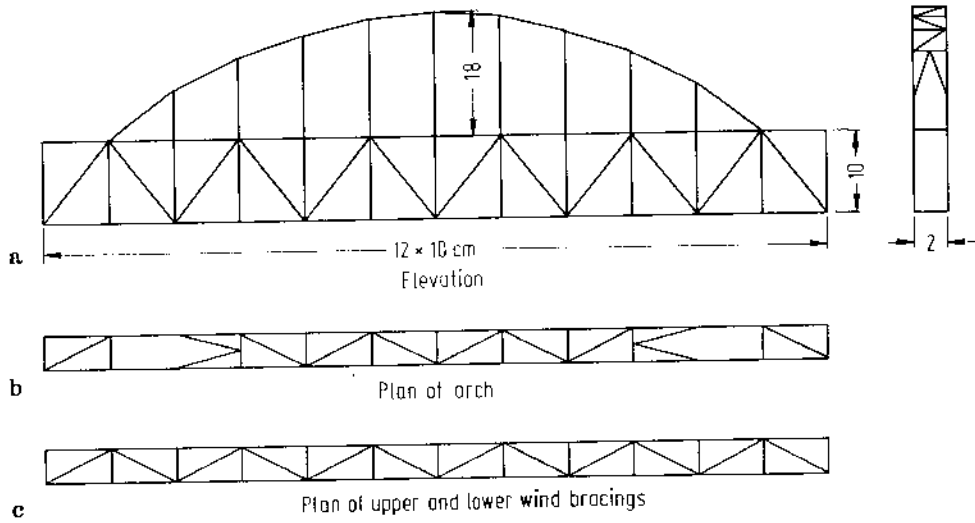


Fig. 10.13a-c. The dimensions of model

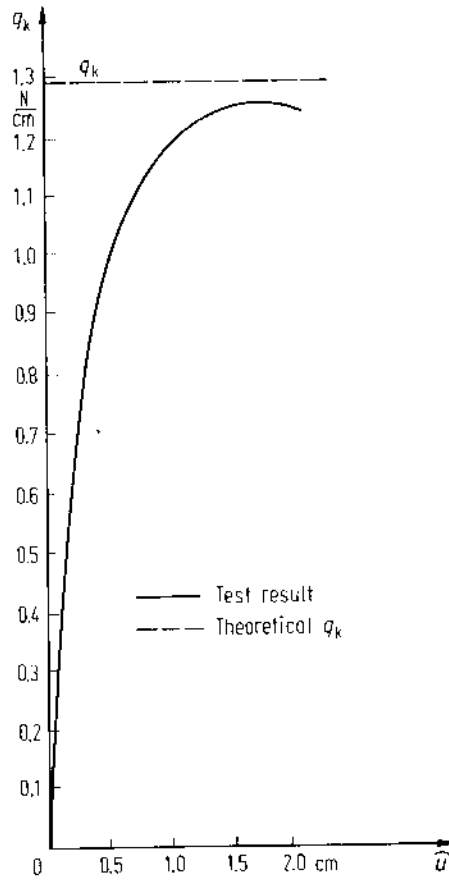


Fig. 10.14. Results of buckling test

the inplane internal forces  $v\{S\}$  and  $\{\delta\}$ , are as follows:

$$\{F\}_G^e = v[g]\{\delta\}^e = v([g]_T + [g]_A + [g]_F)\{\delta\}^e, \quad (10.20)$$

where  $[g]$  is the geometric matrix, and can be obtained according to the principle described in Chap. 8. For details see Li et al. 1983.

Equating the elastic nodal forces  $\{F\}_k^e$  with the additional nodal loads at all nodes, i.e. expressing the indifferent equilibrium of the bridge, we obtain the general lateral buckling equations:

$$[(K) - v(G)]\{\delta\} = 0. \quad (10.21)$$

For further calculation see Chap. 8.

### 10.9 Model Test of the Lateral Buckling of Arch-Truss Bridge

A Plexiglass model (Fig. 10.13) of an arch-truss bridge with a very small ratio of width to span was made for the elastic lateral buckling test, and the critical load  $q_k$  has been computed according to the method previously described; for details see Li et al. (1983).

The results are shown in Fig. 10.14, where  $\hat{u}$  is the lateral displacement at the arch crown. It can be seen that  $q_k$  obtained from the test agrees well with the theoretical value.

The calculation made for arch-truss bridges in engineering shows that the lateral buckling occurs, as in case of the actual truss bridges analyzed in Chap. 8, within the plastic deformation range.

## References

- Alam KM, Hongladaromp T, Lee SL (1973) Curved Box Girder Bridges with Intermediate Diaphragms and Supports. IABSE Proc., 33(II):17-35
- Al-Rifaie WN, Evans HR (1979) An Approximate Method for the Analysis of Box Girder Bridges that are Curved in Plan. IABSE Proc., P-21/79
- Bornscheuer FW (1952) Systematische Darstellung des Biege- und Verdrehvorganges unter besonderer Berücksichtigung der Wölbkrafttorsion. Stahlbau 21(1):1, 22(2):32
- Cao FM (1982) The Lateral Stability Analysis of Trapezoidal Truss Bridges. The Master Thesis of Tongji University (unpublished)
- Cheung MS, Cheung YK (1971) Analysis of Curved Box Girder Bridges by Finite Strip Method. IABSE Proc., 31(I):1-19
- Cheung YK (1976) Finite Strip Method in Structural Analysis. Pergamon Press, England
- Cheung YK, Cheung MS (1969) Free Vibration of Curved and Straight Beam-Slab or Box-Girder Bridges. IABSE Proc., 29(II):41-52
- Clough RW, Penzien J (1975) Dynamics of Structures. McGraw-Hill, New York
- Culver CG (1967) Natural Frequencies of Horizontally Curved Beams. J. of Struct. Div., ASCE, 93(4):189-203
- Dabrowski R (1968) Curved Thin-Walled Girders. Translation No. 144, Cement and Concrete Association, London
- Dalton DC, Richmond B (1968) Twisting of Thin-Walled Box Girders of Trapezoidal Cross-Section. Proc. of Inst. Civ. Engrs., 39(1):61-73
- Dshanelidze GU, Panovko YG (1948) Statics of Elastic Thin-Walled Members (in Russian). National Publishing House of Technical Theoretical Literatures, Moscow
- Evans HR, Al-Rifaie WN (1975) An Experimental and Theoretical Investigation of the Behaviour of Box Girders Curved in Plan. Proc. of Inst. Civ. Engrs., Part 2, Vol. 59, Jun.:323-352
- Gjelsvik A (1981) The Theory of Thin-Walled Bars. John Wiley & Sons, New York
- Hayashi Y, Tanaka Y, Higuchi K (1977) Three-Dimensional Oscillation Analysis of Truss Girders by the Thin-Walled Elastic Beam Theory Considering Cross-Sectional Deformations (in Japanese). Proc. of Japan Society of Civil Engineers, No. 261:7-20
- Heins CP, Humphreys RS (1979) Bending and Torsion Interaction of Box Girders. J. of Struct. Div., ASCE, 105(5):891-904
- Heins CP, Jr., Oleinik JC (1976) Curved Box Beam Bridge Analysis. Int. Journal of Computers & Structures, 6:65-73
- Heins CP, Sahin MA (1979) Natural Frequency of Curved Box Girder Bridges. J. of Struct. Div., ASCE, 105(12):2591-2600
- Hirashima M, Iura M, Yoda T (1979) Finite Displacement Theory of Naturally Curved and Twisted Thin-Walled Members (in Japanese). Proc. of JSCE, No. 292:13-28
- Hu HC (1981) Variational Principles in Elasticity with Applications (in Chinese). Science Press, Beijing, pp 139-206
- Huang JY (1983) Analysis of Torsion of Thin-Walled Structures (in Chinese). China Railway Publishers, Beijing
- Huang J, Shi D, Li MZ (1986), Practical Space Analysis of Sway Bracings of Truss Bridges (in Chinese). J. of Tongji Univ., 14(3):299-309
- Issa RRA, Aven RR (1984) Superelement Stiffness Matrix for Space Trusses. J. of Struct. Div., ASCE, 110(5):1163-1179

- Kolbrunner CF, Hajdin N (1972) *Dünnwandige Stäbe*. Springer-Verlag, Berlin, Heidelberg, New York
- Komatsu S, Nakai H (1966) Study on Forced Vibration of Curved Girder Bridges. *Japan Society of Civil Engineers*, 2(I): 37–42
- Kotsubo S, Teruhiko, Takanishi, Uno K, Matsushita S (1977) Earthquake Response Characteristics of Three Spans Continuous Truss Bridge with High Piers (in Japanese). *Proc. of JSCE*, No. 266
- Kristek V (1979) *Theory of Box Girders*. John Wiley & Sons, New York
- Li GH (1975) *Torsion, Stability and Vibration of Truss Bridges* (in Chinese). Communication Publishers, Beijing
- Li GH (1978) Analysis of Stress, Stability, and Vibration of Truss Bridges. *Scientia Sinica* 21(6): 757–766
- Li GH (1980) Analysis of Lateral Buckling of Truss Bridge (in Chinese). *China Civil Engineering Journal*, 13(1): 2–10
- Li GH (1980) *Dynamics of Earthquake-Resistant Structural Analysis* (in Chinese). Scientific and Technical Literature Publishers, Shanghai
- Li GH (1983) *Research on Bridge and Structural Theory* (in Chinese). Scientific and Technical Literature Publishers, Shanghai
- Li GH, Shi D (1978) The Finite Element Method for the Spatial Analysis of Arch and Truss Combined System (in Chinese). *J. of Tongji Univ.*, 6(4): 1–20
- Li GH, Shi D (1982) Finite Element Analysis of Seismic Response of Curved Girder Bridges. In: *Proceedings of Sino-American Symposium on Bridge and Structural Engineering*, Beijing, 4-01-1, China Academic Publishers
- Li GH, Shi D, Feng Q (1982) The Finite Element Method for the Lateral Stability of Truss Bridge. In: *Proc. of Inter. Conf. on FEM*. Science Press, Beijing, pp 922–925
- Li GH, Shi D, Huang DZ (1983) A Finite Element Method for the Lateral Buckling Analysis of Arch-Truss Beam Bridge (in Chinese). *J. of Tongji Univ.*, 11(1): 1–14
- Lie KH (Li GH) (1944) Berechnung der Fachwerke und Verwanetter Systeme auf neuem Wege. *Stahlbau* 17(819): 35, (10/11): 41
- Lie KH (Li GH) (1949) Analysis of Lattice Trusses. *Science Record*, 2(4): 393
- McManus PF, Nasir GA (1969) Horizontally Curved Girders — State of the Art. *J. of Struct. Div., ASCE*, 95(5): 853–870
- The Ministry of Railway Transportation of the People's Republic of China (1976) *Bridges and Tunnels, the Second Part of the Criteria of the Techniques of Railway Engineering* (in Chinese). People Railway Publishers, Beijing
- Moffat KR, Lim PTK (1977) Some Finite Elements Having Particular Application to Box Girder Bridges. *IABSE Proc.*, P1-177, Zürich
- Murakami T, Aida T (1979) Three-Dimensional Analysis of Free Vibration of Long Span Truss Bridges (in Japanese). *Proc. of JSCE*, No. 283: 1–12
- Nakai H, Tani T (1978) An Approximate Method for the Evaluation of Torsional and Warping Stresses in Box Girder Bridges (in Japanese). *Proc. of JSCE*, No. 277: 41–56
- Przemieniecki JS (1968) *Theory of Matrix Structural Analysis*. McGraw-Hill, New York
- Rabizadeh RO, Shore S (1975), Dynamic Analysis of Curved Box Girder Bridges. *J. of Struct. Div., ASCE*, 101(9): 1899–1912
- Richmond B (1969) Trapezoidal Boxes with Continuous Diaphragms. *Proc. of Inst. of Civ. Engrs.*, 43(8)
- Roik, Carl, Lindner (1972) *Biegetorsionsprobleme Gerader Dünnwandiger Stäbe*. Verlag von Wilhelm Ernst & Sohn, Berlin
- Roik K, Sedlacek G (1970) Erweiterung der technischen Biege- und Verdrehtheorie unter Berücksichtigung von Schubverformungen. *Bautechnik* 47(1): 20
- Sakai F, Nagai M (1977) A Recommendation on the Design of Intermediate Diaphragms in Steel Box Girder Bridges (in Japanese). *Proc. of JSCE*, No. 261: 21–34
- Scordelis AC (1871) Analytical Solutions for Box Girder Bridges. In: *Developments in Bridge Design and Construction*. Crosby Lockwood, Cardiff
- Scordelis AC, David RE (1969) Stresses in Continuous Box Girder Bridges. In: *Proceedings of 2nd International Symposium of Concrete Bridge Design*. American Concrete Institute
- Sedlacek G (1971) Die Anwendung der erweiterten Biege- und Verdrehtheorie auf die Berechnung von Kastenträgern mit verformbarem Querschnitt. *Strasse Brücke Tunnel*, Heft 9 241–329
- Sisodiya RG, Cheung YK, Ghali A (1970) Finite Element Analysis of Skew, Curved Box-Girder Bridge. *IABSE Proc.*, 30(II): 191–199

- Sisodiya RG, Ghali A (1973) Analysis of Box Girder Bridges of Arbitrary Shape. *IABSE Proc.*, 33(1): 203-218
- Tan CP, Shore S (1968) Dynamic Response of a Horizontally Curved Bridge. *J. of Struct. Div., ASCE*, 94: 761-781
- Task Committee on Curved Box Girders (1978) Curved Steel Box-Girder Bridges: State-of-the-art. *J. of Struct. Div., ASCE*, 104(11): 1719-1739
- Taya T (1977) Coupled Vibration of Continuous Truss-Bridge on Many Piers. *Proc. of JSCE*, No. 261: 113-122
- Timoshenko SP (1921) On the Correction for Shear of the Differential Equation for Transverse Vibration of Prismatic Bars. *Phil Mag* 41: 744
- Timoshenko S (1936) *Theory of Elastic Stability*. McGraw-Hill, New York
- Timoshenko SP, Goodier JN (1970) *Theory of Elasticity*. McGraw-Hill, New York
- Timoshenko S, Young DH, Weaver Jr. W (1974) *Vibration Problems in Engineering*, Third Edition. John Wiley & Sons, New York
- Vlasov VZ (1961) *Thin-Walled Elastic Beams*. National Science Foundation, Washington, D.C.
- Zhang SH (1984) A Thin-Walled Box Beam Finite Element for Curved Bridge Analysis. *Inter. Journal of Computers & Structures*, 18(6): 1035-1046
- Zienkiewicz OC (1977) *The Finite Element Method (Third Edition)*. McGraw-Hill, London

